INFLAMMATION-ON-A-CHIP: A MICROPHYSIOLOGICAL HUMAN LIVER MODEL

Dissertation

To fulfill the
requirements for the degree of
doctor rerum naturalium (Dr. rer. nat.)

Submitted to the Council of the Faculty
of Medicine
of the Friedrich Schiller University Jena

by Dipl.-Troph. Marko Tobias Gröger
born on Juli 7th, 1988 in Plauen

1st Reviewer: Prof. Dr. Otmar Huber; University Hospital Jena

2nd Reviewer: Prof. Dr. Michael Bauer; University Hospital Jena

3rd Reviewer: Prof. Dr. Frank Tacke; University Hospital Aachen

Date of the public disputation: October 16th, 2018

TABLE OF CONTENTS

ABBREVIATIONS III

SUMMARY V

ZUSAMMENFASSUNG VII

1 INTRODUCTION 1

1.1 Microphysiological Models 1

1.1.1 Novel concepts of *in vitro* liver modeling 1

1.1.1.1 Regulation of hepatic function by NPCs 2

1.1.1.2 Liver-on-a-chip as a new research tool 2

1.2 Liver inflammation - aspects in biomedical research 5

1.2.1 Pathophysiological role of the liver in sepsis 5

1.2.2 Hepatocellular dysregulation during inflammation 5

1.2.2.1 Macrophage polarization and regulation 6

1.2.3 Models of sepsis and sepsis-related liver dysfunction 8

1.3 Hypothermal liver-on-a-chip preservation 9

1.3.1 Cellular alterations during cold storage 10

1.3.2 Protective effect of storage solution components on liver cells 12

2 AIM OF THESIS 13

3 MANUSCRIPTS 14

3.1 Manuscript I - A microfluidically perfused three dimensional human liver model 15

3.2 Manuscript II - Monocyte-induced recovery of inflammation-associated hepatocellular dysfunction in a biochip-based human liver model 30

3.3 Manuscript III - Preservation of cell structure, metabolism and biotransformation activity of liver-on-chip organ models by hypothermic storage 56

4 DISCUSSION 74

4.1 Liver-on-a-chip - complexity matters 74

4.1.1 Biochip design and technical variables 74

4.1.2 Vascular perfusion as a critical parameter for endothelial and hepatocyte cell function 76

4.1.3 Cellular diversity - the key to hepatic microphysiology 77

4.2 Inflammation-on-a-chip - a suitable tool for translational medicine? 79

4.2.1 TLR-mediated liver dysfunction in a microphysiological liver-on-a-chip 79

4.2.1.1 Hepatocytes as inflammatory targets 79
4.2.1.2 Sinusoidal activation and recruitment of immune cells 80
4.2.2 Monocyte-macrophage interaction during hepatic inflammation 82
4.3 Novel hypothermal preservation strategy for liver-on-a-chip models 83
4.3.1 Basic components of cold storage solutions 84
4.3.2 Iron chelators and chloride - critical elements for cold storage of liver cells 84
4.3.3 Dextran and PEG enhance liver-on-a-chip storage 85
5 CONCLUSION 88
A REFERENCES ..... A
B ACKNOWLEDGEMENT ..... B
C CURRICULUM VITAE C
D LIST OF PUBLICATIONS ..... D
E AUTHOR CONTRIBUTION STATEMENT ..... E
F EHRENWÖRTLICHE ERKLÄRUNG ..... F

ABBREVIATIONS

ALAT	Alanine aminotransferase
ApoB	Apolipoprotein B
ASAT	Aspartate aminotransferase
ATP	Adenosine triphosphate
CD	Cluster of differentiation
CDF	5 (and 6)-carboxy-2′,7′ -dichlorofluorescein
COC	Cyclic olefin copolymer
CYP	Cytochrome P_{450}
DAMPs	Damage-associated molecular patterns
ECs	Endothelial cells
ECM	Extracellular matrix
GLDH	Glutamate dehydrogenase
HGF	Hepatocyte growth factor
HiF-1α	Hypoxia-inducible factor-1α
HSCs	hepatic stellate cells
HTK	Histidine-tryptophan-ketoglutarate solution
HUVECs	Human umbilical vein endothelial cells
ICAM-1	Intercellular adhesion molecule-1
IL	Interleukin
IFN	Interferon
KCs	Kupffer cells
LDH	Lactate dehydrogenase
LPS	Lipopolysaccharide
LSECs	Liver sinusoidal endothelial cells
MOTiF	Multi Organ Tissue Flow
MRP-2	Multi drug resistance protein-2
NPCs	Non-parenchymal cells
PCI	Peritoneal contamination and infection
PAMPs	Pathogen-associated molecular patterns
PDMS	Polydimethylsiloxane
PEG	Polyethylene glycol
PS	Polystyrene

ROS	Reactive oxygen species
TLRs	Toll-like receptors
TNF	Tumor necrosis factor
UW	University of Wisconsin solution
VCAM-1	Vascular cell adhesion molecule-1
VEC	Vascular endothelial cadherin

SUMMARY

A major challenge in the current development of complex biotechnological systems remains in its miniaturization to enable an efficient and economic use in biomedical research. Microphysiological organ-on-a-chip models enter the stage as an enhanced *in vitro* method to emulate physiological processes *ex vivo*. In addition, this approach offers new possibilities to model organ failure and to study systemic inflammatory diseases like sepsis. Due to the lack of appropriate treatment options, sepsis is one of the leading causes of death in intensive care units. Sepsis-related liver dysfunction severely affects the patient survival and causes high mortality underlining the importance of this organ in host defense. Therefore, the versatile organ-on-a-chip technology could be a promising *in vitro* tool to investigate the pathophysiological role of organs, such as the liver, during inflammation under humanized conditions.

The objective of this work was the establishment of a human liver-on-a-chip and its application as a model of inflammatory hepatic dysfunction. In the first study, four major cell types of the liver were integrated in the Multi Organ Tissue Flow (MOTiF) biochip and examined by functional as well as morphological characteristics (manuscript I). Inspired by the basic microanatomy of the liver sinusoid, human umbilical vein endothelial cells and primary human, monocyte-derived macrophages were co-cultured with HepaRG and LX-2 cells representing the vascular and hepatic cell layer, respectively. A porous membrane served as a culture surface for the distinct layers and forms an artificial space of Disse. The combination of vascular perfusion and cellular interaction led to functional stabilization and polarization of the hepatocytes, which was associated with improved biliary excretion via self-formed bile canaliculi, increased albumin and urea synthesis as well as cytochrome P_{450} (CYP) 3A4 activity compared to static liver-on-a-chip culture. Moreover, continuous evaluation of cellular oxygen consumption measured by luminescence-emitting sensor spots enabled the assessment of the metabolic activity.

To verify the applicability of the liver-on-a-chip model as a new biomedical research tool we investigated toll-like receptor (TLR)-mediated inflammation (manuscript II). TLR stimulation for three days led to hepatocellular dysfunction accompanied by the specific release of the pro-inflammatory cytokine interleukin (IL)-6 as well as the anti-inflammatory IL-10 depending on the pathogen-associated molecular pattern. Incubation with lipopolysaccharide (LPS) further revealed a time-dependent cytokine

profile. The results were comparable to data obtained from patients suffering from sepsis as well as data from murine sepsis models, where fecal stool samples were injected into the peritoneum to trigger systemic inflammation (peritoneal contamination and infection, PCI). Hepatocellular dysfunction in our liver-on-a-chip model was characterized by a loss of vascular barrier integrity, diminished biliary excretion rate and reduced apolipoprotein B expression. Interestingly, hepatic damage was prevented by integration of circulating monocytes, which resulted in inflammatory resolution. Furthermore, we identified IL-10 as a potential mediator directing the polarization state of tissue-resident macrophages to an anti-inflammatory, regenerative phenotype in the presented model.

The utilization of organ-on-a-chip applications is limited by their challenging culture protocols and time-consuming establishment. Additionally, handling of these *in vitro* models requires expertise, which is necessary to grant reproducibility and reliable results. Therefore, we developed novel protocols for hypothermic storage of liver-on-a-chip models to maintain their microstructure after assembly (manuscript III). Five different storage solutions were tested for their ability to preserve morphology and function of the respective cell layers. The study confirmed that the preservation of the liver model in an adapted formulation of the TiProtec® storage solution is possible for up to two days at 4 °C. Apart from the structural conservation, the inflammatory responsiveness to LPS was verified by the secretion of tumor necrosis factor, IL-1β, IL-10 and IL-6 as well as the characteristic activated macrophage morphology. Unfortunately, we were not able to extend the cold storage period beyond two days without significantly effecting cell viability and function. Nevertheless, to our best of knowledge this was the first successful approach of a liver-on-a-chip preservation.

Our hepatic model featured characteristics of human tissue samples and clinical observations during liver inflammation. Nonetheless, sequential integration of primary liver cells will be necessary to assess benefits and drawbacks of this concept. In summary, this thesis demonstrates the characterization, application and utilization of a human liver-on-a-chip as a new alternative to conventional *in vitro* and *in vivo* test systems. The complex hepatic microenvironment created in perfused multi-layered tissue models was shown to be important for improving cell type specific functions closely resembling the *in vivo* situation. This model has the potential to become a valuable alternative to overcome the limitations in translational research and will help to close the gap between conventional cell culture and animal experimentation.

ZUSAMMENFASSUNG

Eine der größten Herausforderungen in der aktuellen Entwicklung komplexer biotechnologischer Systeme ist deren Miniaturisierung zur effizienten und ökonomischen Nutzung in der Biomedizin. Mikrophysiologische *organ-on-a-chip* Modelle sind eine verbesserte *in vitro* Technik zur Untersuchung physiologischer Prozesse *ex vivo* und daher von besonderem Interesse für die Forschung. Außerdem könnte dieses Konzept neue Möglichkeiten zur Abbildung von Organversagen und Untersuchung systemischer, inflammatorischer Krankheiten, wie Sepsis, eröffnen. Sepsis ist aufgrund der eingeschränkten Behandlungsmöglichkeiten eine der führenden Todesursachen auf Intensivstationen. Dabei korreliert die Sepsis-assoziierte Leberdysfunktion mit einer schlechten Prognose und hohen Mortalität der Patienten, was die Wichtigkeit des Organs in der Immunabwehr unterstreicht. Daher könnte die vielseitige *organ-on-a-chip* Technologie ein vielversprechendes *in vitro* Werkzeug darstellen, um die pathophysiologische Rolle von humanen Organen wie der Leber während einer Entzündung zu untersuchen.

Das Ziel dieser Arbeit war es, ein humanes, biochip-basiertes Leber Modell zu etablieren und dessen Tauglichkeit zur Untersuchung inflammatorischer Vorgänge zu verifizieren. In der ersten Studie wurden die vier Hauptzelltypen der Leber in den *Multi Organ Tissue Flow* (MOTiF) Biochip integriert und anhand von morphologischen und funktionellen Aspekten charakterisiert (Manuskript I). In Anlehnung an die prinzipielle Mikroanatomie eines Lebersinusoids wurden humane Endothelzellen der Nabelschnurvene und primäre, aus Monozyten abgeleitete humane Makrophagen (vaskuläre Zellschicht) mit HepaRG und LX-2 Zellen (hepatische Zellschicht) ko-kultiviert. Dabei diente eine poröse Membran als artifizieller Disse-Raum sowie als Kulturoberfläche für die verschiedenen Zellschichten. Die Kombination aus vaskulärer Perfusion und zellulärer Interaktion führte zu einer funktionellen Stabilisierung und Polarisierung der Hepatozyten. Diese war gekennzeichnet durch eine verbesserte biliäre Exkretion durch im Chip selbst ausgebildete Gallenkanälchen und Cytochrom P_{450} (CYP) 3A4 Enzymaktivität sowie einer erhöhten Albumin- und Harnstoffsynthese im Vergleich zur statischen Kultur. Zusätzlich konnten durch eine kontinuierliche Ermittlung des zellulären Sauerstoffverbrauchs mittels integrierter Lumineszenz-emittierender Sensorspots Rückschlüsse auf die metabolische Aktivität gezogen werden.

Um die Anwendbarkeit des Leber-Modells als neues Werkzeug in der präklinischen Forschung darzulegen, wurde über Stimulation von Toll-ähnlichen Rezeptoren (TLR) eine Entzündung induziert (Manuskript II). Eine dreitägige Inkubation mit TLR Agonisten führte zu einer hepatozellulären Dysfunktion, die in Abhängigkeit vom pathogen-assoziierten molekularen Muster zur spezifischen Freisetzung des pro-inflammatorischen Zytokins Interleukin (IL)-6 sowie des anti-inflammatorischen IL-10 führte. Weiterführend konnten durch Applikation von Lipopolysacchariden (LPS), anhand des zeitabhängigen Zytokinprofils Übereinstimmungen zu Daten von Sepsis-Patienten und eines murinen Sepsismodells, bei dem durch Injektion von Faeces in das Peritoneum eine systemische Inflammation ausgelöst wurde (peritoneale Kontamination und Infektion, PCI), nachgewiesen werden. Die hepatische Dysfunktion im *liver-on-a-chip* Modell war mit einem Verlust der Integrität der vaskulären Barriere, einer verminderten biliären Exkretionsrate und einer reduzierten Apolipoprotein B Expression assoziiert. Interessanterweise konnte durch Integration von zirkulierenden Monozyten eine Auflösung des Schadens und damit die inflammatorische Regression induziert werden. Zusätzlich wurde IL-10 als ein potentieller Vermittler für die Polarisierung der Makrophagen zu einem anti-inflammatorischen, regenerativen Phänotyp in unserem Modell identifiziert.

Bis heute ist die Nutzbarkeit von *organ-on-a-chip* Modellen durch anspruchsvolle Assemblierungsprotokolle und die damit verbundene, zeitaufwändige Etablierung limitiert. Zusätzlich erfordert deren Handhabung Expertise, um reproduzierbare und verlässliche Ergebnisse zu garantieren. Deshalb wurden in dieser Arbeit neue Protokolle zur hypothermalen Lagerung von komplett assemblierten *liver-on-a-chip* Modellen entwickelt, um deren Mikrostruktur zu konservieren (Manuskript III). Im Zuge dessen wurden fünf verschiedene Lagerungslösungen hinsichtlich der Aufrechterhaltung von Morphologie und Funktion der jeweiligen Zellschichten bewertet. Die Untersuchungen zeigten, dass eine Konservierung der Lebermodelle für zwei Tage bei 4 °C in einem Derivat der TiProtec® Lösung möglich war. Außerdem konnte anhand der Sekretion des Tumornekrosefaktors, IL-1β, IL-10 und IL-6 einhergehend mit der charakteristischen Morphologie der aktivierten Makrophagen ein Erhalt der inflammatorischen Responsivität nachgewiesen werden. Leider war es nicht möglich die Lagerung ohne Schädigung der Zellschichten auf mehr als zwei Tage zu verlängern. Dennoch beschreibt diese Studie nach unserem Wissen zum ersten Mal eine Methode zur hypothermalen Konservierung eines *liver-on-a-chip* Modells.

Unser hepatisches Modell wies zu humanen Gewebeschnitten vergleichbare Merkmale auf und zeigte Übereinstimmungen zu klinischen Beobachtungen im Verlauf einer Leberentzündung. Jedoch ist in Zukunft eine sequenzielle Integration von primären Leberzellen nötig, um die Vor- und Nachteile unseres Konzepts zu bewerten. Zusammenfassend wurde in dieser Arbeit die Charakterisierung, Anwendung und mögliche Nutzung eines humanen biochip-basierten Lebermodells als neue Alternative zu konventionellen *in vitro* und *in vivo* Testsystemen gezeigt. Dabei ist die komplexe Mikroumgebung der mehrschichtigen, perfundierten Gewebemodelle entscheidend für eine verbesserte zelluläre Funktion in Annäherung an die *in vivo* Situation. Diese Applikationen stellen eine wertvolle Alternative dar, um die limitierte Übertragbarkeit von translationalen Forschungsergebnissen zu verbessern und dadurch die Lücke zwischen konventioneller Zellkultur und Tierexperimenten zu schließen.

1 INTRODUCTION

1.1 Microphysiological Models

To date, translational research and understanding of molecular as well as cellular processes of disease progression are highly influenced by the used model system, which needs to be considered when interpreting collected data. On the one hand, static cell culture can barely mimic the complex physiology of the human body or even a single organ. On the other hand, animal models possess a complex systemic interaction but the results gained by them show differences in pathophysiological mechanisms compared to humans (Seok et al. 2013) or fail to be translated into clinical practice (Kingsley and Bhat 2016). Nonetheless, there is an ongoing debate about the future of murine models, especially regarding inflammation and sepsis (Efron et al. 2015). Most recently, microphysiological systems rapidly emerged in biomedical research and have the potential to provide a promising alternative to tackle these issues.

It has been shown that the increased complexity of organ-on-a-chip applications has several advantages compared to static *in vitro* models. This is mainly achieved by a combination of microfluidics, tissue engineering and multi-cell culture in biochips (Meyvantsson and Beebe 2008). Until now, there are various approaches to mimic the physiology of the respective organs. They range from biochip-based cultivation of heart, blood-brain barrier, gut, lung or liver tissue up to multi-organ devices in order to study systemic interaction (Materne et al. 2015, Coppeta et al. 2016).

1.1.1 Novel concepts of *in vitro* liver modeling

The liver is the central organ regarding the immune response to pathogens and biotransformation of drugs. Hence, a set of various cell types is necessary to fulfill these diverse functions. With approximately 80 %, the hepatocytes contribute the largest amount of cells to the liver tissue volume (Ishibashi et al. 2009). In addition, non-parenchymal cells (NPCs), namely liver sinusoidal endothelial cells (LSECs), hepatic stellate cells (HSCs) and Kupffer cells (KCs), are essential to maintain liver physiology and immunological homeostasis. Therefore, it is supposed that multi-cellular liver-on-a-chip models are a valuable new strategy to mimic functional aspects of the hepatic microenvironment *in vitro*, possibly improving the outcome of disease and toxicity studies (Vernetti et al. 2016, Starokozhko and Groothuis 2017).

1.1.1.1 Regulation of hepatic function by NPCs

Physiologically, hepatocytes and NPCs closely interact to fulfill a variety of functions as a mutually dependent unit (Ishibashi et al. 2009). One of the most prominent features of the liver is its drug metabolizing capacity. In general, the process of biotransformation can be divided into three phases: phase I (modification), phase II (conjugation) and phase III (transport and excretion). Before all molecules get in contact with hepatocytes they must pass the liver sinusoids, which are lined with LSECs. These cells form a selective barrier to prevent the hepatic parenchyma from vascular shear stress. Moreover, they are involved in the recruitment of circulating immune cells during liver injury, enable the exchange of nutrients as well as drugs with hepatocytes via fenestrations and scavenge different molecules from the blood (Poisson et al. 2017).

Monoculture of primary hepatocytes rapidly results in dedifferentiation accompanied by a loss of important phase I and II enzyme activities (Rodríguez-Antona et al. 2002, Chen et al. 2012, Godoy et al. 2013). In contrast, co-culture with LSECs led to long-term stabilization of native cytochrome P_{450} (CYP) 1A1 activity (Bale et al. 2015a). The authors concluded that introduction of extracellular matrix (ECM) and cellular interaction were critical for the maintenance of hepatocyte function in their model. Furthermore, it was observed that LSECs could prevent unfavorable HSC activation through paracrine signaling via vascular endothelial growth factor (Deleve et al. 2008). Nonetheless, activation of quiescent HSCs in pathophysiological states results in an increased production of extracellular matrix aligned with a secretion of several cytokines, important for regulating hepatic damage and tissue repair (Weiskirchen and Tacke 2014). Krause et al. (2009) showed that hepatocyte differentiation *in vitro* was stabilized in co-culture with HSCs. Additionally, it was investigated that a cross talk between these cell types is bidirectional, notably under inflammatory conditions (Coulouarn et al. 2012). Due to these observations the interaction of different NPCs with hepatocytes appears to be necessary to support hepatic function and to regulate their pathophysiological response. This statement is fostered by the presence of KCs as specialized macrophages, which were able to enhance albumin and urea synthesis in co-culture with hepatocytes (Zinchenko et al. 2006) and represent important immunological regulators in the liver (Sica et al. 2014).

1.1.1.2 Liver-on-a-chip as a new research tool

Mimicking the liver *in vitro* is still a challenge and far from being fully developed and

validated. Despite the cellular composition and related arrangement, micro-physiological systems comprise several technical variables, e.g. the design and material of the biochip device. Further, exogenous factors like shear stress, oxygenation and nutrient supply need to be monitored continuously to emulate a stable hepatic microenvironment. Hence, it is necessary to analyze the specific physiological characteristics of the human sinusoid to cover a wide range of different aspects by liver-on-a-chip modeling (Figure 1). Dependent on the application, different cell sources (i.e. primary cells, cell lines) and proper evaluation of their individual advantages as well as disadvantages is necessary.

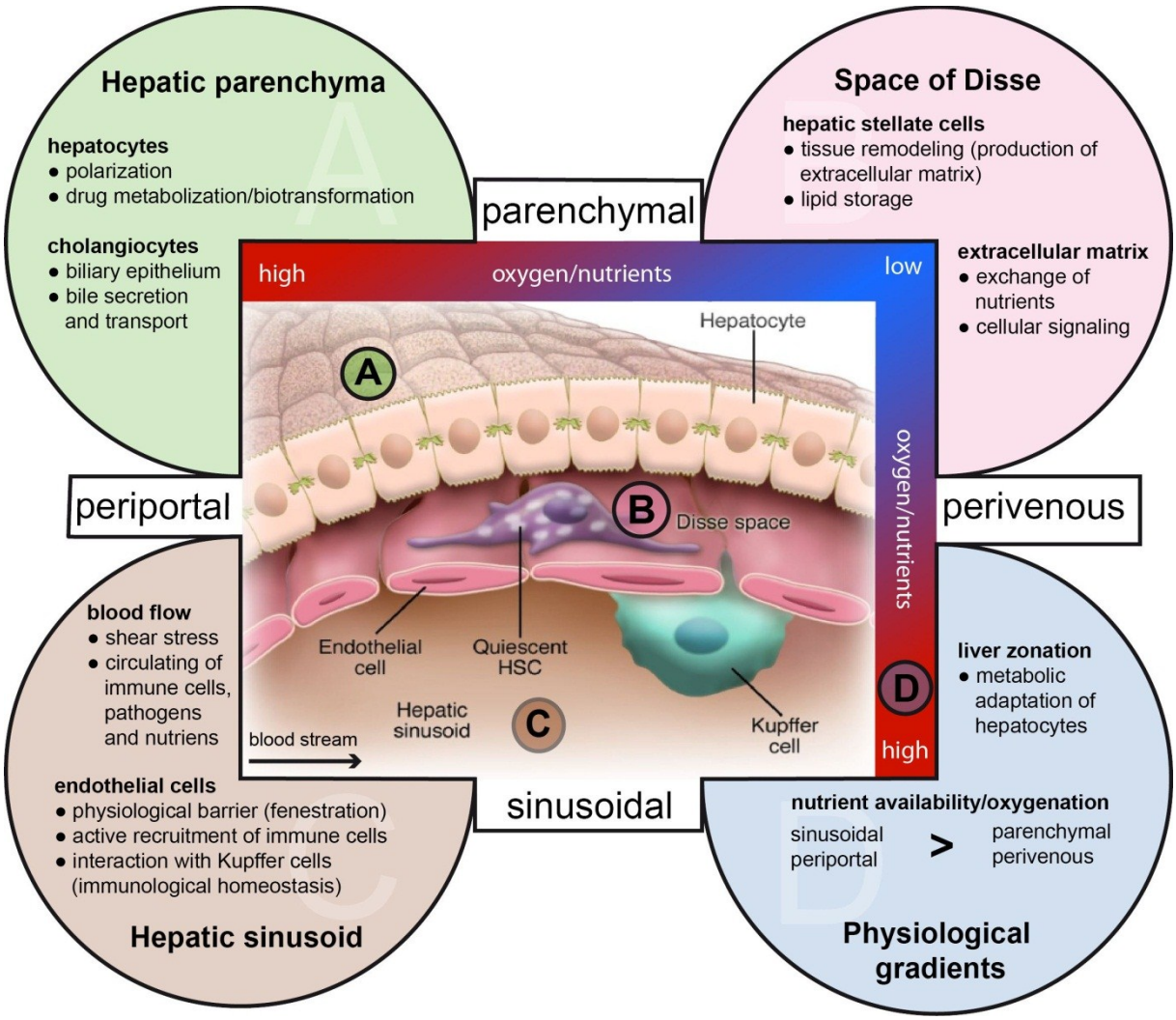

Figure 1. *Important characteristics of the liver that need to be considered in the establishment of a microphysiological hepatic in vitro model. Figure modified from Iredale et al. (2007).*

To protect the hepatic parenchyma from harmful shear stress different cell culture strategies were applied. McCarty et al. (2014) used ultrathin layers of modified collagen to cover primary hepatocytes. Their results demonstrated that hepatocyte

morphology and function were maintained for up to 14 days under slow perfusion rates of 20 µl/h (McCarty et al. 2014). An extension of this approach consisted in the integration of LSECs as a barrier with a physiological ECM mimicking the space of Disse, similar to the *in vivo* situation. Kang et al. (2015) emulated the sinusoidal structure by use of single channel cell culture chambers with stacked endothelial cells (ECs) and hepatocytes divided by a layer of BD Matrigel™. Additionally, the authors of this study compared their model with a dual channel setup where the vascular and hepatic cells grew on different sides of a porous membrane. The membrane served as a permeable cell culture surface, providing an artificial space of Disse for a better control of cellular growth, cell-medium interaction and long term stabilization of the microenvironment (Kang et al. 2015). Prodanov and colleagues further adapted this approach by integration of U937 (tissue-resident macrophages) and LX-2 (stellate cell line), additionally to ECs and primary hepatocytes in two distinct layers. They were able to maintain this liver-on-a-chip model for 28 days with stable albumin and urea secretion as well as CYP3A4 activity (Prodanov et al. 2016). In a similar device with primary murine cells it was also proven that the presence of all four major hepatic cell types led to a higher amount of recruited neutrophils after lipopolysaccharide (LPS) stimulation (Du et al. 2017), most likely via up-regulation of adhesion molecules in LSECs (Edwards et al. 2005). This promising membrane-based approach with a vascularized compartment and a separated epithelial cell layer was also used for other organ models, i.e. emulation of the intestine (Kim et al. 2016), lung (Jain et al. 2018) and the blood-brain barrier (Raasch et al. 2016).

Besides cellular adaptations within microphysiological systems, exogenous factors play an important role in modulating the microenvironment. First of all the biochip material, used for fabrication, needs to be considered. Various microfluidic cell culture devices were made of polydimethylsiloxane (PDMS) due to practical advantages in processing of the material (Leclerc et al. 2003, Maschmeyer et al. 2015, Du et al. 2017, Kang et al. 2017). However, the unspecific binding capacity of PDMS for hydrophobic drugs as well as other molecules could cause variable drug concentrations exposed to cells and tissues possibly affecting the obtained results from associated drug testing (Toepke and Beebe 2006). Therefore, Marx and colleagues suggested the use of materials already established for standard cell culture dishes, such as polystyrene (PS), as the future of organ-on-a-chip manufacturing (Marx et al. 2016). Another important step to promote microphysiological systems is the integration of miniaturized sensors allowing a

continuous monitoring of the critical cell culture parameters thereby contributing to the formation of an organ-specific microenvironment and related cell function (Zhang et al. 2017). Overall, the utilization of biochip-based organ models is critically affected by two variables, the choice of cellular composition and consideration of exogenous influencing factors.

1.2 Liver inflammation – aspects in biomedical research

1.2.1 Pathophysiological role of the liver in sepsis

Recently, Singer and colleagues defined sepsis as a cause of infection that leads to life-threatening organ failure accompanied by a dysregulated immune response (Singer et al. 2016). Recent clinical data indicate that severe courses of systemic inflammation and multi-organ failure still lead to mortality rates over 40 % (Fleischmann et al. 2016). Additionally, there is evidence that liver dysfunction during sepsis is associated with a poor prognosis of patients (Brun-Buisson et al. 2004, Abraham et al. 2005).

Sepsis-associated liver dysfunction leads to metabolic and functional adaptation of the liver cells as a consequence of various factors modulating the immune response. Bacterial clearance and hepatic immune surveillance are mainly regulated at the endothelium of the liver sinusoid (Brunt et al. 2014). The complex interaction of immunological, physiological and molecular mechanisms however is still not fully understood and needs to be further elucidated.

1.2.2 Hepatocellular dysregulation during inflammation

Liver dysfunction is driven by an exuberant immune reaction associated with a loss of synthesis and clearance capacity of hepatocytes due to cholestasis, cholangitis, fibrosis or ischemia (Strnad et al. 2017). Basic clinical indicators for liver damage with functional impairment are increased serum concentrations of hepatic transaminases (Bakker et al. 2004) and bilirubin (Singer et al. 2016). Further, hepatic dysfunction is closely related to signaling of hepatocytes and NPCs, because LSECs as well as the tissue-resident KCs are in the first line of defense encountering pathogens. Additionally, increased expression of vascular cell adhesion molecule-1 (VCAM-1), intercellular adhesion molecule-1 (ICAM-1) and E-selectin leads to active recruitment of circulating immune cells during inflammation (Wu et al. 2001).

LSECs clear macromolecular waste and scavenge circulating antigens from the blood (Smedsrød 2004, Schurich et al. 2009), whereas KCs engulf cellular debris and microorganisms like *S. aureus* or *E. coli.* (Falasca et al. 1996, Ono et al. 2006). These functions are realized partly via pathogen recognition receptors located on the surface of NPCs as well as parenchymal cells (Szabo et al. 2006). As an example, toll-like receptors (TLRs) are involved in the recognition of pathogen-associated molecular patterns (PAMPs) and the initiation of signaling cascades that trigger specific inflammatory reactions depending on the individual receptor involved (Ospelt and Gay 2010). LPS is a well characterized activator of TLR-4 and requires complexation with the LPS-binding protein, the receptor cluster of differentiation (CD) 14 and MD-2 (Lu et al. 2008). Stimulation of TLR-4 activates the transcription factors NFκB and interferon (IFN) regulatory factor 3 leading to the release of different IFNs and other pro-inflammatory cytokines (Takeuchi and Akira 2010). The release of interleukin (IL)-1β, tumor necrosis factor (TNF), IFN-γ or IL-6 by immune cells (i.e. macrophages, monocytes, natural killer cells) in turn triggers the production of various acute phase proteins in hepatocytes (Tacke et al. 2009). The mentioned chemokines possess pleiotropic functions and are centrally involved in the regulation of immunological processes within the liver (Shah et al. 2006).

In the course of inflammation, the metabolic activity of hepatocytes is severely deregulated. *In vitro,* LPS stimulation of hepatocytes altered albumin synthesis (Wang et al. 2004) and decreased mRNA levels as well as related activity of several CYP-enzymes (Aitken and Morgan 2007, Rubin et al. 2015). Moreover, bile canaliculi-associated transporter multi drug resistance protein-2 (MRP-2) protein expression in human liver slices is reduced after 24 h of LPS treatment (Elferink et al. 2004). These observations support the assumption that liver inflammation involves a complex cascade of immunomodulatory signaling molecules driven by NPCs ultimately affecting the function of hepatocytes.

1.2.2.1 Macrophage polarization and regulation

KCs account for 80-90 % of all tissue macrophages of the human body (Ishibashi et al. 2009), which highlights their importance in balancing the immunological homeostasis of the liver. This is supported by the fact that macrophage depletion in mice led to reduced hepatic fibrogenesis after LPS challenge (Seki et al. 2007) and insufficient resolution of fibrosis during healing (Duffield et al. 2005). KCs form a heterogeneous population depending on their origin and physiological state of the

hepatic microenvironment (Tacke and Zimmermann 2014). Furthermore, polarization of tissue-resident macrophages in the liver guides their function and molecular signaling (Figure 2). The classical activated M1-phenotype is involved in inflammation by secretion of pro-inflammatory cytokines, such as TNF and IL-1β, as well as inducible nitric oxide synthase (Sica et al. 2014). In contrast, M2 macrophages mediate the resolution of liver inflammation, i.e. through efficient phagocytosis of cell debris and the secretion of transforming growth factor-β as well as IL-10 (Wynn and Barron 2010, Krenkel and Tacke 2017).

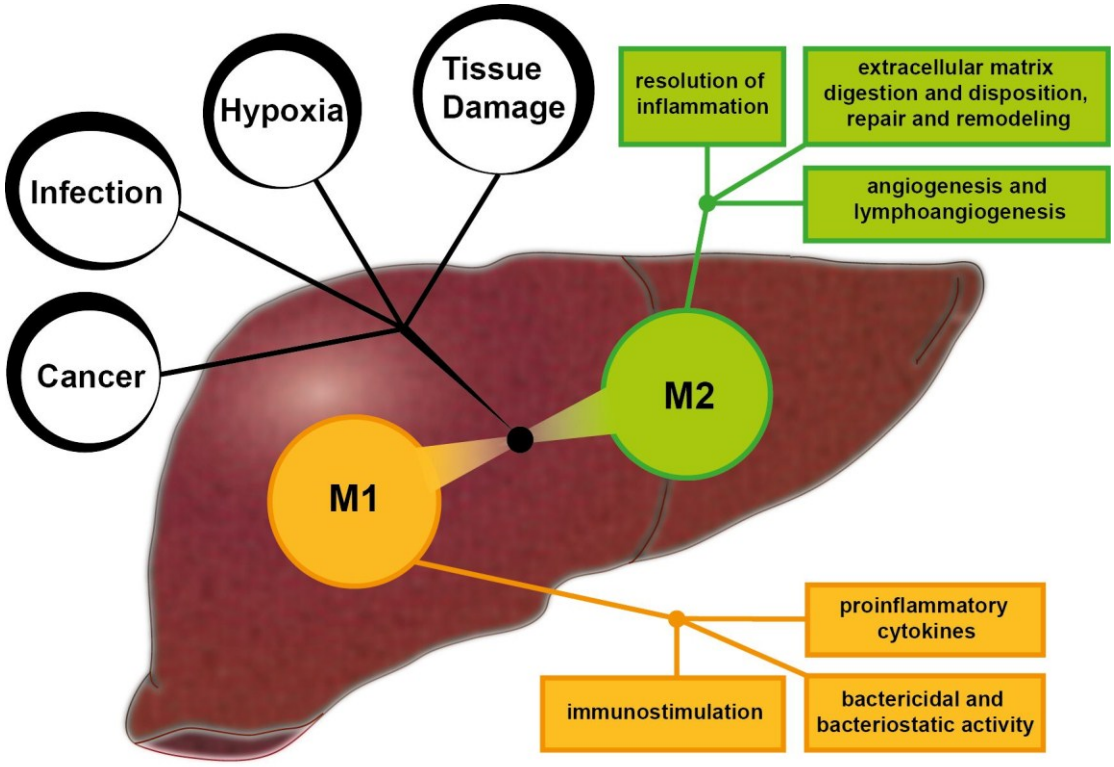

Figure 2. *Schematic overview of macrophage functions depending on their polarization state in the liver (M1/M2). Figure modified from Sica et al. (2014).*

Macrophage polarization states are well regulated and far from being strictly distinguishable. Intermediary conditions were defined by Mantovani and colleagues who classified M2 macrophages into different subtypes dependent on the inducer and related functional response (Mantovani et al. 2004). The difficulty of macrophage distinction was further highlighted by Barros et al. (2013) who examined the expression of CD68 and CD163 in respect to M1 and M2 polarization. They concluded that different activation states co-exist in their disease model, which supports the assumption of at least partially overlapping activation patterns (Barros et

al. 2013). Another critical regulator of inflammatory signaling is the possible transition of tissue-resident macrophages during inflammation. In this regard, IL-10 is considered to be an important regulator of macrophage metabolism accompanied with inhibition of their inflammatory response (Ip et al. 2017). In contrast, recent results indicate that a direct polarization change might not be possible, as INFγ-induced M1 macrophages failed to shift to the M2 phenotype after IL-4 treatment (van den Bossche et al. 2016). In the same study they rather suggested a replacement of macrophages by circulating monocytes instead of tissue macrophage repolarization.

1.2.3 Models of sepsis and sepsis-related liver dysfunction

Due to the complexity of hepatic inflammation, understanding of cellular and molecular regulators is still a challenge in translational medicine. Human *in vitro* models of the liver largely differ in their ability to mimic the hepatic microphysiology. Thus, Dejager and colleagues propagated the murine cecal puncture and ligation model as the gold standard for sepsis research, due to the similarities in regard to the human pathophysiology (Dejager et al. 2011). Mimicking systemic inflammation in an animal organism however possesses important drawbacks, such as interindividual gene changes in response to i.e. burn, trauma or endotoxemia, which are differentially regulated compared to men (Seok et al. 2013). Furthermore, there is evidence that mice have a higher resistance to PAMPs, i.e. LPS, than humans (Fink 2014). To overcome species-related differences, transgenic mice should serve as a host for the engraftment of myeloid cells (Rathinam et al. 2011, Willinger et al. 2011) or HSCs (Brehm et al. 2012) to “humanize” the observed immunological response. But this genetic modification leads to certain disorders accompanied by inadequate cytokine signaling (Rongvaux et al. 2013).

Humanization of mice is quite ambitious and ethically questionable. Therefore, human liver-on-a-chip models are a promising alternative for emulation of host defense and biotransformation during hepatic inflammation. These microphysiological systems generate complex 3D tissue structures with related functional improvements, critical for the response to PAMPs. This was proven by the sinusoidal *in vitro* model of Bale et al. (2016) who observed an adapted release of IL-10 and TNF after LPS stimulation depending on the presence of hepatocytes and NPCs. Their results showed the advantage over *in vivo* models, where individual contribution of cell types to the inflammatory response can hardly be distinguished (Bale et al. 2016).

Microfluidically supported cell culture further creates opportunities to integrate specific, circulating leucocyte subtypes as immunomodulatory elements. In this regard ICAM-1 and CXCL10 were identified as important mediators of T-cell recruitment to LSEC monolayers during viral infection (Bruns et al. 2015). Du et al. (2017) proved that neutrophil attraction to the hepatic endothelium is increased in a multi-cellular liver-on-a-chip compared to LSECs alone. Further, they suggested a direct correlation of complexity and microphysiology, which could be critical to investigate the course of inflammation *in vitro* (Du et al. 2017). In contrast, liver-on-a-chip applications are still limited by the use of murine cells (Kang et al. 2015, Prodanov et al. 2016), lack of important cell types (Toh et al. 2009, Kang et al. 2017) or non-physiological cellular arrangement (Vernetti et al. 2016). Thus, their utilization for studying hepatic inflammation close to the human physiology is still lacking and creates the need for new *in vitro* approaches to remedy existing drawbacks.

1.3 Hypothermal liver-on-a-chip preservation

Microphysiological liver-on-a-chip models constantly emerge in biomedical research. Assembly and microenvironmental control of those *in vitro* systems is still challenging and requires particular expertise as well as experience. To date, there is no available technique to preserve the structure and metabolic function of such models for distribution between different facilities. A possible solution for this problem could be the storage under hypothermal conditions, which is widely used to create a morphological and metabolic stasis of liver cells, tissues and different organs for medical or research purposes (Kozlova et al. 2003, Guibert et al. 2011, Pless et al. 2012). Especially in transplantation medicine hypothermal preservation is a requirement to prevent a rapid loss of viability and tissue damage (Guibert et al. 2011).

In the past, various storage solutions were used to maintain the liver function efficiently. Two of the most prominent solutions are the University of Wisconsin solution (UW) and histidine-tryptophan-ketoglutarate solution (HTK/Custodiol), which showed comparable post-transplant outcomes after cold storage (O'Callaghan et al. 2014). Both include specific ingredients to tackle cold-induced tissue alterations. HTK is characterized by its strong buffering capacity through histidine, low ion concentrations (Na^+, K^+ and Mg^{2+}) and minimal viscosity allowing rapid cooling as well as organ flushing. In contrast, UW has a higher viscosity and is supplemented

with adenosine as a precursor for adenosine triphosphate (ATP), antioxidants and osmotic regulators (lactobionate) to prevent cell swelling (Guibert et al. 2011). In this regard, these solutions have proven to be applicable for whole liver transplantation and were able to prevent cellular damage. In contrast to the medical use of organ preservation, which needs to be approved for surgery, cold storage of hepatic cells and small tissue samples for preclinical research can be individualized dependent on the utilization.

Human hepatocytes were stored efficiently in the HTK derivative Custodiol-N over two weeks. This chloride-rich solution, supplemented with the iron chelator deferoxamine, had advantages in metabolic recovery of the cells compared to the UW (Pless et al. 2012). Further, Custodiol-N was able to increase viability of ECs after cold storage compared to HTK (Wille et al. 2008). In contrast to UW and HTK, it is characterized by a lower buffer capacity and a higher amount of ions, which supports the idea of individualization dependent on the size and complexity of the preserved material. Novel approaches in liver tissue engineering enabled the implementation of parenchymal cells and NPCs that require advanced storage protocols. Hypothermal preservation represents a promising storage strategy for pre-assembled microphysiological systems and potentially offers a better accessibility to organ-on-chip technology by a larger field of researchers.

1.3.1 Cellular alterations during cold storage

Ultimately, hypothermal preservation results into a loss of cell viability over time. This could be explained by the fact that cold storage does not fully stop the cellular metabolism. Thus, the reduced metabolic activity of cells still leads to continuous accumulation of several meta- and catabolites even under cold conditions. In the 1990's it was believed that cell death during hypothermal preservation is a result of the ATP shortage that causes Na^+/K^+-ATPase blocking and finally cellular edema (swelling) through excessive Cl^- influx (Blankensteijn and Terpstra 1991). However, this mechanism was controversial, because of the cell-type specific variations dependent on the chloride concentration (Rauen et al. 2007a, Wille et al. 2008). Other studies showed that iron-dependent formation of reactive oxygen species (ROS) represents a main mediator of cold-induced apoptosis and cell damage, involving i.e. chromatin condensation, DNA fragmentation and a loss of plasma membrane integrity of ECs and hepatocytes (Rauen et al. 1999, Rauen et al. 2000). Thereby, cellular alterations are related to the redox-active, chelatable, intracellular

iron pool, which is increased shortly after hypothermal storage (Rauen et al. 2000), causing mitochondrial permeability transition (Rauen et al. 2004). Furthermore, cold-induced cell death triggers the release of damage-associated molecular patterns (DAMPs) leading to the unfavorable activation of different immune cells, commonly observed during ischemia and reperfusion of liver grafts (Le Moine et al. 2000, Tomiyama et al. 2008, Kimura et al. 2016). This causes damage to hepatocytes and ECs through various humoral factors (Abu-Amara et al. 2010). In summary, three important mediators affect cellular injury during cold storage: iron-dependent apoptosis, impaired intracellular ion homeostasis and cell death-related activation of immune cells (Figure 3).

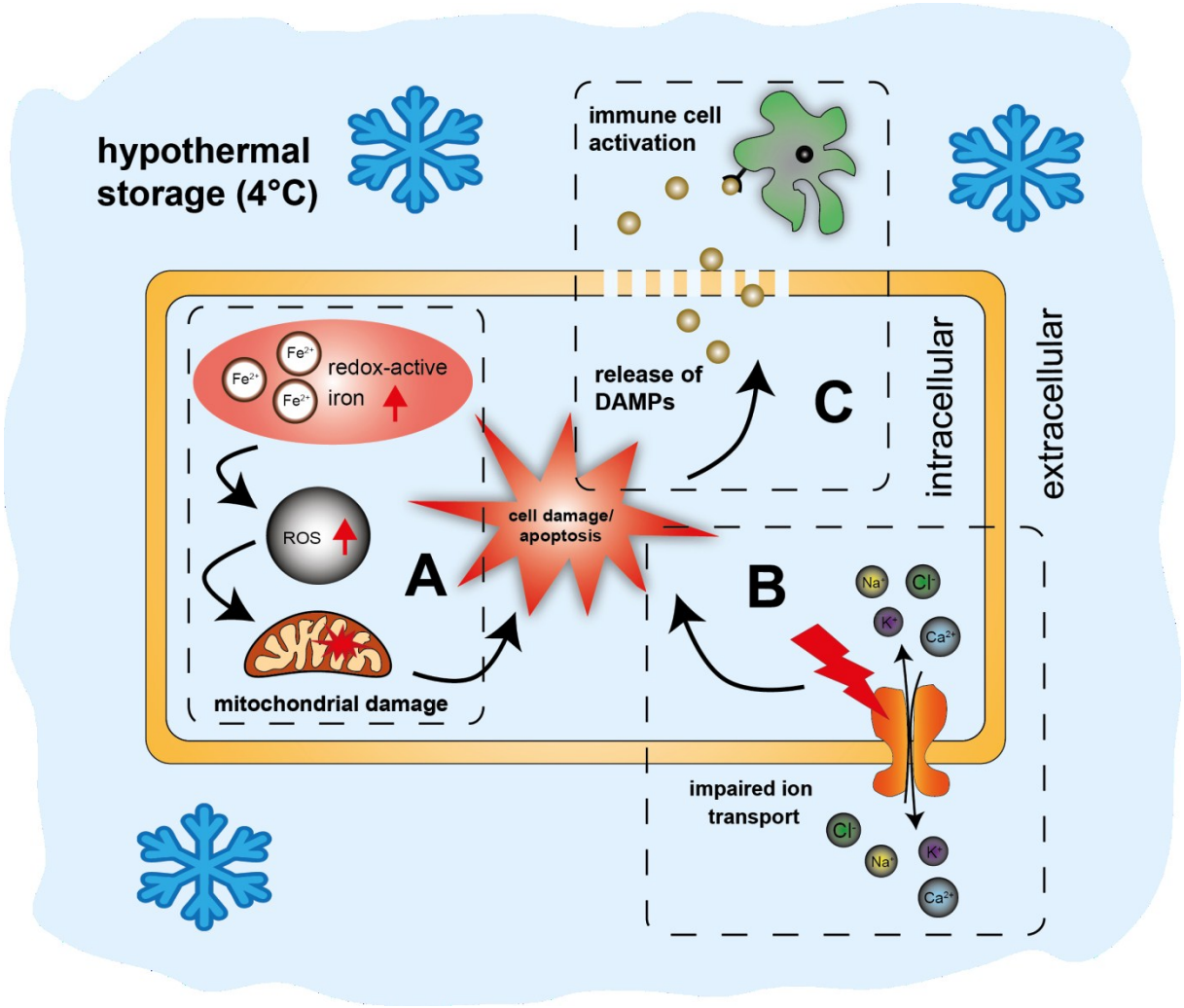

Figure 3. *Important factors of cellular damage during cold storage: A) Mitochondrial damage through ROS formation due to increased intracellular redox-active iron; B) Disturbed ion transport affecting intracellular homeostasis; C) DAMP release and immune cell activation.*

1.3.2 Protective effect of storage solution components on liver cells

In order to prevent cold-induced alterations, specific supplementation of storage solutions is necessary for an optimized protection. As mentioned earlier, iron-dependent cell damage is a main trigger of cold-induced apoptosis (Rauen et al. 2000). It was observed that membrane permeable iron chelators, such as deferoxamine and LK614, markedly increased viability of ECs after storage at 4 °C and contributed to an improved mitochondrial membrane potential (Wille et al. 2008, Zatschler et al. 2009). Their protective effect was also proven for primary human hepatocytes, which displayed significantly reduced lactate dehydrogenase (LDH) release after seven days of hypothermal storage (Pless et al. 2012). Furthermore, injury of whole rat livers was diminished by deferoxamine, demonstrating the applicability of these components for complex tissue preservation (Arthur et al. 2013).
In contrast to the clear benefit of iron chelators on cell viability, adaptation of the ion concentrations needs to be evaluated carefully. High chloride concentrations were shown to be advantageous for cold-preservation of ECs (Wille et al. 2008) and human hepatocytes (Pless et al. 2012). Surprisingly, LDH release was decreased in murine hepatocytes stored in solutions with reduced chloride (Rauen et al. 2007b). This species-related effect is not fully understood and might be the result from a complex alteration of different ion-dependent transporters during hypothermal storage. However, there is evidence that a stable intracellular ion homeostasis is beneficial for hypothermal storage of cells and tissues (Kozlova et al. 2003).
Despite the mentioned additives and adjustments, novel strategies emerge for further improvement of cold storage. Recently, polyethylene glycol (PEG; 35 kDA) supplementation of UW was found protective against lipid peroxidation in hepatocytes, making it a promising additional component (Puts et al. 2015). Furthermore, adjustment of pH to a mild acidosis (Nishimura et al. 1998) and substitution of toxic buffer components such as histidine (Rauen et al. 2007b) improved the applicability of hypothermal storage solutions. To support the preservation of the vascular endothelium, the composition of Custodiol-N was optimized (commercially available as TiProtec®). This solution was successfully utilized for storage of human blood vessels (Garbe et al. 2011) as well as murine hepatocytes (Pless-Petig et al. 2012).

2 AIM OF THESIS

The main objective of this thesis was the establishment of a microphysiological liver-on-a-chip to study inflammation-related dysfunction as a new tool and alternative to conventional cell culture methods. Most hepatic *in vitro* models lack the physiological complexity thereby affecting their outcome, usefulness and benefit in biomedical research (LeCluyse et al. 2012). Therefore, the versatile organ-on-a-chip technology is a promising tool to mimic the microenvironment of the human liver with complex cellular interaction, thereby creating benefits for the investigation of pathophysiological conditions (Ingber 2016). Furthermore, monocytes will be perfused and investigated due to the critical involvement of leucocytes in immunological signaling during hepatic inflammation (Oo et al. 2010). Liver-on-a-chip assembly is associated with complex and challenging culture protocols, which are important for a beneficial utilization of this technology. Cold storage is already used to preserve the function of liver cells and tissues (Hart et al. 2005, Ostrowska et al. 2009). Thus, this method might be suitable to maintain microphysiological models and enhance their applicability.

Specific objectives of the thesis were:

- Establishment of a human liver model including ECs, tissue-resident macrophages, stellate cells and hepatocytes in a microfluidically perfused biochip **(manuscript I)**
- Morphological and functional characterization of the biochip-embedded liver tissue **(manuscript I)**
- Integration of oxygen sensors for monitoring of metabolic activity of liver-on-a-chip models **(manuscript I)**
- Establishment of a disease model of inflammation-associated hepatocellular dysfunction **(manuscript II)**
- Integration of circulating monocytes **(manuscript II)**
- Development of novel hypothermal storage solutions and protocols for liver-on-a-chip models (**manuscript III)**

3 MANUSCRIPTS

Manuscript I

Rennert K, Steinborn S, Gröger M, Ungerböck B, Jank AM, Ehgartner J, Nietzsche S, Dinger J, Kiehntopf M, Funke H, Peters FT, Lupp A, Gärtner C, Mayr T, Bauer M, Huber O, Mosig AS. 2015. A microfluidically perfused three dimensional human liver model. **Biomaterials**, 71:119-131.

Manuscript II

Gröger M, Rennert K, Giszas B, Weiß E, Dinger J, Funke H, Kiehntopf M, Peters FT, Lupp A, Bauer M, Claus RA, Huber O, Mosig AS. 2016. Monocyte-induced recovery of inflammation-associated hepatocellular dysfunction in a biochip-based human liver model. **Scientific Reports**, 6:21868.

Manuscript III

Gröger M, Dinger J, Kiehntopf M, Peter FT, Rauen U, Mosig AS. 2018. Preservation of cell structure, metabolism and biotransformation activity of liver-on-chip organ models by hypothermic storage. **Advanced Healthcare Materials**, 7(2).

3.1 Manuscript I

A microfluidically perfused three dimensional human liver model

---

Rennert K, Steinborn S, Gröger M, Ungerböck B, Jank AM, Ehgartner J, Nietzsche S, Dinger J, Kiehntopf M, Funke H, Peters FT, Lupp A, Gärtner C, Mayr T, Bauer M, Huber O, Mosig AS

Published in:
Biomaterials, 2015, 71:119-131.

Here we described the establishment of a biochip-based sinusoid model of the human liver. Based on a porous membrane, mimicking the space of Disse, we implemented vascular endothelial cells (HUVECs) and primary human, monocyte-derived macrophages in co-culture with a separate layer containing stellate cells (LX-2) and hepatocytes (HepaRG). Vascular perfusion and integration of non-parenchymal cells improved hepatocyte polarization comparable to primary human tissue. Morphological features of the artificial liver tissue were analyzed by immunostaining of the central hepatic markers CYP3A4, MRP-2 and transferrin. Within the multilayered, three-dimensional liver model, hepatocytes displayed improved MRP-2 transporter activity, a higher density of microvilli at the cell surface and enhanced drug metabolization compared to static liver-on-a-chip culture. Furthermore, measurement of oxygen saturation in the media by luminescence-emitting sensor spots was used to evaluate the metabolic activity of cells in our model. In conclusion, the microphysiological model of the human liver holds the potential as a novel and valuable tool for *in vitro* studies under physiological conditions.

Biomaterials 71 (2015) 119–131

Contents lists available at ScienceDirect

Biomaterials

journal homepage: www.elsevier.com/locate/biomaterials

A microfluidically perfused three dimensional human liver model

Knut Rennert [a, 1], Sandra Steinborn [a, 1], Marko Gröger [a, i], Birgit Ungerböck [b], Anne-Marie Jank [c], Josef Ehgartner [d], Sandor Nietzsche [e], Julia Dinger [f], Michael Kiehntopf [g], Harald Funke [c], Frank T. Peters [f], Amelie Lupp [h], Claudia Gärtner [b], Torsten Mayr [d], Michael Bauer [i, j], Otmar Huber [a, j], Alexander S. Mosig [a, j, *]

[a] Institute of Biochemistry II, Jena University Hospital, 07743 Jena, Germany
[b] Microfluidic ChipShop GmbH, Stockholmer Straße 20, 07747 Jena, Germany
[c] Molecular Hemostaseology, Jena University Hospital, Jena, 07743 Jena, Germany
[d] Institute of Analytical Chemistry and Food Chemistry, Graz University of Technology, Graz, Austria
[e] Center for Electron Microscopy, Jena University Hospital, 07743 Jena, Germany
[f] Institute of Forensic Medicine, University Hospital Jena, 07743 Jena, Germany
[g] Department of Clinical Chemistry and Laboratory Medicine, Jena University Hospital, 07743 Jena, Germany
[h] Department of Pharmacology and Toxicology, Jena University Hospital, 07747 Jena, Germany
[i] Clinic of Anesthesiology and Intensive Care, Jena University Hospital, 07747 Jena, Germany
[j] Center for Sepsis Control and Care, Jena University Hospital, 07747 Jena, Germany

ARTICLE INFO

Article history:
Received 10 July 2015
Received in revised form
17 August 2015
Accepted 19 August 2015
Available online 25 August 2015

Keywords:
Liver
Organoid
Microfluidic biochip
Dynamic cell culture
Oxygen

ABSTRACT

Within the liver, non-parenchymal cells (NPCs) are critically involved in the regulation of hepatocyte polarization and maintenance of metabolic function. We here report the establishment of a liver organoid that integrates NPCs in a vascular layer composed of endothelial cells and tissue macrophages and a hepatic layer comprising stellate cells co-cultured with hepatocytes. The three-dimensional liver organoid is embedded in a microfluidically perfused biochip that enables sufficient nutrition supply and resembles morphological aspects of the human liver sinusoid. It utilizes a suspended membrane as a cell substrate mimicking the space of Disse. Luminescence-based sensor spots were integrated into the chip to allow online measurement of cellular oxygen consumption. Application of microfluidic flow induces defined expression of ZO-1, transferrin, ASGPR-1 along with an increased expression of MRP-2 transporter protein within the liver organoids. Moreover, perfusion was accompanied by an increased hepatobiliary secretion of 5(6)-carboxy-2′,7′-dichlorofluorescein and an enhanced formation of hepatocyte microvilli. From this we conclude that the perfused liver organoid shares relevant morphological and functional characteristics with the human liver and represents a new *in vitro* research tool to study human hepatocellular physiology at the cellular level under conditions close to the physiological situation.

1. Introduction

The liver plays a central role in metabolism, biotransformation of endogenous and exogenous substrates, and detoxification of xenobiotica. Non-parenchymal cells (NPCs) are essential for the physiological function of the liver. NPCs including Kupffer cells, stellate cells and endothelial cells account for about 40% of total liver cells. *Ex vivo* it has been shown that the presence of NPCs is a requirement for hepatocyte function [1]. Kupffer cells are specialized tissue macrophages that represent 15% of total liver cells and almost 80–90% of all tissue macrophages in the body [2]. Macrophages are key regulators of inflammatory response during infection and the major source of inflammatory cytokines such as interleukin (IL)-6 driving acute phase protein production in hepatocytes [3,4]. However, macrophages as well as hepatic stellate cells (HSCs) also mediate tissue regeneration in response to drug-induced liver damage [5], regulate the complex balance of inflammation and tissue regeneration [6,7], and facilitate cell–cell

* Corresponding author. Institute of Biochemistry II, Jena University Hospital, Nonnenplan 2-4 07743 Jena, Germany.
E-mail address: alexander.mosig@med.uni-jena.de (A.S. Mosig).
[1] These authors contributed equally to this publication.

http://dx.doi.org/10.1016/j.biomaterials.2015.08.043
0142-9612/

communication between hepatocytes and endothelial cells (ECs) [8]. HSCs and ECs represent 6% and 19% of total liver cells, respectively [9]. ECs do not simply form a barrier to restrict access of blood-borne compounds to the parenchyma, but also mediate clearance of i.e. endotoxins and bacteria, and regulate migration of leukocytes into the liver. The integrity of the liver microvasculature is thus fundamental for maintaining liver perfusion and cell viability [10].

In vitro monolayer cultures of hepatocytes are well-established in research but are accompanied by a reduction of major hepatic functions such as secretion of plasma proteins or detoxification due to down-regulation of several phase-I, -II and phase-III enzymes [11–13]. Co-culture approaches with NPCs have been shown to prevent hepatocyte dedifferentiation. Hepatocytes show improved urea production and a stable up-regulation of CYP1B1, CYP2C9, CYP2E1, and CYP3A4 during long-term co-culture with ECs [14–16]. Similarly, co-culture of hepatocytes and HSCs was reported to increase albumin secretion and CYP2B1/2 expression [17]. In addition to simple co-culture, three-dimensional liver tissue culture involving NPCs in contact with hepatocytes is required for improved maintenance of hepatocyte function [18,19]. In two-dimensional hepatocyte cultures a loss of hepatocyte cell polarization is frequently observed and associated with a diminished expression of distinct transporter proteins at the sinusoidal, basolateral and canalicular membranes [20].

So far, no *in vitro* model of the human liver is available that integrates ECs, macrophages and HSCs in co-culture with hepatocytes and also mimics the specific three-dimensional morphology of the human liver sinusoid, including the endothelial cell layer. While cells in the body are embedded and oriented in a complex three-dimensional network, *in vitro* tissue models need optimized perfusion strategies for a continuous supply of oxygen and nutrients. In addition, the removal of waste products is critical for culture of complex three-dimensional tissues with a high cellular density as diffusion of endogenous catabolites within tissues is impeded in static conditions. We recently introduced the Multi-Organ-Tissue-Flow (MOTiF) biochip design that features a suspended and freely perfusable membrane acting as a cell culture substrate [21]. Here, we report the establishment of a three-dimensional liver organoid embedded in microfluidically-supported biochips, which is structurally inspired by the morphology of the liver. HepaRG cells were used for the assembly of the liver organoids since preparation of primary liver cells is time- and cost-consuming. Moreover, availability of primary liver tissue specimens is often limited to donors suffering from pre-existing liver disorders and receiving extended medication. This likely affects liver cell function and contributes to experimental bias. To overcome these limitations, we used freshly isolated human umbilical vein endothelial cells (HUVEC) instead of liver sinusoidal endothelial cells (LSEC), since LSEC rapidly tend to de-differentiate *in vitro*, which is associated with a loss of fenestrae and re-organization of the cytoskeleton [22]. This de-differentiation process is difficult to monitor or control, and potentially adds an additional bias in day-to-day experimentation. Monocyte-derived macrophages were used to mimic Kupffer cell function and the immortalized human stellate cell line LX-2 as primary stellate cell surrogate. Immortalized cell lines have the advantage of continuous growth, unlimited availability and their clonal origin usually guarantees a constant phenotype allowing reproducible experimentation [23,24]. During culture in the biochip HepaRG cells consistently differentiate into cells exhibiting a hepatocyte phenotype and into cells with biliary epithelial cell phenotype that self-organize into a hepatocyte layer with functional bile ducts between hepatocyte-like cells [25] essential for liver function [26].

2. Material & methods

2.1. Cell culture

HepaRG: HepaRG cells were obtained from Biopredic International (Rennes, France). They were seeded at a density of 2.7×10^4 cells/cm^2 and cultured in William's Medium E (Biochrom, Berlin, Germany) containing 10% (v/v) FCS (Life Technologies, Darmstadt, Germany), 5 μg/ml insulin (Sigma–Aldrich, Steinheim, Germany), 2 mM glutamine (GIBCO, Darmstadt, Germany), 50 mM hydrocortisone-hemisuccinate (Sigma-Aldrich) and 100 U/ml Penicillin/100 μg/ml Streptomycin mixture (Pen/Strep) (GIBCO). The cells were cultured in a humidified cell incubator at 5% CO_2 and 37 °C for 14 days before differentiation. Medium was renewed every 3–4 days. Cell differentiation was induced as described [27] and cells were used up to 4 weeks. Endothelial cells: Human umbilical cord vein endothelial cells (HUVECs) were isolated from human umbilical cord veins as described [28]. Donors were informed about the aim of the study and gave written consent. HUVEC cells were seeded at a density of 2.5×10^4 cells/cm^2 and cultured in Endothelial Cell Medium (ECM) (Promocell, Heidelberg, Germany) up to passage 4. LX-2 stellate cells (kindly provided by Scott L. Friedman, Division of Liver Diseases, Mount Sinai School of Medicine, New York City, NY, USA) were seeded at a density of 2.0×10^4 cells/cm^2 and cultured in Dulbecco's Minimum Essential Medium (DMEM) (Biochrom) supplemented with 10% (v/v) FCS, 1 mM sodium pyruvate (GIBCO) and Pen/Strep. Peripheral Blood Mononuclear Cells (PBMCs) were isolated by Ficoll density gradient centrifugation as described previously [29] and seeded at a density of 1.0×10^6 cells/cm^2 in X-VIVO 15 medium (Lonza, Cologne, Germany) supplemented with 10% (v/v) autologous human serum, 10 ng/ml human granulocyte macrophage colony-stimulating factor (GM-CSF) (PeproTech, Hamburg, Germany) and Pen/Strep. After 3 h incubation in a humidified cell incubator at 5% CO_2 and 37 °C the cells were washed twice with X-VIVO 15 medium. Adherent monocytes were cultivated for 24 h in X-VIVO 15 medium and seeded into the liver organoid.

2.2. Liver organoid assembly

Liver organoids were assembled by staggered seeding of vascular and hepatic cell layers. In each sterilized biochip 2.7×10^5 HUVEC's/cm^2 (in total 3.0×10^5 cells) and 0.9×10^5/cm^2 monocytes (in total 1×10^5 cells) were mixed and seeded on top of the membrane in the upper chamber. HUVEC/monocytes were co-cultured for at least 5 days with a daily medium exchange in endothelial cell culture medium (ECM) supplemented with 10 ng/ml epidermal growth factor, 90 μg/ml heparin, 2.8 μM hydrocortisone, endothelial cell growth supplement, 10 ng/ml GM-CSF to induce macrophage differentiation, 100 U/ml penicillin/100 μg/ml streptomycin and 10% (v/v) autologous human serum (Life Technologies, Karlsruhe, Germany). M-CSF was not supplemented to the medium as human serum contains sufficient amounts for the differentiation of the macrophages [30–33]. Subsequently, 2.7×10^5/cm^2 differentiated HepaRG (in total 3×10^5 cells) and 3.6×10^5/cm^2 LX-2 (in total 4×10^4 cells) were seeded on the membrane at the opposite side of HUVEC cells and cultured for 24 h in DMSO-free William's Medium E (Biochrom, Berlin, Germany) hepatocyte growth medium containing 50 μM hydrocortisone, 10% (v/v) FBS containing, 5 μg/ml insulin, 2 mM glutamine and 100 U/ml penicillin/100 μg/ml streptomycin prior to experimental use.

2.3. Biochips

MOTiF biochips were made from cyclic olefin copolymers (COC) – TOPAS® and obtained from microfluidic ChipShop GmbH (Jena,

Germany). Biochips were manufactured as described previously [21]. Briefly, chips were made by injection molding. A 12.2 μm thick PET membrane (TRAKETCH) with a pore diameter of 8 μm and a pore density of 1×10^5 pores/cm^2 (Sabeu, Radeberg, Germany) was integrated. Chips and channel structures were sealed on top and bottom side with an extruded 140 μm thick COC foil using a low-temperature proprietary bonding method. Gas permeable silicon tubing was used for perfusion allowing oxygen equilibration during experiments. Ramping structures to avoid step transitions between membrane edges and channel structures have been introduced into the chip bulk to prevent unfavorable flow conditions and trapping of stationary bubbles. Stirring the cell culture medium and equilibration under perfusion conditions overnight reduced bubble formation within the chip. Further, oxygen plasma treatment for hydrophilization of the whole chip surface was performed to reduce in-chip air bubble formation. Details on dimensions of biochip structures and applied flow rates with corresponding shear stress rates (calculated for cell culture media used) are given in Supplementary Table 1.

2.4. Oxygen sensors

Oxygen sensors were applied via spray coating at the inlet and outlet of each chamber, allowing online detection of oxygen consumption of cultivated cells. These sensors are based on dynamic quenching principle of luminescence by molecular oxygen and allow contactless measurements of oxygen via frame positioned polymer fibers. Read-out and data acquisition were accomplished by a commercially available oxygen meter (Firesting, Pyroscience, Aachen, Germany). Characterization of COC for oxygen rediffusion was performed in a hypoxia incubator. Briefly, after equilibrating the gas- and medium-filled chamber of a biochip overnight at 0.5% oxygen level, rediffusion of oxygen into the locked chip at normoxic conditions was recorded. Where indicated, experiments at normoxic conditions were performed in a standard cell culture incubator. Oxygen consumption of static cultured cells in a locked COC-biochip was recorded over a time period of at least 16 h. Treatment of cells with 20 μM staurosporine (Sigma-Aldrich, Germany) was introduced as an assay control to induce cell death in the cells, resulting in loss of oxygen consumption and later in oxygen rediffusion into the biochip. Dynamic cultivation of the HepaRG cells was performed using a syringe pump (neMESYS, cetoni GmbH, Korbuβen, Germany) at the indicated flow rates.

2.5. Immunofluorescence microscopy, CDF-DA assay and ADP/ATP assay

Cells were fixed for 10 min with 4% paraformaldehyde at room temperature (RT). Staining was done with antibodies against: CYP3A4 (Merck-Millipore, Schwalbach, Germany), CD68 and ASGPR1 (BD Biosciences/Pharmingen, Heidelberg, Germany), ZO-1 (Life Technologies/Molecular Probes, Karlsruhe, Germany), MRP-2 (Cell Signaling Technology, Frankfurt, Germany), GFAP and Transferrin (Dako, Hamburg, Germany), and secondary antibodies goat-anti-rabbit-AF488, goat-anti-mouse-AF555 (Life Technologies/Molecular Probes), goat-anti-mouse-Cy3 and goat anti-rabbit Cy5 (Dianova, Hamburg, Germany), and DAPI (Life Technologies). Samples were embedded into fluorescent mounting medium (Dako). Image analyses and quantification of mean fluorescence intensities were performed by random field analyses with ImageJ2 software. MRP-2 activity was analyzed by incubation of HepaRG cell layers in serum-free Williams E medium (GIBCO) containing 5 μM 5(6)-Carboxy-2′,7′-dichlorofluorescein diacetate (CDFDA) (Sigma-Aldrich) at 37 °C for 15 min. Imaging was performed on an Axio Observer Z1 fluorescence microscope with ApoTome.2 equipment (Carl Zeiss AG, Jena, Germany). Images were analyzed using ImageJ2 software (Fiji). For measurement of cellular ADP and ATP content of HepaRG and LX-2 cells they were cultured at the bottom sealing foil of the biochip. For ADP/ATP measurement, the foil with attached cells was carefully cut out and adhesive cells treated with Nucleotide Releasing Buffer (abcam Cambridge, UK). Cells of the vascular layer were cultured at the membrane as described. ADP/ATP content and ratio was analyzed with the ADP/ATP Ratio Assay Kit (abcam) according to manufacturers instructions.

2.6. Analysis of CYP3A4 metabolite formation

Liver organoids were cultured for 72 h in absence or presence of LPS, respectively. Medium was exchanged every 24 h. Subsequently, liver organoids were incubated for 6 h with serum-free hepatocyte culture medium containing Midazolam (Rotexmedica, Trittau, Germany), provided as an aqueous solution at 13.8 mM (5 mg/ml) and diluted to a final concentration of 3 μM. After protein precipitation and concentration, samples were analyzed using an LC-MS/MS system consisting of an ABSciex QTrap 4000 tandem mass spectrometer (Darmstadt, Germany) equipped with a Turbo V ion spray source and coupled to an LC-20 liquid chromatography system (Shimadzu, Jena, Germany). Separation was performed on a ZORBAX Eclipse XDBC18 column (4.6 × 150 mm, 5 μm) from Agilent (Böblingen, Germany) using a gradient program with 50 mM ammonium formiate buffer plus 0.75% (v/v) formic acid (eluent A) and acetonitrile (eluent B). The mass spectrometer was operated in scheduled multiple reaction monitoring (MRM) mode using the target transition *m/z* 342 to 324 for quantification of 1-OH-midazolam. Instrument control, data acquisition, and data evaluation were performed using Analyst software 1.6.2 (ABSciex, Darmstadt, Germany).

2.7. Scanning electron microscopy

Cells were fixed with 2.5% (v/v) glutaraldehyde in cacodylate buffer for 120 min. Afterwards the samples were washed thrice with cacodylate buffer for 10 min and dehydrated in ascending ethanol concentrations (30, 50, 70, 90 and 100%) for 10 min each. Subsequently, the samples were critical-point dried using liquid CO_2 and sputter coated with gold (thickness approx. 4 nm) using a SCD005 sputter coater (BAL-TEC, Liechtenstein) to avoid surface charging. Finally the specimens were investigated with a field emission (FE) SEM LEO-1530 Gemini (Carl Zeiss NTS GmbH, Oberkochen, Germany).

Lactate, Glucose, Albumin, Urea, ASAT, ALAT, GLDH and LDH measurements.

The respective parameters were measured in cell culture supernatants using the Abbott Architect ci8200 Integrated System (Abbott Laboratories, Abbott Park, IL, USA) according to the manufacturer's protocol.

2.8. Statistics

All results are reported as average of the performed experiments with standard deviation. Where indicated, statistics were done with two-tailed, non-paired Student's t-test or One-way ANOVA with Tukey's multiple comparison test. Statistical analysis was performed using GraphPad Prism 6.07 software (Graphpad Software, La Jolla, CA, USA).

3. Results

A human liver sinusoid is formed by the sinusoidal wall composed of endothelial cells interspersed with immune-

modulatory monocyte-derived macrophages. This vascular layer is separated from the underlying hepatic tissue of hepatocytes and stellate cells by the space of Disse (Fig. 1). We adapted this morphological structure in our human liver model by assembling a vascular and a hepatic cell layer grown on the opposite sides of a suspended micro-porous membrane. The membrane serves as a substrate for both cell layers thereby separating them from each other and concomitantly mimicking the space of Disse (Fig. 1).

The vascular cell layer is composed of HUVECs which are co-cultured with differentiated primary monocyte-derived macrophages at the apical side of the suspended membrane. On the opposite side of the membrane, the hepatic cell layer is formed by differentiated HepaRG hepatocyte-like cells, which are co-cultured with LX-2 stellate cells. This setting facilitates stabilization of the multilayered three-dimensional tissue and allows intercellular cross-communication of co-cultured cell layers through the 12 μm thick membrane containing pores of 8 μm diameter (Fig. 2A). As shown in Fig. 2 B and C, artificial tissue sheets in the biochip showed structural similarities to primary precision cut liver tissue slices with a similar density and distribution of macrophages and stellate cells, respectively. Primary stellate cells in liver slices were stained for glial fibrillary acidic protein (GFAP), a well-established marker protein for non-activated stellate cells [34].

Prolonged culture of human primary hepatocytes is associated with a significant loss of expression of phase-I cytochrome P450 enzymes [35,36]. Therefore, we tested whether co-culture with endothelial cells in the biochip improves growth and morphology of HepaRG and CYP expression. Under these conditions CYP3A4 expression was clearly increased in HepaRG cells. Furthermore, no adverse effects on CYP3A4 expression levels by co-culturing macrophages or stellate cells in this setup were observed (Fig. 2D, E).

Oxygen saturation of the cell culture medium is a critical parameter for the regulation of the metabolic capacity of hepatocytes. To perform contactless, real-time in-chip measurements of oxygen levels during cell culture luminescence-based sensor spots were integrated into the biochips at the inlets and outlets of both perfusion channels [37] (Fig. 3 A, B). To individually characterize oxygen uptake of cell layers, we measured the time-dependent decline of oxygen saturation in the upper vascular (via sensor spots 1 and 2; Fig. 3 A, B) as wells as the HepaRG compartment (via sensor spots 3 and 4; Fig. 3 A, B) during static cell culture. A significant decline of oxygen saturation within approximately 16 h down to 47% of the maximal oxygen saturation within the culture medium (max. O_2 sat.) was observed in the vascular compartment containing HUVEC cell layers, and a nearly complete oxygen depletion down to 4% max. O_2 sat. in the HepaRG compartment. A similar oxygen decline was observed after replacing of the medium by fresh, air equilibrated cell culture medium. After more than 37 h of static culture we found a comparable kinetic of oxygen consumption in the culture medium indicating that cell layers within the biochip are unaffected, still viable and metabolic active (Fig. 3C, D). To verify that the decline of oxygen levels within the biochip depends on the metabolic activity of cultured cells, apoptosis was induced by treatment with staurosporine [38] (Fig. 3C, D). After a short initial phase of oxygen depletion, the oxygen consumption subsequently decreased in response to death of the embedded cells and passive oxygen re-diffusion through the chip bulk material. The oxygen resupply by diffusion throughout the biochip bulk material was slightly slower than diffusion rates observed in control experiments without cultured cells (Supplementary Figure 1), indicating some remaining cell viability after staurosporine treatment.

Next, we wanted to determine the impact of different perfusion rates on oxygen consumption by HepaRG cells, calculated as the difference between oxygen saturation at the inlet and outlet of the chamber (Δ oxygen saturation). For the first 200 min the co-culture was perfused with 1 μl/min at both cell layers. A significant drop of oxygen levels at the inlet of the perfusion channel, which however was significantly lower than under static culture conditions was detectable. This indicates that oxygen consumption through HepaRG cells is faster than oxygen re-supply through media perfusion at 1 μl/min (Fig. 3 E). Increasing the perfusion rate up to 3 μl/min resulted in a stable oxygen level at the inlet of the HepaRG cell chamber of around 95% max. O_2 saturation. Analysis of the difference in oxygen saturation at the inlet and outlet of the channel system allowed to estimate the metabolic activity of the HepaRG cell layer. Interestingly, HepaRG oxygen consumption was elevated in response to increased perfusion rate (Fig. 3 F).

Moreover, we addressed the impact of medium perfusion under normoxic and hypoxic conditions on cellular energy levels by measurement of intracellular ATP and ADP contents of HepaRG cells. ATP levels were found significantly decreased under hypoxic conditions in static as well as perfused cultures of the liver organoids (Fig. 4 A). Intracellular ADP levels seemed unaffected by medium perfusion under normoxic conditions, but slightly declined in the dynamic culture of organoids under hypoxic conditions. In order to determine the cell fate, intracellular ADP/ATP ratio was calculated (Fig. 4 B). A low ADP/ATP ratio based on the high ATP and low ADP levels was assumed to correlate with a

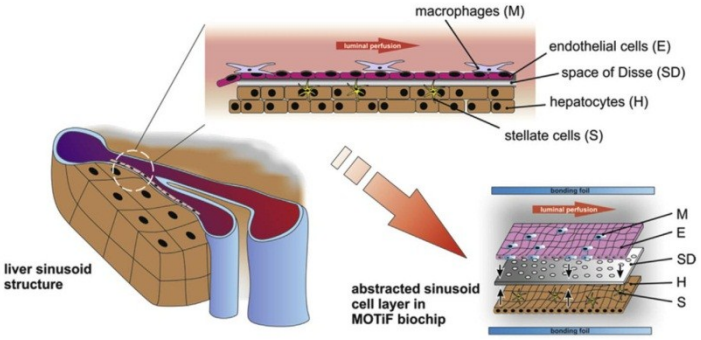

Fig. 1. Adaption of the *in vivo* morphology of the human liver sinusoid in a multi-layered liver organoid. The three-dimensional liver organoid consists of a vascular layer formed by endothelial cells (E) and primary macrophages (M), and a hepatic layer comprising hepatocyte-like HepaRG cells (H) co-cultured with stellate cells (S). The space of Disse (SD) is mimicked by the biochip-embedded membrane serving as a scaffold allowing cell–cell communication through its pores.

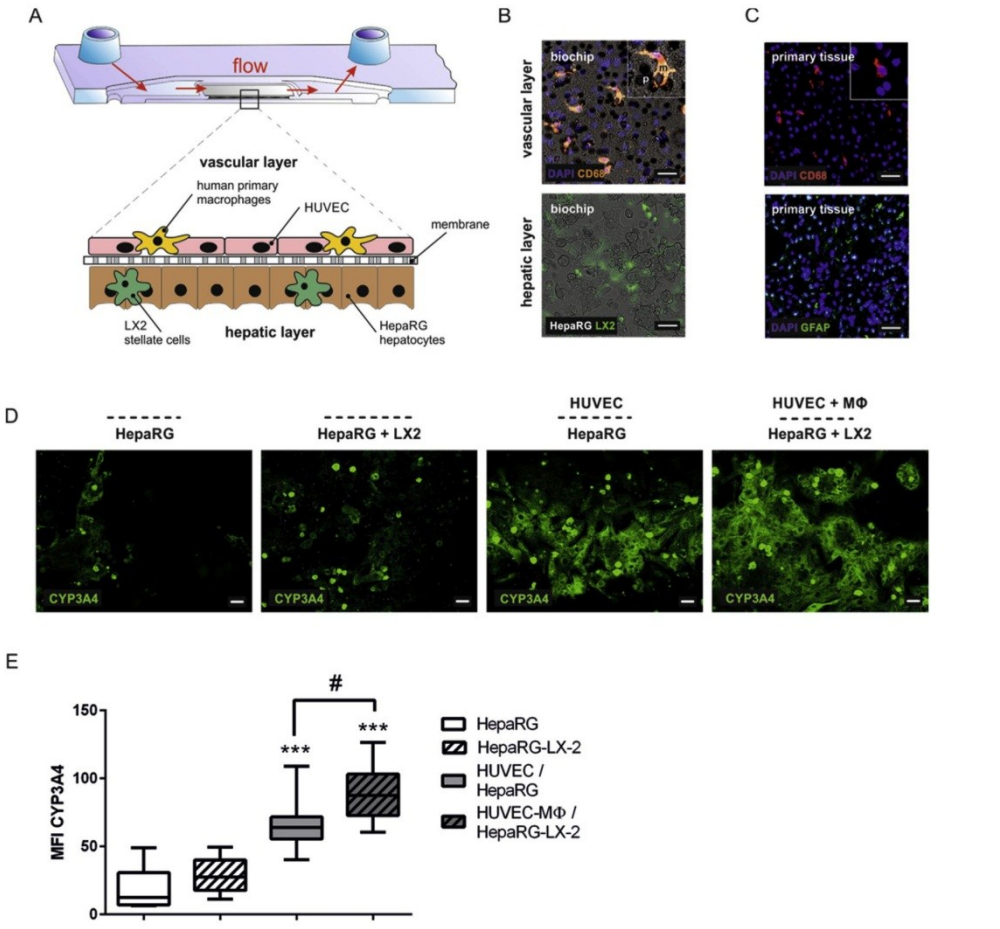

Fig. 2. Establishment of a three-dimensional liver model in a microfluidic biochip. A) Cross-section of the biochip-embedded liver model. B) Immunostaining of macrophages (CD68, orange) and nuclei (DAPI, blue) of cells of the vascular layer. Bright field microscopic image of the HepaRG layer. For visualization purposes LX-2 stellate cells were labeled with CellTracker Green CMFDA dye immediately before seeding the cells. Liver organoids were cultured for 4 days. C) Immunostaining of macrophages (CD68, red) and primary stellate cells (GFAP, green) in primary liver tissue. B–C) scale bar 50 μm; D) Effect of NPC co-culture on CYP3A4 protein expression (green) in HepaRG cells. The black bar above the microscopic image represents the chip membrane and localization of individual cell types relative to the membrane is noted. Scale bar 50 μm. E) Quantification of CYP3A4 mean fluorescence intensity (MFI) in regions of interest (ROI) of three independent experiments. Significance was calculated using One-Way-ANOVA with Tukey's multiple comparison test (***$p < 0.01$ vs. HepaRG mono-culture, #$p < 0.05$ between indicated conditions). D-E) Liver organoids were cultured for 4 days. (For interpretation of the references to color in this figure legend, the reader is referred to the web version of this article.)

proliferative state of cells cultured under normoxic conditions, irrespective of medium perfusion. Under hypoxic conditions however, the ADP/ATP ratio was significantly increased under static but not dynamic conditions. As the cellular ATP content in static, hypoxic culture was also lower than the ADP level, this is indicative for cell death under these conditions. In dynamic, hypoxic cultures, ATP levels were found increased relative to ADP levels resulting in a low ADP/ATP ratio pointing to a growth arrest (Supplementary Table 2).

An appropriate polarization of hepatocytes is a prerequisite for the formation of functionally active hepatic bile canaliculi and represents an important characteristic of the HepaRG cell line. To address this point, the expression and localization of various hepatic differentiation and polarization marker proteins including the differentiation marker proteins asialoglycoprotein receptor-1 (ASGPR-1), zonula occludens-1 (ZO-1) and multidrug resistance-associated protein-2 (MRP-2) was analyzed. ASGPR-1 is a transmembrane protein that is specifically expressed in the liver at the sinusoidal and basolateral hepatocellular membranes, but not on the bile canalicular (also called apical) membrane [39–41]. ZO-1, which is located at the tight junctions (TJs) marks the margins of the bile canaliculi [42], and the multidrug resistance-associated protein-2 (MRP-2), a major hepatic transporter protein, defines the apical membrane of polarized hepatocytes [43]. Normal ASGPR-

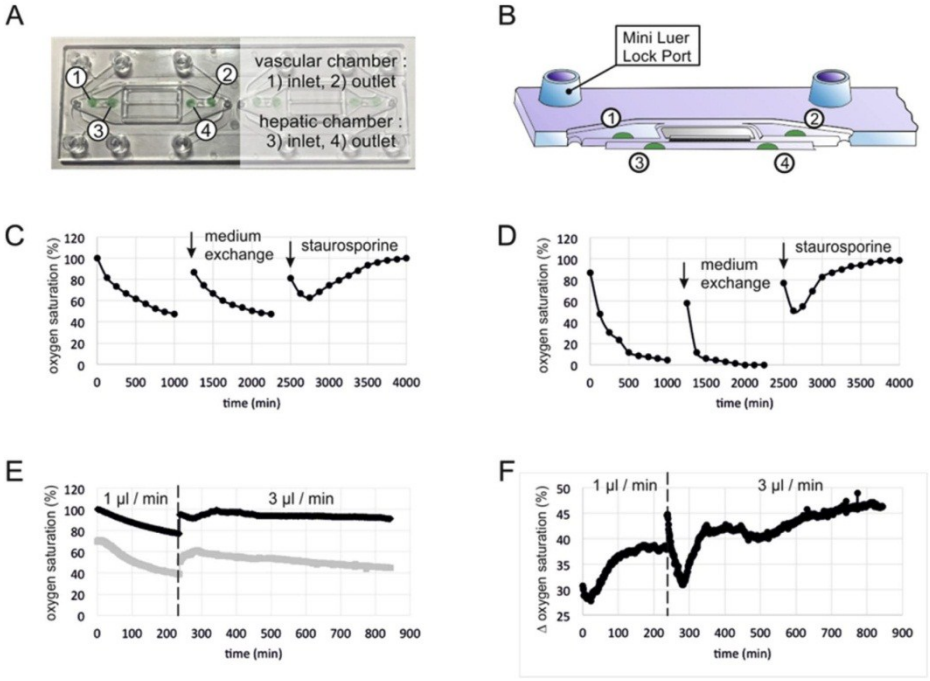

Fig. 3. Measurement of oxygen saturation in cell culture medium by fluorescence emitting sensor spots. A) Integration of oxygen sensor spots in the microfluidically supported biochip. Sensor spots were integrated at the inlets (1, 3) and the outlets (2, 4) of the upper and lower channel systems, respectively. B) Schematic cross-section of the biochip with integrated oxygen sensor spots. C, D) Oxygen saturation of the medium measured at the outlets of the upper vascular compartment containing HUVECs (C), and the lower compartment containing hepatocyte-like HepaRG cells (D). Both cell layers were co-cultured within the MOTiF biochips. The time point of medium exchange with fresh, air-equilibrated medium and exchange for fresh, air-equilibrated medium containing 20 µM staurosporine are indicated by arrows above the graph lines. E) Measurement of oxygen consumption of HepaRG cell layer co-cultured with an HUVEC cell layer at the membrane under microfluidic flow. Oxygen saturation was measured at the inlet (black line) and the outlet (gray line) of the HepaRG biochip compartment. F) Calculated oxygen consumption of perfused HepaRG cell layers calculated from the difference between oxygen saturation at the inlet and outlet of HepaRG biochip compartment. E–F) Oxygen saturation was initially measured at a cell perfusion rate of 1 µl/min and was subsequently increased to 3 µl/min (right to the dashed line). C–F) Oxygen saturation measurements were performed with cell layers pre-cultured for 24 h within the biochip.

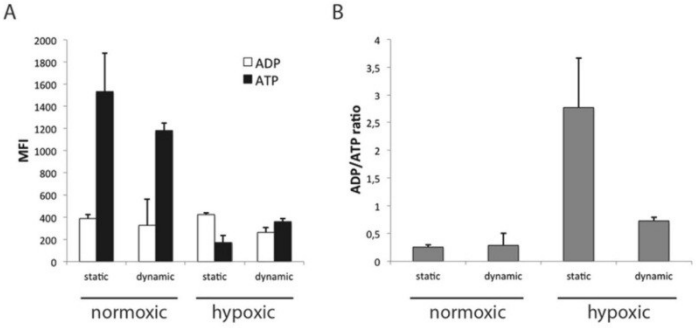

Fig. 4. Cellular ADP and ATP content of HepaRG cell layers co-cultured with HUVEC cell layer on the opposite sides of the membrane within MOTiF biochips for 4 days under static and dynamic culture conditions. A) Cellular ADP (open bars) and ATP (black bars) levels in cells cultured under normal oxygen levels (21% O_2) and under hypoxic conditions (5% O_2) for 72 h. B) ADP/ATP ratios measured with luciferase assays. Mean fluorescence intensity (MFI) represents cellular ATP and ADP content.

1 expression and distribution was observed within HepaRG monocultures. However, the compact co-culture of stellate cells, endothelial cells or/and macrophages under static conditions resulted in a loss of defined ASGPR-1 protein expression and a delocalization of the protein from the basolateral membrane (Fig. 5 A). Also ZO-1 was diminished and delocalized in HepaRG when co-cultured with NPCs under static conditions (Fig. 5 B). MRP-2 expression was found highly expressed in monolayer cultures of HepaRG, and its expression pattern was lost in static co-cultures of HepaRG and NPCs (Fig. 5 C). In agreement with this finding the activity of MRP-2, as assayed by release of the fluorescent dye 5-(and 6)-carboxy-2′,7′-dichlorofluorescein (CDF) into bile canaliculi-like structures of HepaRG [44] was decreased. In consequence, the CDF dye was trapped within the cytoplasm of HepaRG cells resulting in unfocused staining (Fig. 5 D).

In the human liver a shear stress at the sinusoidal endothelium of 10–50 mPa has been reported [45]. However, the direct shear stresses experienced by hepatocytes is difficult to estimate as the effects of flow are dampened by the separation of hepatocytes from sinusoidal blood by liver sinusoidal ECs and the space of Disse [10]. It even appears that hepatocytes are sensitive to the application of shear stress and that only extremely low shear stress is tolerated [46]. We observed increased oxygen consumption of HepaRG cells in response to elevated cell perfusion with increased shear forces that might induce cellular stress. To avoid this stress effect and to prevent potential cell damage the liver organoids were perfused in

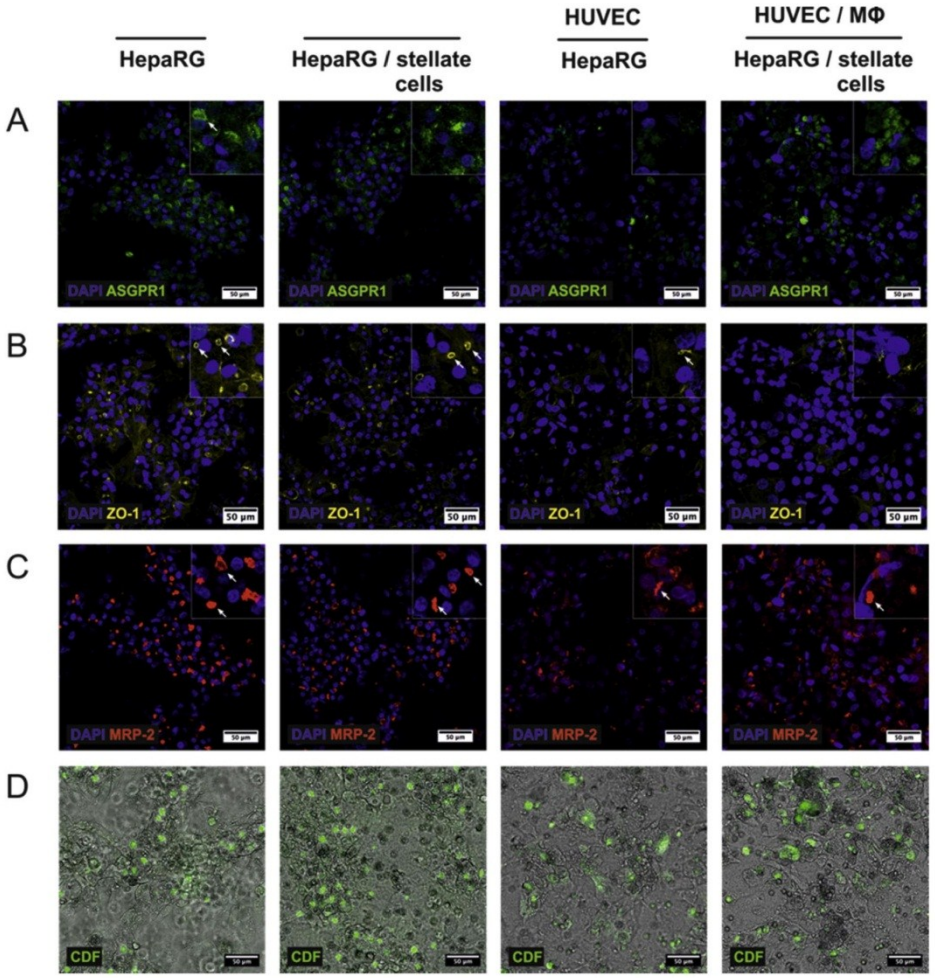

Fig. 5. Immunostaining of specific markers in the HepaRG cell layer during step-wise assembly of the liver organoids. A) ASGPR-1 (green), B) ZO-1 (yellow), C) MRP-2 (red). A-C) Cell nuclei (DAPI, blue). D) Assessment of MRP-2 activity in HepaRG cells by measurement of CDF-release (green) into bile canaliculi-like structures. Scale bar 20 μm. The line above the images represents the chip-embedded membrane and indicates localization of each individual cell type relative to the membrane. A-D) Cell layers were cultured for 4 days within biochips. (For interpretation of the references to color in this figure legend, the reader is referred to the web version of this article.)

a more physiological way only at the vascular side ("vascular perfusion") resembling the *in vivo* situation with a shear stress rate of 50 mPa·(0.5 dyn/cm^2), which equals a perfusion rate of 50 μl/min in the MOTiF biochip. Vascular perfusion for 96 h resulted in the formation of a highly confluent EC layer with an increased expression of VE-cadherin at endothelial cell–cell contacts revealing similarities with the VE-cadherin expression pattern observed in primary human precision cut liver slices (Fig. 6 A). Thus dynamic perfusion significantly improves the polarization of ECs in the vascular layer of the liver organoids.

In static co-cultures of HepaRG and LX-2 cell clusters are surrounded by cells with a biliary epithelial phenotype. In contrast, the vascular perfusion induced the formation of a confluent homogenous HepaRG cell layer without cluster formation (Fig. 6 B). Moreover, the HepaRG cell layers in perfused liver organoids displayed an increased and stable expression of CYP3A4 (Fig. 6 B, 7 A) that was associated with elevated metabolization of midazolam as detected by the formation of its metabolite 1-hydroxy-midazolam (1-OH-midazolam) after 6 h incubation. In addition, perfused organoids exhibited a defined and stable pattern of ASGPR-1 expression that highly correlated with the morphology and expression pattern observed in primary human liver tissue (Fig. 6 C). Compared to static cultures, transferrin expression was also markedly increased in perfused liver organoids with expression levels close to the levels detectable in primary liver tissue slices (Fig. 6 D). Furthermore, perfused liver organoids revealed a ZO-1 staining along elongated structures correlating with an enhanced formation of bile canaliculi-like structures between HepaRG cells (Fig. 6 E). MRP-2 expression (Fig. 6 F) and function was also significantly increased in perfused liver organoids as detected by CDF excretion assays displaying a focused release of CDF into self-organized bile canaliculi-like structures not observable under static conditions (Fig. 7 C).

MRP-2 is located along the microvilli of hepatocytes [47]. When perfused liver organoids were compared with static tissue culture by scanning electron microscopy. HepaRG cells exhibited an increased plasticity with a higher density of microvilli compared to static tissue culture that showed a flattened cell structure with significantly reduced numbers of microvilli (Fig. 8 A). This finding correlated well with the defined expression pattern of ZO-1 and MRP-2 (Fig. 6 B) and the enhanced CDF secretion in perfused liver organoids (Fig. 7 A). In addition to the enhanced MRP-2 secretory capacity, perfused liver organoids also exhibited significantly enhanced synthesis of albumin and urea, compared to statically cultured liver organoids or conventional monolayer cultures of hepatocytes (Fig. 8 B–C).

Next we addressed the cellular oxygen consumption in the whole liver organoid during vascular perfusion. In contrast to static culture, where a fast drop of oxygen saturation was observed, vascular perfusion with 50 μl/min was sufficient for stable oxygen supply to the vascular cell layer of the liver organoid (Fig. 8 D). Similarly, in the HepaRG compartment of the lower biochip chamber a rapid oxygen consumption was detectable under static cell culture conditions. However, in contrast to the vascular cell layer a medium perfusion only temporally increased oxygen saturation at the chamber inlet that declined within 8 h to a virtually complete oxygen exhaustion within the HepaRG chamber (Fig. 8 E). In this context we were interested whether the adaption of HepaRG cells to hypoxia is reversible. Therefore, we measured oxygen consumption of HepaRG cells as surrogate of their metabolic activity under static conditions as well as direct perfusion conditions. After complete oxygen exhaustion within the HepaRG compartment we initiated perfusion of the HepaRG layer by a stepwise increase in perfusion rates. At a perfusion rate of 1 μl/min, oxygen levels still declined with time at the channel inlet, and dissolved oxygen was entirely consumed during media flow through the organoid. Applying a perfusion rate of 3 μl/min, oxygen supply at the channel inlet was constant. However, after an initial increase, oxygen levels at the chamber outlet still declined over time (Fig. 8 F). An increase of the flow rate up to 10 μl/min resulted in stable oxygen levels at the inlet and outlet of the chamber. Highest difference of oxygen saturation at the inlet and outlet of the chamber was measured at a perfusion rate of 3 μl/min (Fig. 8 G).

Taken together, oxygen consumption correlated with increasing perfusion rates. During cell culture the air pressure was 760 mmHg and oxygen solubility in the cell culture medium was estimated k = 1.19 nmol/ml/mmHg [48,49]. Under these conditions we calculate mean oxygen saturation difference as $\Delta_{\text{saturation}}$

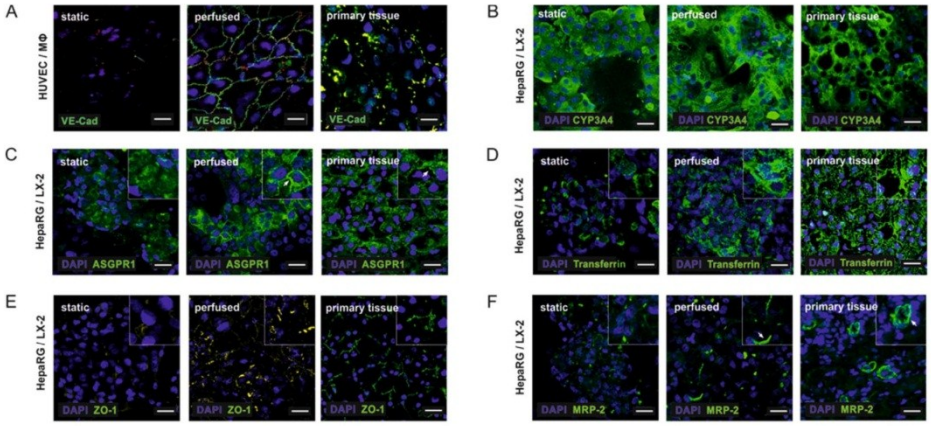

Fig. 6. Immunostaining of liver organoids cultured under static and perfused conditions. Perfused liver organoid share morphological similarities with primary human precision cut liver tissue (primary tissue). A) VE-cadherin (green) expression and localization within the vascular layer of the organoid. Cell nuclei (DAPI, blue) (scale bar 20 μm). B–F) Immune staining of B) CYP3A4 (green), C) ASGPR-1 (green), D) transferrin (green), E) ZO-1 (yellow) and F) MRP-2 (green). B–F) Cell nuclei (DAPI, blue). Scale bar 50 μm. A-F) Liver organoids were cultured for 4 days under indicated conditions. (For interpretation of the references to color in this figure legend, the reader is referred to the web version of this article.)

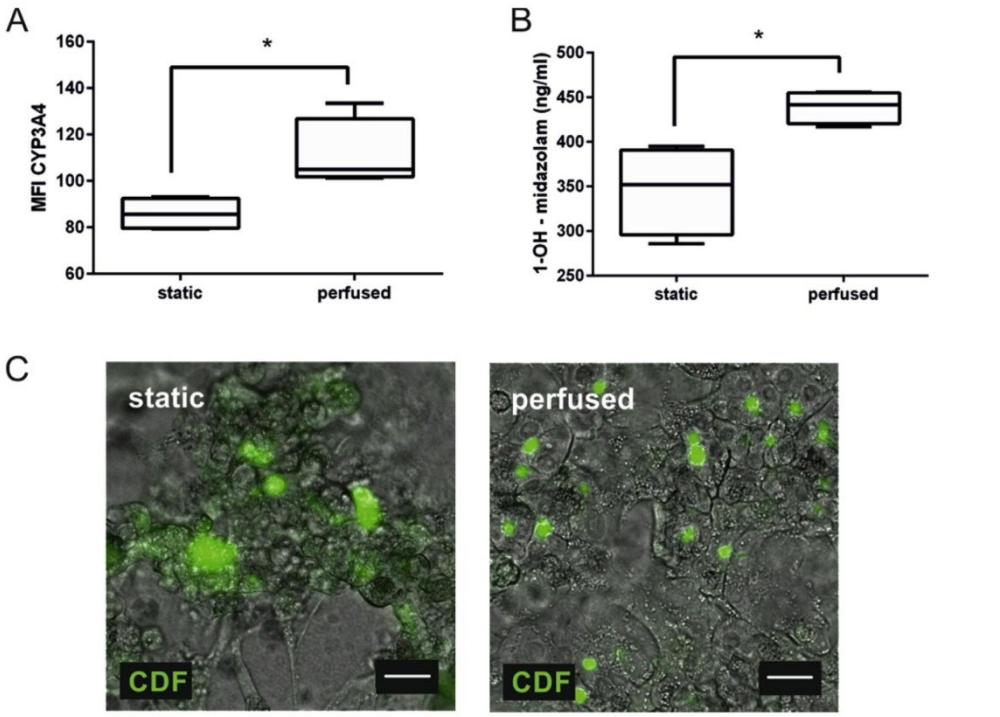

Fig. 7. Comparison of metabolic activities in the liver organoid under static and dynamic culture conditions. A) Analysis of CYP3A4 expression by immunofluorescence image analysis. B) Formation of the metabolite 1-OH-midazolam by CYP3A4 A-B) Significance was calculated using Student's t-test (*$p < 0.05$) C) Assessment of MRP-2 activity in hepatocytes of organoids cultured under static or perfused conditions by measurement of CDF-release (green) into bile canaliculi-like structures (scale bar 20 μm). A-C) Liver organoids were cultured for 4 days under static or perfused conditions. (For interpretation of the references to color in this figure legend, the reader is referred to the web version of this article.)

$_{\text{level}} = O_2\ sat\cdot_{\ inlet} - O_2\ sat\cdot_{\ outlet}$, where $O_2\ sat.$ is the mean oxygen saturation level measured at the inlet and outlet of the chamber, respectively. Oxygen consumption is then calculated $O_2\ con\cdot = (k{*}0,209{*}760\ mmHg){*}(O_2\ sat\cdot_{\ inlet} - O_2\ sat\cdot_{\ outlet}){*}flow\ rate$, where $O_2\ sat.$ is the mean oxygen saturation level measured at the inlet and outlet of the chamber, respectively. Our results indicate that increasing liver organoid perfusion rates correlate with elevated cellular oxygen consumption likely due to improved nutrient supply and associated higher metabolic activity under well-perfused culture conditions (Table 1).

4. Discussion

Most studies addressing liver physiology or organ dysfunction were performed using animal models of mice and rats. However, a controversial debate about the usefulness of rodent models and the transferability of the obtained data to human conditions was raised [50,51]. *In vitro* organoid models of the liver facilitate studies with human liver tissue and prevent potential bias due to interspecies differences and thus offer an attractive alternative to animal models. *In vitro* models can be used under reproducible and standardized conditions and are reasonably cost effective, whereas animal models need extensive service and maintenance to ensure i.e. sufficient environmental control for reliable experimentation [52,53].

In vitro hepatocyte monolayers are a frequently used tool. However, under static conditions in conventional cell culture dishes, unfavorable high media-to-cell volume ratios exist. Recently, it was shown that decreasing media-to-cell volume ratios resulted in the formation of higher concentrations of drug metabolites [54]. Cell culture of 3×10^5 HepaRG/LX-2 cells in MOTiF biochips requires only 120 μl of culture medium (0.4 nl/hepatocyte) making it a suitable tool for substance screening on a micro-scale basis with minimized wastage of test compounds. The low media-to-cell ratio in our biochip-based assays increases the resulting medium concentrations of metabolites and thereby facilitates application of assays to measure metabolites.

A close interaction between endothelial cells and hepatocytes is required to maintain normal morphology and sufficient CYP enzyme expression [16,55]. These stabilizing effects of ECs on the expression as well as the activity of CYP3A4 in HepaRG cells are mediated through the pores of the scaffold membrane in our biochip model. Layer-wise assembling strategies were also applied by other groups. When rat hepatocytes and bovine aortic endothelial cells were co-cultured on opposing sides of a transwell filter, hepatocytes remained differentiated and secreted urea [55]. Similar results were obtained in a model of stacked cell layers of rat hepatocytes and bovine carotid artery endothelial cells [56]. However, these models do not allow investigations under humanized

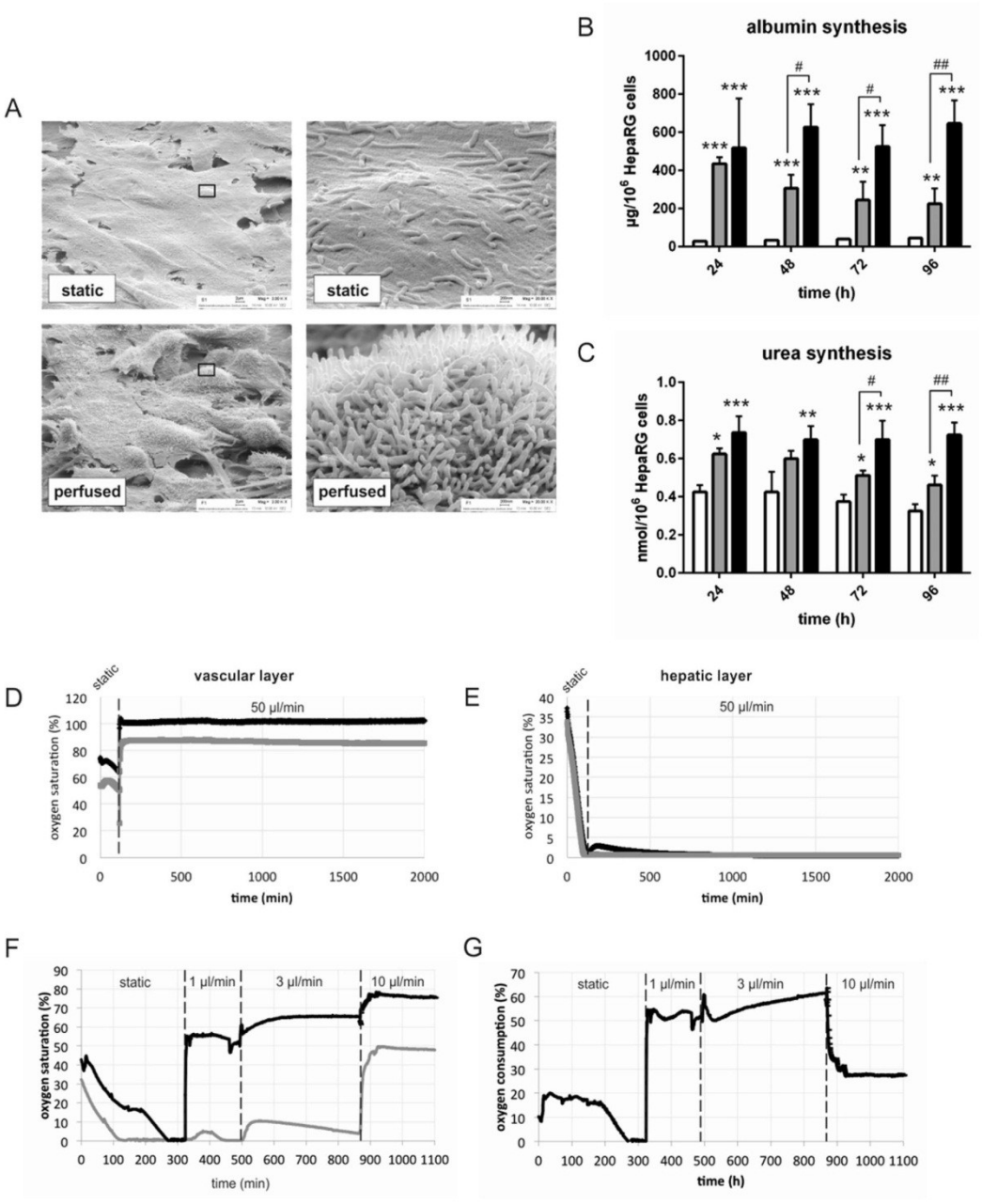

Fig. 8. Comparison of microstructure and oxygen consumption of liver organoids under static and dynamic culture conditions. A) Scanning electron microscopic images of HepaRG cells in the liver organoids cultured under static or perfused culture conditions. Rectangle in left side images marks magnified area of images shown at the right side. HepaRG cells under perfusion revealed higher cell plasticity with increased microvilli formation at the cell surface (scale bar 2 µm left side, 200 nm right side). Release of B) albumin and C) urea by monocultures of HepaRG cells under static conditions in a cell culture dish (open bars) and organoids cultured within MOTiF biochips under static (gray bars) and dynamic

Table 1
Oxygen consumption of liver organoids under flow conditions.

Perfusion rate	Mean $\Delta_{inlet/outlet}$ Saturation level (%)	Total O_2 consumption (nmol/min/10^6 cells)
1 μl/min	51.91	0.3271
3 μl/min	56.50	1.0680
10 μl/min	29.30	1.8461

conditions. Other studies have shown that extracellular matrix (ECM) proteins such as collagen, fibronectin and laminin produced by endothelial cells promote hepatocyte differentiation [56] and preserve hepatocyte morphology concomitant with a stable secretion of albumin and urea, and an elevated hepatocyte drug metabolizing ability [57,58]. Moreover, hepatocyte growth factor (HGF), which is produced by LSEC and also HUVEC, was reported to mediate long-term survival and polarization of hepatocytes in co-culture with HUVEC [56,59–61]. We suppose that similar effects contribute to HepaRG phenotype preservation in our liver model. Larkin et al. reported a more complex model of rat LSEC and Kupffer cells separated by a chitosan-hyaluronic acid polymer layer from collagen embedded primary rat hepatocytes. Under static culture conditions the hepatocytes maintained their phenotype without signs of dedifferentiation [62]. A biodegradable chitosan membrane was also used by Salerno et al. for co-culture of human primary hepatocytes with HUVEC, where beneficial effects of the co-culture on hepatocyte albumin production, urea synthesis and drug biotransformation again was reported [63]. All these observations underline the importance of NPCs on maintenance of hepatocellular function.

An important step forward to further optimize culture conditions in our liver organoid model was the application of microfluidic flow mimicking *in vivo* vascular perfusion. The more complex and highly packed cell layers formed on the membrane within the biochip apparently consume more oxygen and produce considerably more waste products in limited volumes of available cell culture medium. Thus, the perfusion of the multilayered organoids is advantageous for efficient supply with oxygen and removal of waste products, to stabilize the morphology, polarization and excretory function of HepaRG cells. Other perfused *in vitro* liver models have been previously reported. Toh et al. utilized micropillars mimicking fenestrated ECs that act as a shield to protect hepatocytes during perfusion with culture medium [64]. However, due to the absence of NPCs and the lack of essential cell–cell contacts or paracrine signals this model does not really reflect the physiological regulation of hepatocellular function and polarization. Cell–cell communication between ECs and hepatocytes under perfusion was established in a model published by Domansky et al., in which flow-mediated simulation of physiological shear stress conditions allowed to maintain viability and phenotype of hepatocytes up to 13 days [65]. Recently, Esch et al. reported the establishment of a three-dimensional model of the human liver, consisting of defined ratios of hepatocytes and non-parenchymal cells (fibroblasts, stellate cells, and Kupffer cells) [66]. Fluidic flow of medium was emulated by placing the chip on a rocking platform. In this simplified perfusion approach, an increase of albumin and urea synthesis of co-cultured hepatocytes was achieved. However, an organized *in vivo*-like morphology including an endothelial cell layer covering hepatocytes is missing.

A striking feature of the liver is the difference of metabolic activity of hepatocytes depending on oxygen gradient along the liver acinus [67]. *In-chip* oxygen measurement under flow conditions by luminescence emitting sensor spots not only represents a valuable tool for assessment of cellular activity of assembled liver organoids but can also be used as a surrogate of HepaRG metabolic activity. Our measurements indicate that in our biochip under vascular perfusion conditions an oxygen gradient mimicking *in vivo* conditions is formed as a consequence of enhanced oxygen consumption and prevention of free oxygen diffusion from the upper chamber throughout the organoid.

The oxygen gradient formed by vascular perfusion likely restricts uncontrolled cell growth, contributes to the maintenance of the cellular architecture of the organoid and is adaptable by simple adjustment of the perfusion rate. Hepatocytes quickly depolarize upon loss of cell–cell contacts in response to removal from native tissue complexes [68]. Repolarization during liver organoid formation is thus an important prerequisite for an effective excretory activity and the removal of xenobiotics and catabolites from the cells. The localization of ASGPR-1, ZO-1 and MRP-2 confirms functional polarization of hepatocytes necessary for bile secretion and barrier formation [69]. Perfusion of the liver organoid further increased metabolic activity as detectable by enhanced urea and albumin synthesis, which was also reported by other multi-cellular liver models [66,70,71]. Moreover, we assume that the oxygen gradient formed by unilateral perfusion of the vascular layer contributes to the observed hepatocyte polarization. Our microfluidic biochip-based liver organoid thus holds the potential to mimic liver acinus zonation, enabling the development of *in vitro* platforms to study liver zonation [72]. Follow-up studies will be performed to examine this in detail.

Our experiments showed that under microfluidic perfusion HepaRG cells are able to dynamically adapt to normoxic as well as hypoxic conditions as revealed by changes in cellular ADP/ATP ratios. However, in case of static culture with restricted oxygen and nutrition supply together with enrichments of catabolites cellular damage is induced. *In vivo* similar conditions are observed in response to ischemia, which is also associated with cellular damage and organ dysfunction.

In conclusion, we here demonstrated the establishment of a functional liver organoid comprising all major liver cell types. The liver model displays clear differentiation and structural reorganization and enables polarization closely resembling primary human liver tissue *in vitro*. It is functionally stable for at least four days after full assembly and with perfusion. Studies are underway to characterize viability under long-term culture. The compact biochip in the size of a standardized microscope slide further facilitates *on-chip* tissue observation with conventional bright field or fluorescence microscopy [21,73] or spectrometric methods such as near infrared spectroscopy [74] enabling real-time analysis under flow conditions. We are convinced that this liver model is a valuable tool to study liver physiology, metabolism and the underlying molecular processes at the cellular level. It paves the way for detailed *in vitro* studies on the role of particular NPCs on hepatocellular function under physiological and pathophysiological conditions, i.e. in

culture conditions (filled bars) for up to 96 h. Students t-Test: compared to corresponding HepaRG monocell culture: *p < 0.05; **p < 0.01; ***p < 0.001; compared to indicated condition #p < 0.05; ##p < 0.01; E–H) Measurement of oxygen consumption of liver organoids under static and microfluidic flow. Oxygen saturation was measured at the inlet (black line) and the outlet (gray line) of the vascular and HepaRG biochip compartment at indicated perfusion rates. D–E) Oxygen saturation in at the vascular layer (D) and HepaRG layer (E) of the organoid during unilateral vascular perfusion. F-G) Perfusion of the HepaRG cell layer. Oxygen saturation was initially measured at static conditions and subsequently with cell perfusion rates of 1, 3 and 10 μl/min. The vascular layer was simultaneously perfused with 50 μl/ml. F) Oxygen consumption of the liver organoid measured in the HepaRG compartment. G) Calculated oxygen consumption of perfused organoid from the difference between oxygen saturation at the inlet and outlet of HepaRG biochip compartment. A–G) Liver Organoids were cultured for 4 days within biochips.

toxicological or pharmacological screening. The principal utility of biochip-based assays has already been proven for simple endothelial and HepaRG cell cultures in assays aimed to characterize functionalized nanoparticles as new therapeutic treatment options of liver disease [75]. Furthermore, the modular assembly of the liver model described in this study is ideally suited to address the role of specific genes or proteins in the cell types of interest for liver function. Cells with a knock-out/down of the gene of interest or overexpressing a mutated variant thereof can be easily integrated into the liver organoid for subsequent functional analyses. The integration of the organoid into a versatile, microfluidically supported platform with standardized microscopical slide dimensions allows real-time in-chip analyses with established analytical microscopic and/or spectrometric methods and state-of-the-art biosensor applications.

Author contributions

KR, SS, JD, MG, BU, AML, SN performed the experiments. JE, MK, TM, AL, HF, FP contributed reagents/materials/analysis tools. KR, SS, BU, SN, MG, ASM analyzed the data. KR, MB, AL wrote parts of the manuscript. OH, ASM wrote the manuscript. KR and ASM planned experiments. ASM designed and supervised the study.

Acknowledgments

We are grateful to the excellent technical work of Christina Ness, Maria Franke and Margot Voigt. We thank the team of the Placenta Laboratory of the Jena University Hospital for supplying umbilical cords for HUVEC isolation. The authors would further like to acknowledge support of this work by 2011 VF 0005 grant of the Thüringer Aufbaubank (Germany) and by the FK 1328-511 grant from the Federal Agency on Risk Assessment (Germany). This work was further supported by the Federal Ministry of Education and Research (Germany), FKZ: 01EO1002.

Appendix A. Supplementary data

Supplementary data related to this article can be found at http://dx.doi.org/10.1016/j.biomaterials.2015.08.043.

References

[1] D.M. Bissell, D.M. Arenson, J.J. Maher, F.J. Roll, Support of cultured hepatocytes by a laminin-rich gel. Evidence for a functionally significant subendothelial matrix in normal rat liver, J. Clin. Investig. 79 (1987) 801–812.
[2] L. Bouwens, M. Baekeland, R. De Zanger, E. Wisse, Quantitation, tissue distribution and proliferation kinetics of Kupffer cells in normal rat liver, Hepatology 6 (1986) 718–722.
[3] E. Seki, S. De Minicis, C.H. Osterreicher, J. Kluwe, Y. Osawa, D.A. Brenner, et al., TLR4 enhances TGF-beta signaling and hepatic fibrosis, Nat. Med. 13 (2007) 1324–1332.
[4] T.R. Billiar, R.D. Curran, D.L. Williams, P.H. Kispert, Liver nonparenchymal cells are stimulated to provide interleukin 6 for induction of the hepatic acute-phase response in endotoxemia but not in remote localized inflammation, Archives Surg. 127 (1992) 31–36 (discussion 6–7).
[5] M.P. Holt, L. Cheng, C. Ju, Identification and characterization of infiltrating macrophages in acetaminophen-induced liver injury, J. Leukoc. Biol. 84 (2008) 1410–1421.
[6] I.N. Crispe, The liver as a lymphoid organ, Annu. Rev. Immunol. 27 (2009) 147–163.
[7] C. Kordes, I. Sawitza, D. Haussinger, Hepatic and pancreatic stellate cells in focus, Biol. Chem. 390 (2009) 1003–1012.
[8] J. Kasuya, R. Sudo, T. Mitaka, M. Ikeda, K. Tanishita, Hepatic stellate cell-mediated three-dimensional hepatocyte and endothelial cell triculture model, Tissue Eng. Part A 17 (2011) 361–370.
[9] Z. Kmiec, Cooperation of liver cells in health and disease, Adv. Anat. Embryol. Cell Biol. 161 (2001). III-XIII, 1–151.
[10] E.L. LeCluyse, R.P. Witek, M.E. Andersen, M.J. Powers, Organotypic liver culture models: meeting current challenges in toxicity testing, Crit. Rev. Toxicol. 42 (2012) 501–548.
[11] D.F. Clayton, A.L. Harrelson, J.E. Darnell Jr., Dependence of liver-specific transcription on tissue organization, Mol. Cell Biol. 5 (1985) 2623–2632.
[12] J.Z. Tong, P. De Lagausie, V. Furlan, T. Cresteil, O. Bernard, F. Alvarez, Long-term culture of adult rat hepatocyte spheroids, Exp. Cell Res. 200 (1992) 326–332.
[13] P. Godoy, N.J. Hewitt, U. Albrecht, M.E. Andersen, N. Ansari, S. Bhattacharya, et al., Recent advances in 2D and 3D in vitro systems using primary hepatocytes, alternative hepatocyte sources and non-parenchymal liver cells and their use in investigating mechanisms of hepatotoxicity, cell signaling and ADME, Arch. Toxicol. 87 (2013) 1315–1530.
[14] J. Schutte, B. Hagmeyer, F. Holzner, M. Kubon, S. Werner, C. Freudigmann, et al., Artificial micro organs"–a microfluidic device for dielectrophoretic assembly of liver sinusoids, Biomed. Microdevices 13 (2011) 493–501.
[15] M. Ohno, K. Motojima, T. Okano, A. Taniguchi, Induction of drug-metabolizing enzymes by phenobarbital in layered co-culture of a human liver cell line and endothelial cells, Biol. Pharm. Bull. 32 (2009) 813–817.
[16] M. Ohno, K. Motojima, T. Okano, A. Taniguchi, Up-regulation of drug-metabolizing enzyme genes in layered co-culture of a human liver cell line and endothelial cells, Tissue Eng. Part A 14 (2008) 1861–1869.
[17] S.F. Abu-Absi, J.R. Friend, L.K. Hansen, W.S. Hu, Structural polarity and functional bile canaliculi in rat hepatocyte spheroids, Exp. Cell Res. 274 (2002) 56–67.
[18] J. Landry, D. Bernier, C. Ouellet, R. Goyette, N. Marceau, Spheroidal aggregate culture of rat liver cells: histotypic reorganization, biomatrix deposition, and maintenance of functional activities, J. Cell Biol. 101 (1985) 914–923.
[19] F.J. Wu, J.R. Friend, R.P. Remmel, F.B. Cerra, W.S. Hu, Enhanced cytochrome P450 IA1 activity of self-assembled rat hepatocyte spheroids, Cell Transpl. 8 (1999) 233–246.
[20] F. Berthiaume, P.V. Moghe, M. Toner, M.L. Yarmush, Effect of extracellular matrix topology on cell structure, function, and physiological responsiveness: hepatocytes cultured in a sandwich configuration, FASEB J. 10 (1996) 1471–1484.
[21] M. Raasch, K. Rennert, T. Jahn, S. Peters, T. Henkel, O. Huber, et al., Microfluidically supported biochip design for culture of endothelial cell layers with improved perfusion conditions, Biofabrication 7 (2015) 015013.
[22] A.J. Ford, G. Jain, P. Rajagopalan, Designing a fibrotic microenvironment to investigate changes in human liver sinusoidal endothelial cell function, Acta Biomater. 24 (2015) 220–227.
[23] R. Weiskirchen, J. Weimer, S.K. Meurer, A. Kron, B. Seipel, I. Vater, et al., Genetic characteristics of the human hepatic stellate cell line LX-2, PloS One 8 (2013) e75692.
[24] J. Herrmann, A.M. Gressner, R. Weiskirchen, Immortal hepatic stellate cell lines: useful tools to study hepatic stellate cell biology and function? J. Cell Mol. Med. 11 (2007) 704–722.
[25] V. Cerec, D. Glaise, D. Garnier, S. Morosan, B. Turlin, B. Drenou, et al., Transdifferentiation of hepatocyte-like cells from the human hepatoma HepaRG cell line through bipotent progenitor, Hepatology 45 (2007) 957–967.
[26] D.H. Adams, S.C. Afford, The role of cholangiocytes in the development of chronic inflammatory liver disease, Front. Biosci. 7 (2002) e276–85.
[27] P. Gripon, S. Rumin, S. Urban, J. Le Seyec, D. Glaise, I. Cannie, et al., Infection of a human hepatoma cell line by hepatitis B virus, Proc. Natl. Acad. Sci. U.S.A. 99 (2002) 15655–15660.
[28] M. Wallert, S. Mosig, K. Rennert, H. Funke, M. Ristow, R.M. Pellegrino, et al., Long-chain metabolites of α-tocopherol occur in human serum and inhibit macrophage foam cell formation in vitro, Free Radic. Biol. Med. (2014) 43–51.
[29] S. Mosig, K. Rennert, S. Krause, J. Kzhyshkowska, K. Neunübel, R. Heller, et al., Different functions of monocyte subsets in familial hypercholesterolemia: potential function of CD14+ CD16+ monocytes in detoxification of oxidized LDL, FASEB J Fed. Am. Soc. Exp. Biol. (2009) 866–874.
[30] K. Yong, N. Salooja, R.E. Donahue, U. Hegde, D.C. Linch, Human macrophage colony-stimulating factor levels are elevated in pregnancy and in immune thrombocytopenia, Blood 80 (1992) 2897–2902.
[31] J. Cebon, J.E. Layton, D. Maher, G. Morstyn, Endogenous haemopoietic growth factors in neutropenia and infection, Br. J. Haematol. 86 (1994) 265–274.
[32] K.M. Irvine, M.R. Andrews, M.A. Fernandez-Rojo, K. Schroder, C.J. Burns, S. Su, et al., Colony-stimulating factor-1 (CSF-1) delivers a proatherogenic signal to human macrophages, J. Leukoc. Biol. 85 (2009) 278–288.
[33] M. Naito, G. Hasegawa, Y. Ebe, T. Yamamoto, Differentiation and function of Kupffer cells, Med. Electron Microsc. 37 (2004) 16–28.
[34] R. Liao, H. Wu, Y. Yi, J.X. Wang, X.Y. Cai, H.W. He, et al., Clinical significance and gene expression study of human hepatic stellate cells in HBV related-hepatocellular carcinoma, J. Exp. Clin. Cancer Res. 32 (2013) 22.
[35] V.Y. Soldatow, E.L. Lecluyse, L.G. Griffith, I. Rusyn, models for liver toxicity testing, Toxicol. Res. Camb. 2 (2013) 23–39.
[36] G. Luo, T. Guenthner, L.S. Gan, W.G. Humphreys, CYP3A4 induction by xenobiotics: biochemistry, experimental methods and impact on drug discovery and development, Curr. Drug Metab. 5 (2004) 483–505.
[37] C. Gärtner, B. Ungerbröck, I. Schulz, T. Jahn, A. Mosig, T. Mayr, et al., Sensor enhanced microfluidic devices for cell based assays and organs on chip, in: Proceedings SPIE, Smart Biomedical and Physiological Sensor Technology XII, 2015.
[38] M. Andersson, J. Sjostrand, A. Petersen, A.K. Honarvar, J.O. Karlsson, Caspase and proteasome activity during staurosporin-induced apoptosis in lens epithelial cells, Invest. Ophthalmol. Vis. Sci. 41 (2000) 2623–2632.
[39] T. Terada, M. Iwai, S. Kawakami, F. Yamashita, M. Hashida, Novel PEG-matrix

metalloproteinase-2 cleavable peptide-lipid containing galactosylated liposomes for hepatocellular carcinoma-selective targeting, J. Control Release 111 (2006) 333–342.
[40] D.A. Wall, A.L. Hubbard, Galactose-specific recognition system of mammalian liver: receptor distribution on the hepatocyte cell surface, J. Cell Biol. 90 (1981) 687–696.
[41] M. Spiess, The asialoglycoprotein receptor: a model for endocytic transport receptors, Biochemistry 29 (1990) 10009–10018.
[42] J.M. Anderson, J.L. Glade, B.R. Stevenson, J.L. Boyer, M.S. Mooseker, Hepatic immunohistochemical localization of the tight junction protein ZO-1 in rat models of cholestasis, Am. J. Pathol. 134 (1989) 1055–1062.
[43] G. Jedlitschky, U. Hoffmann, H.K. Kroemer, Structure and function of the MRP2 (ABCC2) protein and its role in drug disposition, Expert Opin. Drug Metab. Toxicol. 2 (2006) 351–366.
[44] M.J. Zamek-Gliszczynski, H. Xiong, N.J. Patel, R.Z. Turncliff, G.M. Pollack, K.L. Brouwer, Pharmacokinetics of 5 (and 6)-carboxy-2′,7′-dichlorofluorescein and its diacetate promoiety in the liver, J. Pharmacol. Exp. Ther. 304 (2003) 801–809.
[45] P.F. Lalor, D.H. Adams, Adhesion of lymphocytes to hepatic endothelium, Mol. Pathol. 52 (1999) 214–219.
[46] H. Miyoshi, T. Ehashi, H. Kawai, N. Ohshima, S. Suzuki, Three-dimensional perfusion cultures of mouse and pig fetal liver cells in a packed-bed reactor: effect of medium flow rate on cell numbers and hepatic functions, J. Biotechnol. 148 (2010) 226–232.
[47] P. Recknagel, F.A. Gonnert, M. Westermann, S. Lambeck, A. Lupp, A. Rudiger, et al., Liver dysfunction and phosphatidylinositol-3-kinase signalling in early sepsis: experimental studies in rodent models of peritonitis, PLoS Med. 9 (2012) e1001338.
[48] M.L. Yarmush, M. Toner, J.C. Dunn, A. Rotem, A. Hubel, R.G. Tompkins, Hepatic tissue engineering. Development of critical technologies, Ann. N. Y. Acad. Sci. 665 (1992) 238–252.
[49] Y. Nahmias, Y. Kramvis, L. Barbe, M. Casali, F. Berthiaume, M.L. Yarmush, A novel formulation of oxygen-carrying matrix enhances liver-specific function of cultured hepatocytes, FASEB J. 20 (2006) 2531–2533.
[50] H.S. Warren, R.G. Tompkins, L.L. Moldawer, J. Seok, W. Xu, M.N. Mindrinos, et al., Mice are not men, Proc. Natl. Acad. Sci. U.S.A. 112 (2015) E345.
[51] J. Seok, H.S. Warren, A.G. Cuenca, M.N. Mindrinos, H.V. Baker, W. Xu, et al., Genomic responses in mouse models poorly mimic human inflammatory diseases, Proc. Natl. Acad. Sci. U.S.A. Natl. Acad. Sci. (2013) 3507–3512.
[52] M.H. Tschop, J.R. Speakman, J.R. Arch, J. Auwerx, J.C. Bruning, L. Chan, et al., A guide to analysis of mouse energy metabolism, Nat. Methods 9 (2012) 57–63.
[53] J. Nedergaard, B. Cannon, The browning of white adipose tissue: some burning issues, Cell Metab. 20 (2014) 396–407.
[54] S.S. Bale, G.V. Sridharan, I. Golberg, L. Prodanov, W.J. McCarty, O.B. Usta, et al., A novel low-volume two-chamber microfabricated platform for evaluating drug metabolism and toxicity, Technology 0 (2015) 1–8.
[55] Y.B. Kang, S. Rawat, J. Cirillo, M. Bouchard, H.M. Noh, Layered long-term co-culture of hepatocytes and endothelial cells on a transwell membrane: toward engineering the liver sinusoid, Biofabrication 5 (2013) 045008.
[56] K. Kim, K. Ohashi, R. Utoh, K. Kano, T. Okano, Preserved liver-specific functions of hepatocytes in 3D co-culture witsh endothelial cell sheets, Biomaterials 33 (2012) 1406–1413.
[57] J.C. Dunn, M.L. Yarmush, H.G. Koebe, R.G. Tompkins, Hepatocyte function and extracellular matrix geometry: long-term culture in a sandwich configuration, FASEB J. 3 (1989) 174–177.
[58] A. Bader, E. Knop, A. Kern, K. Boker, N. Fruhauf, O. Crome, et al., 3-D coculture of hepatic sinusoidal cells with primary hepatocytes-design of an organotypical model, Exp. Cell Res. 226 (1996) 223–233.
[59] Y. Toyoda, M. Tamai, K. Kashikura, S. Kobayashi, Y. Fujiyama, T. Soga, et al., Acetaminophen-induced hepatotoxicity in a liver tissue model consisting of primary hepatocytes assembling around an endothelial cell network, Drug Metabol. Dispos. Biol. Fate Chem. 40 (2012) 169–177.
[60] A. Soto-Gutierrez, N. Navarro-Alvarez, H. Yagi, Y. Nahmias, M.L. Yarmush, N. Kobayashi, Engineering of an hepatic organoid to develop liver assist devices, Cell Transpl. 19 (2010) 815–822.
[61] Y. Nahmias, R.E. Schwartz, W.S. Hu, C.M. Verfaillie, D.J. Odde, Endothelium-mediated hepatocyte recruitment in the establishment of liver-like tissue in vitro, Tissue Eng. 12 (2006) 1627–1638.
[62] A.L. Larkin, R.R. Rodrigues, T.M. Murali, P. Rajagopalan, Designing a multicellular organotypic 3D liver model with a detachable, nanoscale polymeric Space of Disse, Tissue Eng. Part C Methods 19 (2013) 875–884.
[63] S. Salerno, C. Campana, S. Morelli, E. Drioli, L. De Bartolo, Human hepatocytes and endothelial cells in organotypic membrane systems, Biomaterials 32 (2011) 8848–8859.
[64] Y.C. Toh, T.C. Lim, D. Tai, G. Xiao, D. van Noort, H. Yu, A microfluidic 3D hepatocyte chip for drug toxicity testing, Lab Chip 9 (2009) 2026–2035.
[65] K. Domansky, W. Inman, J. Serdy, A. Dash, M.H.M. Lim, L.G. Griffith, Perfused multiwell plate for 3D liver tissue engineering, Lab Chip (2010) 51.
[66] M.B. Esch, J.M. Prot, Y.I. Wang, P. Miller, J.R. Llamas-Vidales, B.A. Naughton, et al., Multi-cellular 3D human primary liver cell culture elevates metabolic activity under fluidic flow, Lab Chip 15 (2015) 2269–2277.
[67] T.D. Boyer, T.L. Wright, M.P. Manns, D. Zakim, Zakim and Boyer's Hepatology: a Textbook of Liver Disease, Saunders/Elsevier, Philadelphia, PA, 2006.
[68] G. Elaut, T. Henkens, P. Papeleu, S. Snykers, M. Vinken, T. Vanhaecke, et al., Molecular mechanisms underlying the dedifferentiation process of isolated hepatocytes and their cultures, Curr. Drug Metab. 7 (2006) 629–660.
[69] D. Fu, Y. Wakabayashi, Y. Ido, J. Lippincott-Schwartz, I.M. Arias, Regulation of bile canalicular network formation and maintenance by AMP-activated protein kinase and LKB1, J. Cell Sci. 123 (2010) 3294–3302.
[70] I. Wagner, E.M. Materne, S. Brincker, U. Sussbier, C. Fradrich, M. Busek, et al., A dynamic multi-organ-chip for long-term cultivation and substance testing proven by 3D human liver and skin tissue co-culture, Lab Chip 13 (2013) 3538–3547.
[71] S.S. Bale, I. Golberg, R. Jindal, W.J. McCarty, M. Luitje, M. Hegde, et al., Long-term coculture strategies for primary hepatocytes and liver sinusoidal endothelial cells, Tissue Eng. Part C Methods 21 (2015) 413–422.
[72] S.S. Bale, L. Vernetti, N. Senutovitch, R. Jindal, M. Hegde, A. Gough, et al., In vitro platforms for evaluating liver toxicity, Exp. Biol. Med. (Maywood) 239 (2014) 1180–1191.
[73] H. Becker, I. Schulz, A. Mosig, T. Jahn, C. Gärtner, Microfluidic devices for cell culture and handling in organ-on-a-chip applications, SPIE MOEMS-MEMS SPIE. 8976 (2014) 1–9.
[74] M. Lange, S. Engelhardt, S. Liebold, H. Plettenberg, S. Mosig, M. Hoffmann, Analysis of glucose and fetal calf serum in aqueous solution for Multi Organ Tissue Flow (MOTiF) bioreactors using NIR Spectroscopy, Biomed. Techn. Berl. 58 (2013) 4199.
[75] A.T. Press, A. Traeger, C. Pietsch, A. Mosig, M. Wagner, M.G. Clemens, et al., Cell type-specific delivery of short interfering RNAs by dye-functionalised theranostic nanoparticles, Nat. Commun. (2014) 5565.

Manuscript I – Supplementary information

Supplementary Table 1.

Dimensions:

	length / width / height (mm)
chip body	75.5 / 22.5 / 1.5
upper channel	15.0 / 2 / 0.45
lower channel	16.8 / 2 / 0.40
membrane (8 µm pore diameter)	13 / 8.5 / 0.02
	distance (mm)
membrane to upper sealing foil	0.7
membrane to lower sealing foil	0.8

Flow rates:

	flow rate (µl / min)	*shear stress ((dyn * s) / cm^2)*
upper channel	50	0.7
lower channel (as indicated in corresponding experiments)	1 3 10	0.01 0.03 0.12

Supplementary Table 2. Interpretation of cellular ATP and ATP levels, and ADP/ATP ratios (Abcam ADP/ATP Ratio Assay Kit (Bioluminescent) booklet (2015))

cell fate	**ATP level**	**ADP/ATP ratio**
proliferation	high	low
growth arrest	increased	low
apoptosis	low	high

3.2 Manuscript II

Monocyte-induced recovery of inflammation-associated hepatocellular dysfunction in a biochip-based human liver model

---

Gröger M, Rennert K, Giszas B, Weiß E, Dinger J, Funke H, Kiehntopf M, Peters FT, Lupp A, Bauer M, Claus RA, Huber O, Mosig AS

Published in:
Scientific Reports, 2016, 6:21868.

In this study the liver-on-a-chip model was used to evaluate TLR-mediated hepatocellular dysfunction. Stimulation with TLR-1/2, 4 and 9 agonists led to specific release of pro- and anti-inflammatory cytokines. The resulting loss of vascular endothelial cadherin (VEC) indicates an impairment of the endothelial barrier. Furthermore, hepatic damage was confirmed by the diminished expression of the biliary transporter MRP-2 and apolipoprotein B (ApoB) of the hepatocytes. It was shown that perfusion of primary monocytes restored liver-on-a-chip function, associated with a recovery of albumin as well as urea synthesis, diminished cell death and restored biliary excretion via self-formed bile canaliculi in the HepaRG cell layer. The observed pathophysiological conditions were comparable with data obtained in the murine sepsis model of peritoneal contamination and infection (PCI) as well as in clinical observations of septic patients. Thus, the model proved its ability to mimic inflammation-related hepatic dysfunction as well as immune cell-dependent liver regeneration. It thereby offers novel options for the elucidation of the underlying signaling processes and creates new opportunities in the development of tailored treatment strategies for sepsis-associated liver failure.

www.nature.com/scientificreports

SCIENTIFIC REPORTS

OPEN

Received: 13 October 2015
Accepted: 02 February 2016
Published: 23 February 2016

Monocyte-induced recovery of inflammation-associated hepatocellular dysfunction in a biochip-based human liver model

Marko Gröger[1,7,*], Knut Rennert[1,7,*], Benjamin Giszas[2,7], Elisabeth Weiß[1], Julia Dinger[3], Harald Funke[4], Michael Kiehntopf[5,7,*], Frank T. Peters[3], Amelie Lupp[6], Michael Bauer[2,7], Ralf A. Claus[2,7], Otmar Huber[1,7] & Alexander S. Mosig[1,7]

Liver dysfunction is an early event in sepsis-related multi-organ failure. We here report the establishment and characterization of a microfluidically supported *in vitro* organoid model of the human liver sinusoid. The liver organoid is composed of vascular and hepatocyte cell layers integrating non-parenchymal cells closely reflecting tissue architecture and enables physiological cross-communication in a bio-inspired fashion. Inflammation-associated liver dysfunction was mimicked by stimulation with various agonists of toll-like receptors. TLR-stimulation induced the release of pro- and anti-inflammatory cytokines and diminished expression of endothelial VE-cadherin, hepatic MRP-2 transporter and apolipoprotein B (ApoB), resulting in an inflammation-related endothelial barrier disruption and hepatocellular dysfunction in the liver organoid. However, interaction of the liver organoid with human monocytes attenuated inflammation-related cell responses and restored MRP-2 transporter activity, ApoB expression and albumin/urea production. The cellular events observed in the liver organoid closely resembled pathophysiological responses in the well-established sepsis model of peritoneal contamination and infection (PCI) in mice and clinical observations in human sepsis. We therefore conclude that this human liver organoid model is a valuable tool to investigate sepsis-related liver dysfunction and subsequent immune cell-related tissue repair/remodeling processes.

The liver plays a central role in metabolism of carbohydrates, lipids and proteins, in biotransformation and detoxification. In addition, it is a key player in the host response against infections and damage but the multiple impacts of the liver in sepsis just recently started to emerge[1]. Pathogen-associated molecular patterns (PAMPs) inducing systemic inflammatory conditions often result in liver dysfunction as one of the earliest events. They often progress to liver damage and failure and concomitant sepsis-related multi-organ failure (MOF)[2]. Liver injury or damage before onset of sepsis is associated with a higher risk of poor outcome[3]. Yet, the underlying molecular mechanisms are poorly understood. Most studies on inflammation-associated hepatocellular dysfunction were performed in rodent animal models. However, a controversial debate about the value of these models in inflammatory research and transferability of results to human conditions has been raised[4,5]. To solve this issue it is necessary to establish model systems that allow corresponding tests under physiological relevant conditions using human cell layers, which clearly mirror the disorganization during the underlying disease in the clinical setting.

The immune response within the liver is mainly borne by nonparenchymal cells (NPCs) accounting for about 40% of total liver cells. Kupffer cells, specialized tissue macrophages, represent 15% of total liver cells and almost 80–90% of all tissue macrophages in the body[6], underscoring the important role of the liver for detoxification of endotoxin and for immunological homeostasis. In the context of lipopolysaccharide (LPS) stimulation, a recent

[1]Institute of Biochemistry II, Jena University Hospital, 07743 Jena, Germany. [2]Department of Anesthesiology and Intensive Care, Jena University Hospital, Jena 07747 Jena, Germany. [3]Institute of Forensic Medicine, Jena University Hospital, 07743 Jena, Germany. [4]Molecular Hemostaseology, Jena University Hospital, Jena, 07747 Jena, Germany. [5]Institute of Clinical Chemistry and Laboratory Diagnostics, Jena University Hospital, 07747 Jena, Germany. [6]Institute of Pharmacology and Toxicology, Jena University Hospital , Jena, Germany. [7]Center for Sepsis Control and Care, Jena University Hospital, Jena, 07747 Jena, Germany . *These authors contributed equally to this work. Correspondence and requests for materials should be addressed to A.S.M. (email: alexander.mosig@med.uni-jena.de)

study suggested that macrophages are key regulators of the inflammatory response in the liver *in vivo*, since upon macrophage-ablation hepatocytes do not longer respond toward a challenge with LPS[7]. Further major cell types populating the liver are stellate cells (6%) and endothelial cells (19%)[8]. Hepatic stellate cells (HSCs) also participate in immune regulation and tissue regeneration[9]. In secreting TNFα and IL-1β they promote an inflammatory microenvironment that aggravates initial damage inflicted by PAMPs and drugs[3]. On the other hand, they also secrete TGF-β and proteins of the extracellular matrix (e.g. collagen I) which leads to resolution of inflammation and tissue repair[10]. The lack of efficient cell depletion strategies for HSCs makes it difficult to assess their respective contribution during inflammation *in vivo*. Similarly, the role of endothelial cells (ECs) comprises not only their barrier function by spatially separating the plasma compartment, but also includes receptor-mediated clearance of endotoxins, bacteria and other compounds, and regulation of inflammation, leukocyte recruitment and host immune responses to pathogens[11]. ECs promote the inflammatory process, by sensing cell debris from damaged hepatocytes via TLR, subsequent secretion of chemokines and expression of cell adhesion molecules that recruit leukocytes to the site of activated and damaged tissue. However, it remains to be elucidated whether they also play a role in recruitment of monocytes that can favor regeneration. Furthermore, the integrity of the liver microvasculature preserving an adequate function of sinusoidal ECs, plays a crucial role in maintaining liver perfusion and liver cell viability[12].

To investigate human hepatic inflammatory response, primary hepatocyte monolayers are frequently used as they provide the whole range of liver-specific metabolism, including transporter proteins and CYPs relevant in human biotransformation and detoxification. However, primary hepatocytes as well as most of the commonly used hepatocyte cell lines tend to de-differentiate during culture resulting in a loss of metabolic activity and reduced synthesis of typical hepatic products such as urea and albumin[11]. Under physiological conditions, hepatic inflammation and tissue repair in response to microbial infection is orchestrated by the specifically timed and dynamically regulated action of pro- and anti-inflammatory chemo- and cytokines[13]. Such a complex secretion profile can only barely be mimicked by exogenous cytokine treatment. In order to better reflect the *in vivo* situation it is therefore desirable to include an endogenous source of integrative cytokine secretion such as NPCs into the liver model to imitate spatio-temporal events of host response. Several *in vitro* liver models were reported that allow co-culture of hepatocytes with ECs[14], macrophages[15] and HSCs[16].

We recently reported the establishment of a perfused human liver organoid model composed of a vascular and a hepatic cell layer comprising all major cell types of the liver that are assembled in a in tissue structure mimicking the *in vivo* situation[17]. We here adapted the arrangement of the individual organoid cell layers in order to facilitate the enrichment of secreted cytokines, metabolic marker molecules and released intracellular enzymes in response to TLR-mediated inflammation. We observed a striking resemblance to the sepsis-related liver dysfunction responses in the well-established *in vivo* mouse model of peritoneal contamination and infection (PCI) as well as clinical observations of human sepsis[2]. To assemble the liver organoid we used the recently described microfluidically supported "MOTiF" (multi organ tissue flow) biochips[18] enabling adhesion and transmigration of monocytes under physiological flow conditions to study the impact of invading immune cells on the functional properties of the liver organoid under inflammatory conditions. Strikingly, we observed a restoration of inflammation-induced hepatocellular dysfunction upon adhesion of monocytes to the vascular layer and their invasion into inflamed hepatic tissue. Thus, this model not only mimics inflammation-related processes of liver dysfunction on the cellular level, but also allows analysis of monocyte-mediated processes of tissue repair and immunotolerance known to be important in the course of human sepsis[19].

Results

Design of the biochip-based sinusoidal liver model. The structure of the artificial liver model was inspired by the structure of the human liver sinusoid. A suspended porous membrane within the MOTiF biochips served as a substrate for human umbilical vein endothelial cells (HUVEC) that are co-cultured with primary macrophages mimicking the immune-modulatory function of Kupffer cells. The EC/macrophage layer mimics aspects of the vascular component of the human liver sinusoid in shielding hepatocytes from instant contact to monocytes perfused via the upper channel system thereby imitating the luminal side of the sinusoid. This vascular layer is separated by a medium-filled space of the size of 400 μm from the hepatic cell layer cultured on the sealing foil at the bottom of the biochip. The hepatic layer comprises human HepaRG hepatocytes that differentiate into cells with a hepatocyte phenotype and cells exhibiting a biliary epithelial cell phenotype which self-organize during culture and form hepatocyte layers with functional bile canaliculi[20]. This design allows to also address the important role of the biliary epithelium within the liver. Furthermore, HepaRG cells have been shown to be suitable for studies of hepatic inflammatory response[21,22].

HepaRG cells were co-cultured with HSCs that *in vivo* mostly reside in the space of Dissé with contacts to both endothelial cells and hepatocytes[23]. To keep the endothelial layer intact LX-2 stellate cells were co-cultured in the hepatic layer. This hepatic layer separated from the vascular layer by superposed medium and the membrane allows cross-communication of both layers and cell migration through the vascular to the hepatic tissue layer through the pores of the membrane (*SI Appendix*, Fig. S1A,B).

NPCs stabilize HepaRG differentiation in the absence of dimethyl-sulfoxide. HepaRG cells were used to establish the liver organoid as this cell line in contrast to other hepatic cells lines, i.e. HepG2 or Hep2/C3A, remains functionally stable during prolonged culture and self-organizes functional bile canaliculi-like structures[24]. Moreover, HepaRG cells respond to exogenous inflammatory cytokine treatment[25]. Maintenance of differentiated HepaRG cells depends on the presence of 2% dimethyl-sulfoxide (DMSO) and is a prerequisite for the expression of cytochrome P450 enzymes (CYP proteins), which is diminished in its absence (*SI Appendix*, Fig. S1C). However, during prolonged cell culture DMSO is cytotoxic to HUVEC cells forming the vascular layer. They dramatically lose expression of endothelial von Willebrand factor and PECAM-1, proteins that are involved

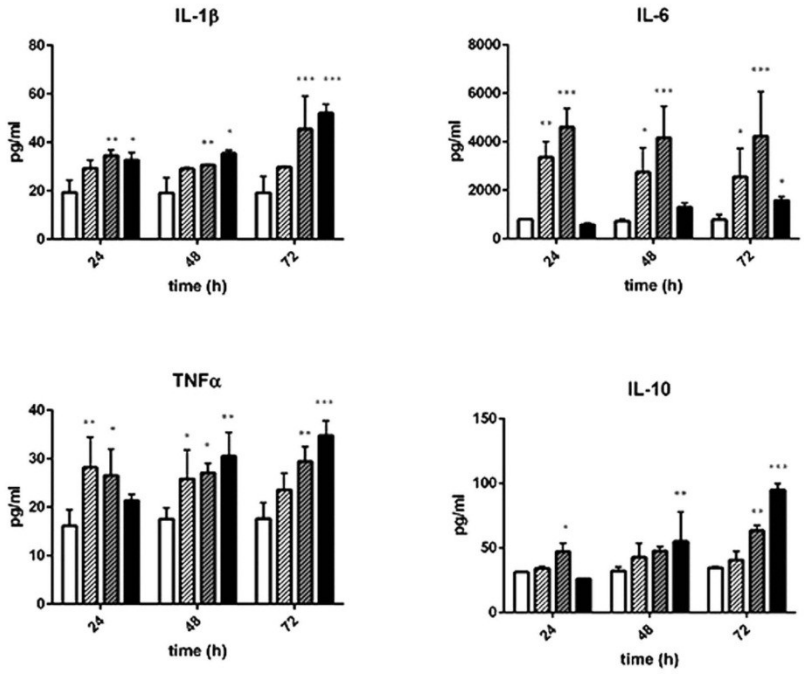

Figure 1. Cytokine profiling of liver organoids stimulated with TLR agonists. Cytokine release of untreated liver organoids (open bars) was compared to liver organoids treated for 24 h, 48 h or 72 h with Pam3CSK4 (open, shaded bars), LPS (grey, shaded bars) or ODN2006 (black bars). Cell culture medium was exchanged every 24 h. Statistical significance was calculated compared to untreated control after 24 h of culture using two-way ANOVA with Dunnett's multiple comparisons test (*$p < 0.05$, **$p < 0.01$, ***$p < 0.001$). Results of five independent experiments are shown.

in regulation of coagulation, immune cell trafficking and maintenance of EC junctional integrity[26,27]. Co-culture of NPCs has been shown to stabilize hepatocyte differentiation[28]. Indeed, when differentiated HepaRG cells were co-cultured with LX-2 stellate cells, HUVEC and macrophages prevented HepaRG dedifferentiation resulting in stabilization of CYP3A4 expression for at least four days of co-culture even in the absence of DMSO (*SI Appendix,* Fig. S1C). From these observations we concluded that co-culture of NPCs stabilizes the differentiated hepatocyte phenotype in the liver organoid.

TLR agonist-specific cytokine secretion profiles. In a first set of experiments, the inflammatory response of the liver organoid was tested in response to treatment with Pam3CSK4 (TLR-1/2 agonist), LPS (TLR-4 agonist) and ODN2006 (TLR-9 agonist) for up to 72 h. A TLR agonist-specific and time-dependent cytokine secretion profile of the pro-inflammatory cytokines IL-1β, IL-6 and TNFα and the anti-inflammatory cytokine IL-10 was observed. The release of pro-inflammatory cytokines occurred as an acute and sustained pro-inflammatory response for up to three days of stimulation. The release of anti-inflammatory IL-10 was delayed and only induced by LPS and ODN2006 treatment, reaching a maximum after 72 h of stimulation (Fig. 1)

Hepatic enzyme expression is modulated by TLR stimulation. CYP3A4 as one of the major cytochrome P450 enzymes is responsible for the metabolism of >50% of all prescribed drugs[29]. In accordance with previous reports[21,30] we found a down-regulation of CYP3A4 in response to LPS stimulation in mono cell cultures of HepaRG cells. A significant reduction of CYP3A4 expression in response to LPS was also observed in co-cultures of HepaRG with stellate cells (*SI Appendix*, Fig. S2A). Interestingly, at the level of a completely assembled liver organoid including the endothelial layer and macrophages the expression of CYP3A4 was not affected by any of the TLR agonists (Fig. 2A,E). To correlate expression and drug-metabolizing activity we used midazolam as CYP3A4 model substrate and measured the formation rate of its metabolite 1-OH-midazolam over 6 h in HepaRG mono-cell cultures and in liver organoids. Although LPS treatment diminished formation rate of 1-hydroxymidazolam (1-OH-midazolam) in HepaRG mono-cell cultures we observed no significant decline in response to LPS stimulation in the liver organoid (*SI Appendix*, Fig. S2B). These data suggested that ECs and

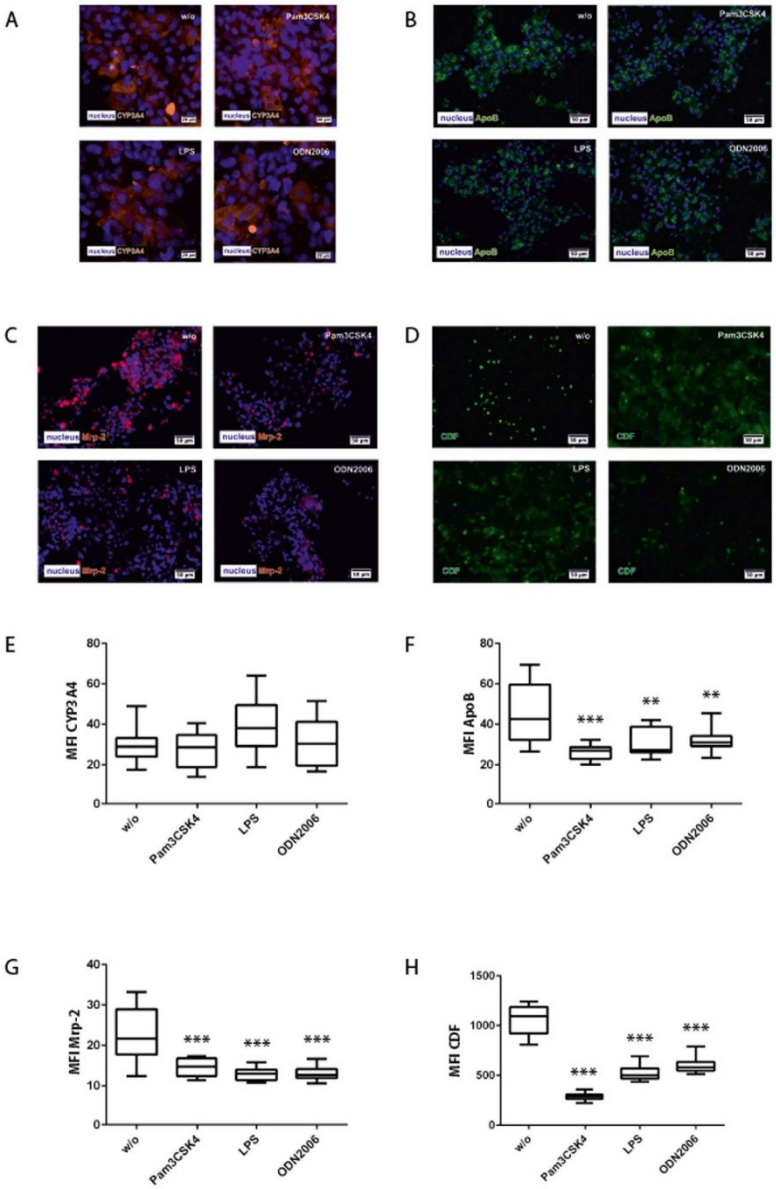

Figure 2. Hepatocyte protein expression and CDF secretion in the hepatic layer. Liver organoids were treated with Pam3CSK4, LPS or ODN2006 for 72 h and compared with untreated control (w/o). (**A**–**D**) Immunofluorescence staining of (**A**) CYP3A4 (orange) (**B**) ApoB (green) and (**C**) MRP-2 (magenta), (**D**) CDF secretion (green) into bile canaliculi after 24 h of stimulation with TLR agonists. (**E**–**H**) Computational analyses of fluorescence signal intensities using random field analyses of at least 20 regions of interest (ROI) per tested condition (labeled as mean immunofluorescence intensity (MFI) of specific staining against the respective protein) of (**E**) CYP3A4, (**F**) ApoB, (**G**) Mrp-2, (**H**) CDF. Nuclei are stained with DAPI (blue). Statistical significance was calculated compared to untreated control using one-way ANOVA with Dunnett's multiple comparisons test (*$p < 0.05$, **$p < 0.01$, ***$p < 0.001$). Results of three independent experiments are shown.

macrophages of the vascular layer contribute to a reduced susceptibility of the hepatocyte response to LPS in respect to CYP3A4 activity.

We further asked whether the liver organoid reflects the inflammation-related lipoprotein dysregulation at the level of apoB expression. In agreement with *in vivo* studies[31], we observed a significantly reduced expression of apoB in the liver organoids after treatment with agonists for TLR1/2, TLR4 and TLR9 (Fig. 2B,F).

Moreover, sepsis-related liver dysfunction is associated with cholestasis[32]. Expression and activity of MRP-2, a major transporter protein involved in bile acid secretion, was used as a read-out. Release of the fluorescent dye 5 (and 6)-carboxy-2′,7′-dichlorofluorescein (CDF) into bile canaliculi was measured as surrogate for MRP-2 efficiency[33]. After 72 h, expression levels of MRP-2 remarkably declined in liver organoids treated with Pam3CSK4, LPS or ODN2006 compared to untreated control (Fig. 2C,G). Moreover, upon TLR stimulation accumulation of CDF in the bile canaliculi was substantially reduced and CDF was trapped within the cytoplasm of the hepatocytes (Fig. 2D,H).

Inflammatory response of the vascular layer. During sepsis a dysregulation of the endothelial barrier is a major pathogenic mechanism promoting septic MOF[34]. Therefore, we next studied the response of ECs and embedded macrophages to TLR agonists in the liver organoid. Both cell types have been shown to bind LPS and mediate endotoxin clearance in the liver[35]. Expression and localization of the junctional proteins VE-cadherin and the zonula occludens-1 (ZO-1) protein in the vascular layer were analyzed in response to inflammation. VE-cadherin is known to be essential for endothelial integrity and the maintenance of endothelial cell-cell contacts[36]. ZO-1 connects integral tight junction proteins to the actin cytoskeleton, and was reported to be involved in the disarrangement of the actin cytoskeleton leading to increased endothelial permeability in response to IL-6[37]. All TLR agonists tested induced a sustainable reduction of VE-cadherin and ZO-1 expression within three days of stimulation (Fig. 3A,B). Concomitantly, actin cytoskeleton fibers within ECs were disassembled in response to TLR stimulation (Fig. 3A,B).

Endothelial injury is associated with the recruitment of circulating immune cells such as monocytes to the endothelial lining, where they are assumed to contribute to local inflammatory hotspots and thereby enhance endothelial leakage. Since in initial experiments LPS provoked a robust and prolonged pro-inflammatory cytokine release among tested TLR agonists, we focused our studies on monocyte adhesion and transmigration into the liver organoid in response to LPS treatment. To assess specific cell recruitment and diapedesis at the vascular layer under flow conditions, liver organoids pre-cultured and stimulated under static conditions were subsequently perfused with Celltracker® Green stained monocytes for 60 min under dynamic flow conditions with a shear stress rate of 3 dyn/cm^2. Primary monocytes as well as THP-1 monocytes were efficiently recruited to the vascular layer upon LPS stimulation, formed filopodia and efficient diapedesis through the vascular layer and migration into the hepatic compartment of the liver organoid was observed (Fig. 3C,D; *SI Appendix,* Fig. S3A). Viability of transmigrated primary monocytes of more than 75% was confirmed by flow cytometry (Fig. 3D). These findings prove that the majority of invading monocytes in the liver model were viable and functionally active in respect to adhesion and endothelial transmigration.

Monocyte adhesion/migration enhances the cytokine release, which activates endothelial cells and thereby induces the expression of ICAM-1 and VCAM-1 and release of sCAMs[38]. Immune cell adhesion and subsequent migration rely on the presence of endothelial cell adhesion molecules (CAMs) whereas release of soluble CAM fragments was shown to correlate with severity of sepsis[39]. An acute increase of endothelial ICAM-1 and VCAM-1 expression in the vascular layer of the liver organoid was observed within 24 h of LPS stimulation. Although ICAM-1 levels went down within the next 48 h, expression was still considerably higher than in unstimulated cells. By contrast VCAM-1 expression returned to basal levels. Interestingly, in the presence of perfused and adhesive monocytes, ICAM-1 expression on EC surfaces was significantly lower under inflammatory conditions triggered by LPS after 72 h compared to LPS-treated organoids without monocyte perfusion. VCAM-1 levels in monocyte-perfused organoids were slightly lower compared to monocyte-free conditions (*SI Appendix,* Fig. S3A).

LPS-treatment induced a prompt release of sICAM-1 and sVCAM-1 from the cell surface within 24 h. Within the next 48 h sICAM-1 levels only slightly increased whereas sVCAM-1 levels decreased. In the presence of monocytes sCAM levels decreased (Fig. 4A). As expected, we further found increased IL-1β, IL-6 and TNFα levels after primary monocyte adhesion in the presence of LPS compared to untreated control. Cytokine levels then declined during subsequent 48 h, but remained significantly higher in LPS-treated liver organoids (Fig. 4B). Also anti-inflammatory IL-10 was regulated in a similar manner in primary monocytes.

In liver organoids perfused with THP-1 monocytes we found a significantly reduced release of cytokine upon LPS challenge and TNFα release was not increased in presence of THP-1 monocytes. In addition, a transient increase of anti-inflammatory IL-10 secretion was detectable in untreated liver organoids and to lower extend in LPS-treated organoids in the presence of THP-1 monocytes (*SI Appendix,* Fig. S4B). In contrast to primary monocytes the release of sICAM and sVCAM was not significantly increased by LPS in the presence of THP-1 monocytes (*SI Appendix,* Fig. S3C).

Invading monocytes modulate endothelial and hepatic protein expression and function in the liver organoid. In LPS stimulation experiments without monocyte perfusion, localization of VE-cadherin and ZO-1 appeared fuzzy and discontinuously aligned along cell-cell contacts. In contrast, only a minor loss of VE-cadherin expression accompanied with an enhanced cytosolic VE-cadherin signal was found within the vascular layer in the presence of adhering/invading primary monocytes in response to 72 h LPS treatment (Fig. 5A).

To characterize the impact of invading monocytes on the hepatic cells, we also measured the expression of CYP3A4, ApoB, MRP-2 and E-cadherin within the hepatic layer. In experiments without monocyte perfusion we observed that LPS treatment did not affect CYP3A4 or E-cadherin expression but induced a decrease of ApoB and

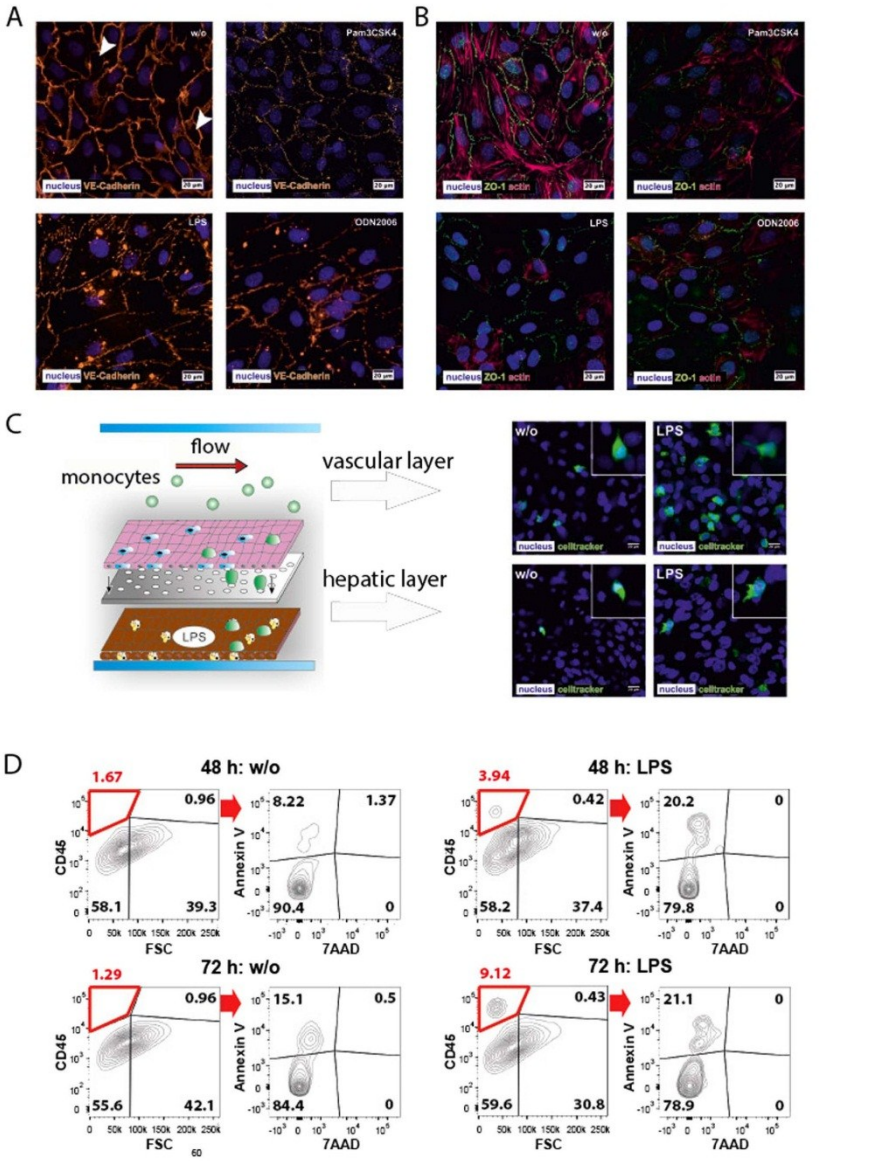

Figure 3. Modulation of endothelial integrity and monocyte adhesion/migration under inflammatory conditions triggered by Pam3CSK4, LPS or ODN2006. (**A**) Expression of VE-cadherin (orange). White arrows indicate gaps in the vascular layer. (**B**) Expression of ZO-1 (green) and actin (red). (**C,D**) Flow-based adhesion and migration assay of primary monocytes stained with Celltracker® Green at the vascular and hepatic layer of untreated liver organoids (w/o) or liver organoids pre-stimulated with LPS. Nuclei are stained with DAPI (blue). (**D**) Analysis of primary monocytes transmigrated for 48 h and 72 h into the hepatic layer in absence (w/o) or presence of LPS. Monocytes within the hepatic chamber were stained and gated based on CD45 expression and analyzed for apoptosis induction (Annexin V staining) and cell death (7AAD). (**A–D**) Results of a representative experiment out of three independent experiments are shown.

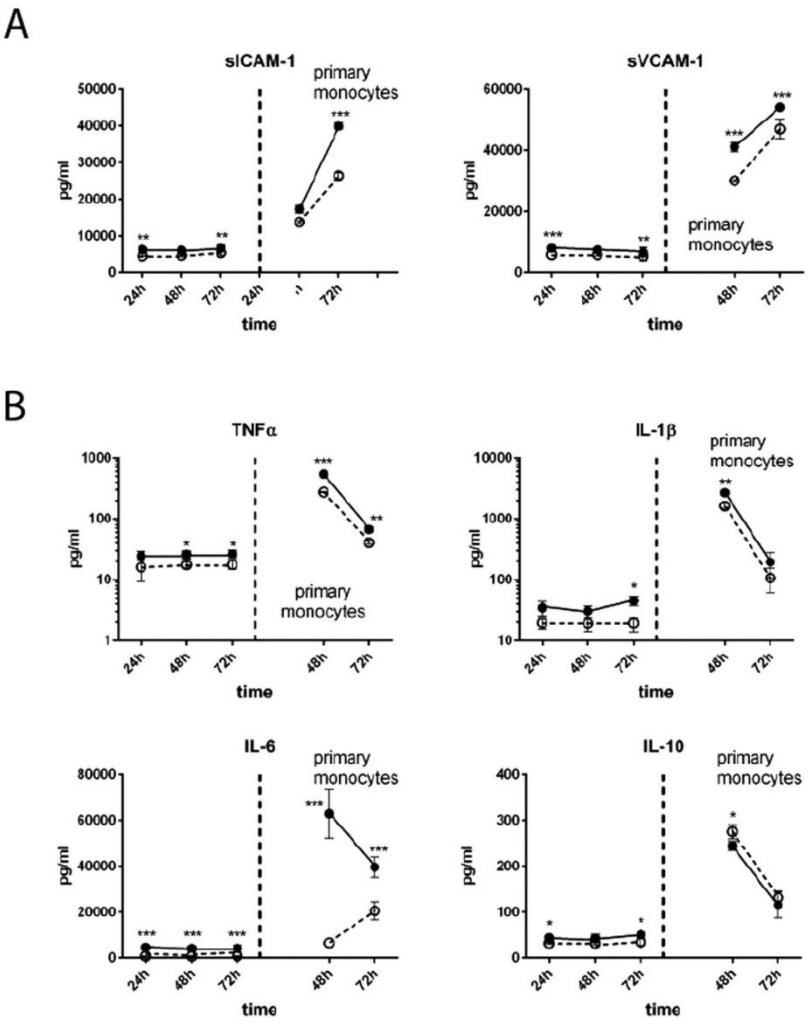

Figure 4. Impact of perfusion with primary monocytes. (**A**) Release of sICAM and sVCAM in response to primary monocyte perfusion and adhesion. (**B**) Secretion of IL-1β, IL-6, TNFα and IL-10 in response to primary monocyte perfusion and adhesion. Liver organoids were untreated (dashed line) or stimulated with LPS (solid line), without monocyte perfusion (left from vertical dashed line) or with monocyte perfusion (right from vertical dashed line). (**A**,**B**) Statistical significance was calculated between untreated and LPS-treated liver organoids of identical time points and perfusion conditions (*$p < 0.05$, **$p < 0.01$, ***$p < 0.001$) using student's t-test. Results of six independent experiments are shown.

MRP-2 expression accompanied by a reduced MRP-2 activity in bile canaliculi under inflammatory conditions (Fig. 5B). Importantly, in the presence of invading monocytes we observed a stabilization of ApoB and MRP-2 expression associated with the secretion of CDF. Although the expression level of these proteins as well as the CDF secretion rate were lower compared to naive organoids, invading monocytes clearly prevented hepatocellular dysfunction observed under inflammatory conditions in absence of migrating monocytes. Similar observations were made upon THP-1 invasion in presence of LPS (*SI Appendix,* Fig. S5A,B).

Next, the impact of monocyte invasion into the liver organoid on viability and metabolic activity of hepatic cells was tested. In this context, the release of intracellular enzymes as reporters of cell-damage

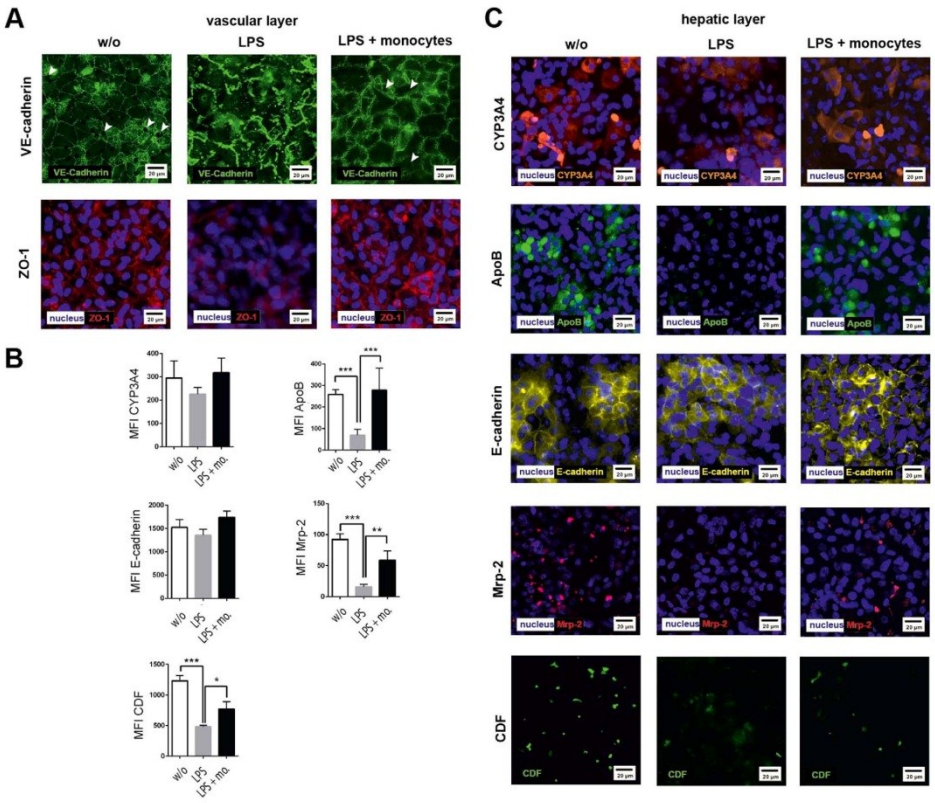

Figure 5. Immunofluorescence staining of endothelial and hepatocyte proteins without stimulation (w/o) and in presence of 100 ng/ml LPS (LPS) or 100 ng LPS and primary monocytes (LPS + monocytes (mo.)). (**A**) Expression of VE-cadherin and ZO-1 at the vascular layer. White arrows indicate gaps in the vascular layer. Representative results of three independent experiments are shown. (**B**) Computational analyses of fluorescence intensities of at least 20 ROI per condition (labeled as mean immunofluorescence intensity (MFI)) of the respective protein using random field analysis in the hepatic layer. Statistical significance was calculated between indicated conditions using student's t-test (*$p < 0.05$, **$p < 0.01$, ***$p < 0.001$). Immunostaining for (**C**) CYP3A4 (red), ApoB (green), E-cadherin (yellow), MRP-2 (red), and detection of CDF secretion (green). Nuclei are stained with DAPI (blue). Representative results of three independent experiments are shown.

in response to LPS-induced inflammation was measured. In the absence of monocytes, a continuously increasing release of the intracellular enzyme lactate-dehydrogenase (LDH) under inflammatory conditions was observed, which was not detectable under LPS-free conditions. Most interestingly, adhesion and invasion of primary monocytes as well as THP-1 monocytes resulted in a rapid decline of LDH-release down to levels observed in the untreated control. Similar results were obtained for the release of the hepatocyte-specific intracellular enzymes glutamate-dehydrogenase (GLDH), aspartate-transaminase (ASAT) and alanine-transaminase (ALAT) with increasing release of GLDH, ASAT and ALAT in response to LPS-triggered inflammation. However, in the presence of transmigrated primary as well as THP-1 monocytes, accumulation of GLDH, ASAT and ALAT in the culture medium of the hepatocyte layer was prevented (Fig. 6A, *SI Appendix,* Fig. S6A).

The metabolic activity of the liver organoid was analyzed at the level of cellular glucose consumption and lactate formation. Liver organoids stressed by inflammation exhibited an increased turnover/consumption of glucose compared to non-stimulated liver organoids. Interestingly, in the presence of transmigrated primary monocytes, inflammatory conditions apparently influenced glucose turnover rates to a lower extent. Concomitant with increased glucose consumption, LPS treatment induced an increase in lactate formation. This effect was diminished in the presence of primary monocytes (Fig. 6B), but not observed for THP-1 monocytes (*SI Appendix,* Fig. 6B).

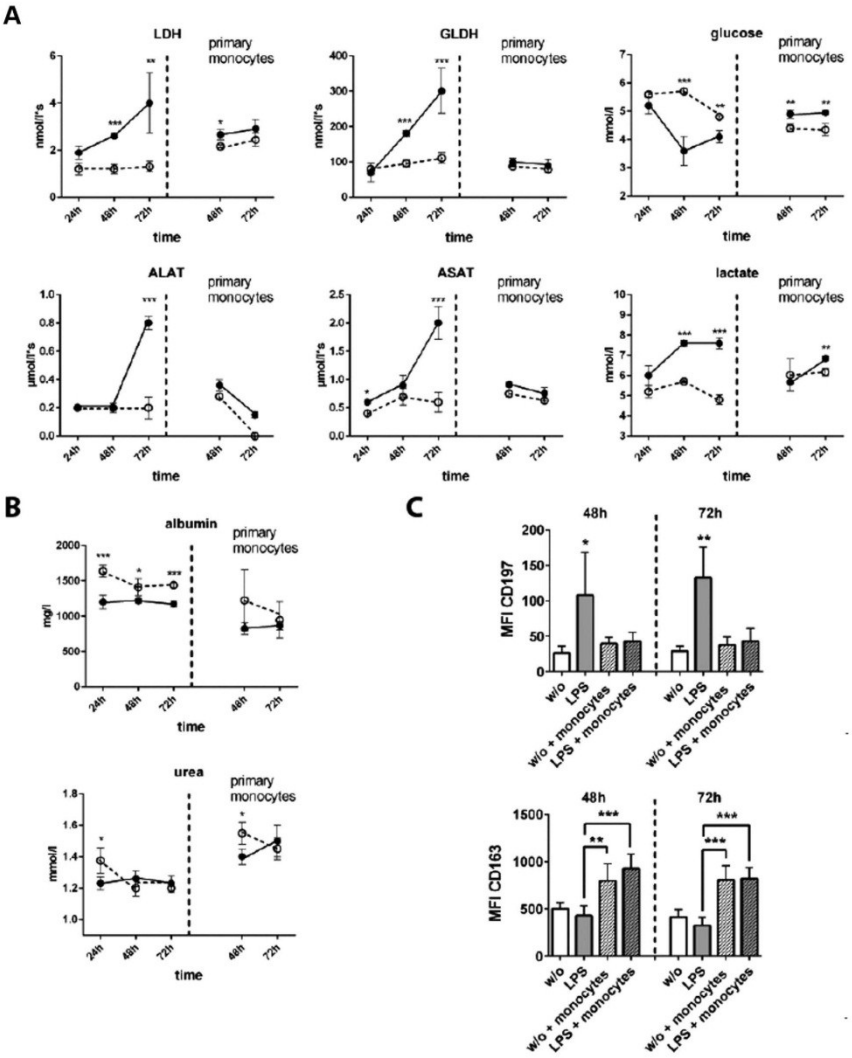

Figure 6. Release of intracellular enzymes and metabolic activity of the liver organoid. Liver organoids were untreated (dashed line) or stimulated with LPS (solid line), without monocyte perfusion (left from vertical dashed line) or with primary monocyte perfusion (primary monocytes, right from vertical dashed line). (**A**) Release of lactate-dehydrogenase (LDH), glutamate-dehydrogenase (GLDH), aspartate-transaminase (ASAT) and alanine-transaminase (ALAT). Changes in glucose, lactate consumption. (**B**) Synthesis of albumin and urea. Statistical significance was calculated between untreated and LPS-treated samples at similar time points and perfusion conditions (*$p < 0.05$, **$p < 0.01$, ***$p < 0.001$) using student's t-test. (**C**) Computational analyses of fluorescence intensity of 20 ROI per condition (labeled as mean immunofluorescence intensity (MFI)) of CD197 or CD163 using random field analyses of macrophages in the vascular layer. Liver organoids were cultured for 48 h or 72 h in absence (w/o) or presence of LPS (LPS). Where indicated liver organoids were perfused with monocytes (+monocytes) 24 h after culture and then sub-cultured for indicated times. Significance of CD197 was calculated for condition "LPS treatment without monocytes perfusion" compared to the remaining conditions. For CD163 significance was calculated between indicated conditions. For statistical analysis of CD196 and CD163 expression one-way ANOVA with Bonferroni multiple testing correction (*$p < 0.05$, **$p < 0.01$, ***$p < 0.001$) was used. (**A**–**C**) Data of three independent experiments are shown.

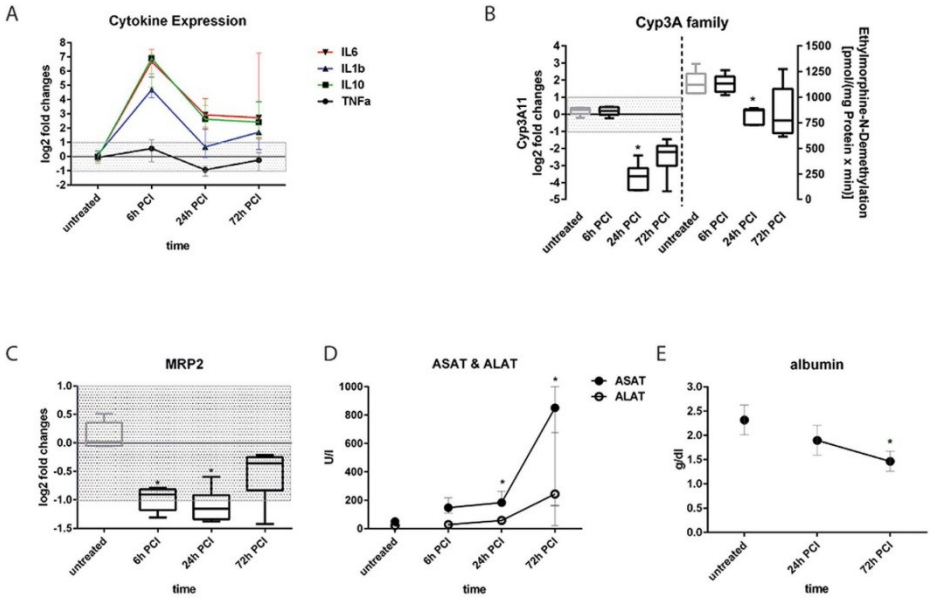

Figure 7. Release of cytokines and intracellular enzymes, and regulation of CYP3A and MRP2 in the PCI model. Messenger RNA expression of cytokines (**A**), CYP3A11 (**B**) and MRP-2 (**C**). Enzyme activity of CYP3A family members using the model reaction ethylmorphine-N-demethylation (**D**,**E**) Serum concentrations of ASAT, ALAT and albumin. Statistically significance was calculated using one-way ANOVA with Dunn's test for multiple testing correction ($^{\#}p < 0.05$). (**A**–**E**) Five animals per time point were analyzed.

In addition, we studied albumin and urea synthesis under inflammatory conditions in the liver organoid. Under unstimulated conditions, liver organoids stably synthesized albumin and urea. However, inflammation induced by LPS resulted in a drop in albumin secretion. This effect was not observed for urea production, which appeared to be unaffected by LPS treatment. In presence of primary monocytes, the impact of LPS treatment was abolished 48 h after monocyte invasion and urea synthesis rate even increased (Fig. 6B). In the presence of transmigrated THP-1 monocytes, a significant decline of albumin and urea formation was detected within the first 24 h. However, 48 h after monocyte perfusion, albumin and urea production returned back to levels typically seen at untreated conditions even in the presence of LPS (*SI Appendix*, Fig. 6B).

To investigate the impact of LPS and migrating monocytes on the activation of macrophages residing in the vascular layer we studied their polarization stage. Resident macrophages were identified by staining the macrophage marker protein CD68[40] and were analyzed for the expression of M1 polarization marker protein (CCR7) and M2 polarization marker protein CD163 (hemoglobin-haptoglobin complex receptor)[41]. We observed an LPS-induced up-regulation of CD197 48 h and 72 h after LPS stimulation, which was prevented in the presence of migrating monocytes. In contrast expression of CD163 was not influenced by LPS but up-regulated in presence of monocytes (Fig. 6C and *SI Appendix*, Fig. 7.). Our data thus indicate a shift from M1 to M2 polarization of macrophages in the presence of LPS upon monocyte migration.

Comparison with the *in vivo* situation in a peritoneal contamination and infection mouse model. Next, we wanted to address whether effects in the liver organoid are similarly detectable in the *in vivo* situation. Murine peritoneal contamination and infection (PCI) is a well-established *in vivo* model for studies on systemic inflammation, sepsis-related liver dysfunction and its long-term sequelae with respect to tissue repair[42–45]. Similar to findings in the liver organoid, cytokine levels rapidly increased in the mouse model within 6 h after induction of systemic inflammation by PCI, however, dropped down to low levels until 72 h at the mRNA level (Fig. 7A). In agreement with other reports we observed a down-regulation of the mRNA levels of CYP3A11, which encodes the human analog of CYP3A4, in response to LPS. In a time series for up to 72 h a maximal repression of the mRNA expression was found 24 h after PCI. Although, gene expression of CYP3A11 appeared to be reduced on the mRNA level as shown by qRT-PCR, a reduction of enzyme activity in response to PCI was only detectable 24 h after PCI (Fig. 7B). In line with our findings in the liver organoid also MRP-2 mRNA expression in the PCI mouse model was down-regulated for up to 24 h after PCI (Fig. 7C). In addition, serum levels of ASAT and ALAT were significantly increased upon PCI induction. Maximal release of ASAT/ALAT was observed three days after PCI, indicating most acute inflammation-related liver damage at this time point

(Fig. 7D). Furthermore, albumin production in the PCI mouse model was significantly decreased with a maximal depression of albumin synthesis three days post PCI procedure (Fig. 7E).

Discussion

Using different protocols to stimulate inflammation we have demonstrated the suitability of our biochip supported liver organoid model to simulate sepsis-related liver dysfunction *in vitro*. Most notably, our studies demonstrated that co-culture of the different cell types of the liver is essential to obtain responses reflecting the *in vivo* situation. In detail, we observed that depending on the TLR agonist used for stimulation a specific and time-dependent profile of pro- and anti-inflammatory cytokines was released. This observation underlines that a complete inflammatory response within the liver not only relies on certain isolated cytokines often used as exogenous stimuli especially in cell culture approaches. In particular, it depends on a concerted action of various pro- and anti-inflammatory activities in response to the PAMP stimulus. The inclusion of NPCs and their intrinsic immune-modulatory capacity into the biochip seems to better reflect inflammatory conditions occurring in human liver.

Under inflammatory conditions we did not observe any reduction of CYP3A4 expression in the liver organoid nor reduced formation of 1-OH-midazolam in response to LPS stimulation. In the PCI mouse model expression and activity of CYP3A11 (the homolog of human CYP3A4) were initially reduced and subsequently increased over time in surviving mice. On the other hand, a down-regulation of CYP3A4 protein expression in primary human hepatocyte culture after stimulation with LPS or pro-inflammatory cytokines (5 ng/ml IL-1 or 10 ng/ml TNFα) was reported[46]. The differences to our observations can be explained by the fact, that in our study a significantly lower dose of LPS was used (100 ng/ml vs. 10 μg/ml LPS). Furthermore, a significantly different amount of secreted cytokines was measured in the liver organoid even in the presence of invading monocytes (IL-1β: 516 ± 16 pg/ml and TNFα: 29 ± 3 pg/ml) compared to more than 9-fold and 340-fold higher concentrations of IL1β or TNFα used in the study of Aitken *et al.*[46]. Thus endogenous cytokine release by the organoid model could avoid stimulation with overdosed cytokine amounts potentially inducing non-physiological responses.

Moreover, the response of the liver organoid to TLR agonists resembles many metabolic and structural changes reported for septic liver dysfunction and damage including down-regulation of ApoB, MRP-2, albumin and increased release of LDH, GLDH, ALAT and ASAT. It has been shown that serum ApoB levels are significantly reduced in patients suffering from a systemic inflammatory response syndrome with associated MOF[31]. Furthermore, it was reported that non-survivors of severe sepsis exhibit diminished serum LDL levels compared to surviving patients[47]. Also MRP-2 expression and function was shown to be restricted during sepsis. In the course of sepsis, MRP-2 is irregularly expressed and disrupted at sides of hepatocellular bile secretion in rats, resulting in a disturbed bile acid transport and secretion[2]. In addition, our experiments suggest that endothelial cells actively participate in the regulation of liver organoid inflammation. Up-regulation and shedding of ICAM-1 and VCAM-1 support observations that enrichment of sCAM fragments in the serum positively correlates with the severity of sepsis and other systemic inflammatory diseases[39,48].

It has been shown that NPCs are the major source of inflammatory cytokines such as IL-6 driving acute phase protein production in hepatocytes[49]. HSCs express TLR4 and TLR9, and in addition, they can secrete potent chemoattractants for macrophages (Mcp-1, RANTES) and neutrophils (Cxcl1/Gro1)[50]. In the liver organoid primary as well as THP-1 monocytes were recruited to the activated vascular layer in response to LPS treatment. Monocyte invasion into the liver organoid triggered by PAMP-induced inflammation resulted on one hand in an increased release of pro-inflammatory cytokines such as IL-1β and IL-6, but on the other side appeared to contribute to a dampening of the inflammation-induced hepatocellular dysfunction. However, variations in the monocyte-mediated modulation of liver organoid function under inflammatory conditions were observed when primary and THP-1 monocytes are compared. It is known that THP-1 monocytes secrete substantially lower amounts of TNFα, IL-6 and IL-10 upon LPS stimulation[51] compared to primary monocytes, which was also detectable in our LPS-stimulated and monocyte-perfused liver organoids. Thus, this different behavior likely explains the observed variations of endothelial ICAM-1 expression and sICAM-1 release upon LPS treatment as these cytokines are critical regulators of ICAM-1 expression and shedding[52,53]. However, we already observed an increased cytokine release in the presence of primary monocytes that was associated with an augmented sICAM/sVCAM shedding in the absence of LPS. This might be a reflection of a higher stimulatory sensitivity of primary monocytes compared to THP-1 cells when they are perfused in the vascular compartment of the liver organoid.

Although expression of ApoB and MRP-2 as well as efficiency of MRP-2-mediated bile acid secretion remained decreased during time of observation, the LPS-mediated decrease in albumin or urea production as well as a nearly complete abolishment of hepatic enzyme release into the cell culture medium upon monocyte invasion was observed. This fact indicates that the presence of monocytes within inflamed liver tissue may contribute to increased survival of the tissue layers of the liver organoid.

Macrophages have also been shown to mediate tissue regeneration in response to drug-induced liver damage depending on their differentiation stage[54,55]. M1 or classically activated macrophages possess pro-inflammatory properties and are triggered by bacterial molecular components such as LPS. M2 or alternatively activated macrophages, are generated in response to cytokines such as IL-10 and have been shown to mediate tissue regeneration[56]. The polarization of tissue macrophages is thereby not a terminal state but a transient polarization status within a continuum of different polarization stages with sometimes overlaying macrophage polarization phenotypes. Based on evaluation of the expression pattern of the M1 and M2 polarization markers CD197 and CD163, respectively, we observed a shift from LPS-induced M1- to M2-polarization upon monocyte invasion. The up-regulated expression of the M1 marker protein CD197 in macrophages of the vascular layer in the liver organoids is likely to be induced by LPS and was described in several studies[41]. Upon monocyte perfusion we found a significant increase of IL-10 release, a cytokine known to facilitate M2-polarization[57]. We speculate that the significant increase of IL-10 secretion contributes to the observed polarization shift upon primary monocyte invasion.

This hypothesis is supported by the observation that up-regulation of the M2-polarization marker CD163 correlates with the release of IL-10 and primary monocyte migration but not with LPS treatment. In addition to increased IL-10 release monocyte migration further increases the phagocytic fraction in the liver organoid. This likely facilitates clearance of soluble LPS by monocytes infiltrating the organoid, which facilitates removal of the primary M1-polarization trigger. In combination these processes can contribute to the observed macrophage polarization shift associated with the restoration of organoid function. In addition to macrophage polarization, a immunosuppressive state of monocytes due to cellular re-programming associated with tissue re-modeling and wound healing was described in sepsis patients[58,59]. Shalova *et al.* recently showed that monocytes of patients suffering from sepsis displayed a pro-inflammatory gene expression profile that was associated with features of endotoxine tolerance when treated *ex-vivo* with LPS[59]. Still, phagocytosis and anti-microbial activity as well as tissue re-modeling and repair functions were found to be increased in blood monocytes of sepsis patients, indicating that monocyte function is re-configured under these conditions[59]. Similar effects were also observed in our liver organoid model, where after an initial acute pro-inflammatory phase further release of pro-inflammatory cytokines was subsequently suppressed. This effect was not observed in absence of invading monocytes where cytokine release was stable up to 72 h of LPS stimulation. From our data, we speculate that a homeostatic situation is established in the liver organoid within 48 h of co-culture with transmigrated monocytes facilitating on the one hand inflammation, and on the other hand mediating endotoxin clearance, immune tolerance as well as enhanced metabolism and viability of hepatocytes.

Recently, Esch *et al.* reported the establishment of a three-dimensional model of the human liver, consisting of defined ratios of hepatocytes and NPCs (fibroblasts, stellate cells, and Kupffer cells)[60]. In this model, stable secretion of albumin and urea, and responsiveness to LPS was shown as detected by secretion of pro-inflammatory IL-8. However, this model did not include an endothelial counterpart. Furthermore, Prodanov *et al.* published a model consisting of collagen-gel-embedded hepatocyte/stellate cell co-cultures which are separated by a porous membrane from a cell layer of endothelial like HUVEC/A549 somatic cell hybrids co-cultured with U937 cells[61]. In a cursory test for its inflammatory response, a stable expression of CYP3A4 was observed in primary hepatocytes co-cultured with non-parenchymal cells similar to our model. Though, to the best of our knowledge, we herein describe for the first time a microfluidically assisted human liver sinusoid model specifically designed to mimic responses to liver inflammation that not only exhibits typical signs of pathophysiological liver dysfunction, but also reflects monocyte-mediated tissue repair and reduction of inflammation-triggered cell death.

Taken together, our biochip-based liver organoid exhibits highly similar responses to inflammatory stimulation as compared to those in mice undergoing sepsis. In absence of invading monocytes we observed an acute response ultimately resulting in hepatocellular dysfunction and cell death. However, circulating monocytes recruited to the vascular layer in response to inflammation that subsequently migrated into the stimulated organoid seem to act as modulators mediating different early and late inflammatory responses. Monocytes abrogated inflammation-related cell death and induced recovery of central metabolic functions in liver organoid even in the presence of LPS. Similar effects of a monocyte-mediated immune tolerance have been reported in animal models of sepsis and clinical studies[62]. Thus, the liver organoid confirms the importance of these processes for hepatocellular functions. *In vivo* models represent the integrated systemic response to sepsis. Nevertheless, they also possess technical limitations. Sophisticated technology, i.e. intravital microscopy is needed for real-time analysis of immune cells interacting with the organ. In addition, the isolation of specific cell types in response to stimulation/intervention for subsequent analyses or even subculture is complex. The risk of a potential bias provoked by time-consuming tissue resection and digestion is increased. The modular structure of the liver organoid allows studying the role of individual cell types, stimuli and factors involved in the specific response. In this context and in contrast to the *in vivo* situation of animal models where e.g. depletion of HSCs is not possible, organoid models offer the advantage of studying the function of specific cell types by omitting or including them within a physiological tissue environment. In principle, also genetically modified cells/cell types can be embedded in a cellular "wild type" environment to study specific gene functions in the course of a simulated pathogenesis. From the practical point of view, the multi-layered assembly of the organoid model allows an easy disassembly of the different layers of the organoid and parallel isolation and analysis of cells from separated vascular and hepatic layers. Moreover, in contrast to the restrictions given in respect to the number of time points for sample collection from severely injured mice due to limitations of repeated blood drawings, the organoid paves the way for analysis of close-meshed trajectories in a more detailed manner. We are aware of the structural limitations of the liver model, i.e. the distance of 400 μm medium-filled space between the vascular and hepatic cell layer in contrast to the Disse space were cell layers are much closer to each other. However, our data demonstrate a selective barrier function of the vascular layer and that the hepatic layer responds to migrating monocytes. In the vascular layer macrophages are also interspersed between endothelial cells. In this setting small gaps at the contact zones between these two cell types are formed. Although this is not a substitution of endothelial fenestrae this cell layer allows passage of larger molecules from the vascular to the hepatic layer. This is demonstrated by action of cytokines that originate from secretion at the vascular compartment of the organoid and the observed active migration of monocytes to the hepatic cell layer. Thus, the liver organoid model presented herein demonstrates the impact and relevance of the cellular crosstalk between major cell types of the liver in the context of inflammation. In this first proof-of-concept study this model system presents itself highly suitable to investigate inflammation-associated liver dysfunction. More detailed follow-up studies using primary human cells are required to further confirm transferability to human sepsis conditions. Furthermore, it is of certain interest to investigate whether culture of primary hepatocytes within biochip organoids prevents loss of the polarized hepatocyte-phenotype and cell dedifferentiation observed in normal cell culture.

Material and Methods

Biochips. MOTiF biochips were made from polystyrol (PS) and obtained from microfluidic ChipShop GmbH (Jena, Germany). Biochips were manufactured as described previously[18]. Briefly, chips were made by injection molding. Within the Biochip an area of 1,1 cm^2 is available for cell culture. The height of the vascular chamber is 700 μm, the hepatic chamber's height is 400 μm. The width of the afferent and efferent channels is 0,8 mm and 2 mm, the height of these channels is 0,6 mm and 0,4 mm, respectively. The medium volume of the upper chamber including the channel system is 220 μl. The lower chamber volume including channel system housing the hepatic layer is 120 μl. A 12 μm thick PET membrane with a pore diameter of 8 μm and a pore density of 1×10^5 pores/cm^2 (TRAKETCH Sabeu, Radeberg, Germany) was integrated. Chips and channels structures were sealed on top and bottom side with an extruded 140 μm thick PS film using a low-temperature proprietary bonding method. Gas permeable silicon tubing was used for perfusion allowing oxygen equilibration during experimentation. In addition, the biochips owe a high re-diffusion of oxygen through the PS bulk material and 140 μm thin PS sealing films. No shortcoming of oxygen inside the chambers could be observed at the vascular or hepatic cell layer during culture (*SI Appendix,* Fig. S8A,B). Oxygen saturation was measured as previously described[17]. Ramping structures have been introduced into the chip bulk to avoid unfavorable flow conditions and trapping of stationary bubbles. Bubble formation was reduced by oxygen plasma treatment for hydrophilization of the whole chip surface and perfusion medium was stirred and equilibrated overnight under perfusion conditions before use.

Oxygen measurement. Oxygen sensors were applied via spray coating at the inlet and outlet of each chamber, allowing online detection of oxygen consumption of cultivated cells. These sensors are based on dynamic quenching principle of luminescence by molecular oxygen and allow contactless measurements of oxygen via frame positioned polymer fibers. Read-out and data acquisition were accomplished by a commercially available oxygen meter (Firesting, Pyroscience, Aachen, Germany).

Cell culture and TLR-Stimulation. *HepaRG hepatocytes:* HepaRG cells were obtained from Biopredic International (Rennes, France). They were seeded at a density of $2,7 \times 10^4$ cells/cm^2 and cultured in William's Medium E (Biochrom, Berlin, Germany) containing 10% (v/v) FCS (GIBCO, Darmstadt, Germany), 5 μg/ml insulin (Sigma-Aldrich, Steinheim, Germany), 2 mM glutamine (GIBCO), 5×10^{-5} M hydrocortisone-hemisuccinate (Sigma-Aldrich) and 100 U/ml Penicillin/100 μg/ml Streptomycin mixture (Pen/Strep) (GIBCO). The cells were cultured in a humidified cell incubator at 5% CO_2 and 37 °C for 14 days before differentiation. Medium was renewed every 3–4 days. Cell differentiation was induced as described[63] and cells were used up to 4 weeks. Primary human cells: primary cell donors were informed about the aim of the study and gave written informed consent. The study and experimental protocols used therein were approved by the ethics committee of the Jena University Hospital (assigned study number 3939-12/13). *Endothelial cells:* HUVECs were isolated from human umbilical cord veins (HUVEC) as described[64]. Experiments were performed with HUVEC cells cultured in Endothelial Cell Medium (ECM) (Promocell, Heidelberg, Germany) up to passage 4, seeded with a density of 1.3×10^5 cells/cm^2 and cultured up to 95% confluence before sub-cultured. *Stellate cells:* LX-2 stellate cells were kindly provided by Scott L. Friedman (Division of Liver Diseases, Mount Sinai School of Medicine, New York City, NY, USA). LX-2 cells were cultured in Dulbecco's Minimum Essential Medium (DMEM) (Biochrom, Berlin, Germany) supplemented with 10% (v/v) FCS, 1 mM sodium pyruvate (GIBCO) and Pen/Strep and seeded with a density of 2.0×10^5 cells/cm^2. Cells were grown up to 95% confluence before sub-cultured. *Primary macrophages:* PBMCs of three different healthy donors were isolated by Ficoll density gradient centrifugation and seeded in 6- well dishes with a density of 1.0×10^6 cells/cm^2 in X-VIVO 15 medium (Lonza, Cologne, Germany) supplemented with 10% (v/v) autologous human serum, 10 ng/ml human granulocyte macrophage colony-stimulating factor (GM-CSF) (PeproTech, Hamburg, Germany) and Pen/Strep. After 3 h incubation in a humidified cell incubator at 5% CO_2 and 37 °C the cells were washed twice with *X-VIVO* 15 medium and subsequently used for liver organoid assembly. Typically, 5×10^5 monocytes per ml whole blood were obtained. Liver organoids were assembled by staggered seeding of vascular and hepatic cell layers. In each sterilized biochip 3×10^5 HUVEC's and 1×10^5 monocytes were mixed and seeded on top of the membrane in the upper chamber. HUVEC/monocytes were co-cultured for at least 5 days with a daily medium exchange in endothelial cell culture medium (ECM) supplemented 10 ng/ml epidermal growth factor, 90 μg/ml heparin, 2,8 μM hydrocortisone, endothelial cell growth supplement, 10 ng/ml GM-CSF to induce macrophage differentiation, 100 U/ml Penicillin/100 μg/ml Streptomycin and 10% (v/v) autologous human serum. Subsequently, 3×10^5 differentiated HepaRG cells and 4×10^4 LX-2 cells were seeded at the bottom sealing foil of the biochip in each bottom chamber and cultured for 24 hours in DMSO-free William's Medium E (Biochrom, Berlin, Germany) hepatocyte growth medium containing 50 μM hydrocortisone, 10% (v/v) FBS containing, 5 μg/ml insulin, 2 mM glutamine and 100 U/ml Penicillin/100 μg/ml Streptomycin prior to experimental use. Endothelial growth medium was used in the upper biochip chamber and hepatocyte growth medium in the lower biochip chamber as specific cell culture media during native liver organoid culture and TLR stimulation experiments for the vascular and hepatic cell layers, respectively. TLR agonist stimulation was performed by medium exchange of the lower cavity chamber with hepatocyte growth medium supplemented with 100 ng/ml lipopolysaccharide (LPS) from *E. coli* 026:B6 (Sigma Aldrich), 1 μg/ml Pam3CSK4 (InvivoGen, Toulouse, France) or 5 μM ODN2006 (InvivoGen). Medium containing TLR agonists was renewed every 24 h. Organoid assembly and experimental setting is shown in Supplementary Fig. 1A.

Monocyte migration assay. *Primary monocytes.* Monocytes were isolated from freshly isolated PBMCs of three different healthy donors using Dynabeads® CD14 Isolation Kit according to manufacturers protocol (Life Technologies, Darmstadt, Germany). Donors were informed about the aim of the study and gave written informed consent. The study was approved by the ethics committee of the Jena University Hospital. Typically, 5×10^5 monocytes per ml whole blood were obtained. *THP-1 monocytes:* THP-1 cells were obtained from DSMZ

(Braunschweig, Germany) and cultured in RPMI 1640 medium (GIBCO) supplemented with 10% (v/v) FCS, 1 mM sodium pyruvate and Pen/Strep. A total of 1×10^6 THP-1 or primary monocytes were suspended in 16,2 ml ECM and perfused for 60 min with a flow rate of 270 µl/min over the the endothelial cell layer. This flow rate corresponds to a relative shear stress of 3 dyn/cm² at the vascular cell layer.

After perfusion non-adherent cells were removed by perfusion of endothelial layer with cell free ECM medium for further 10 min with a flow rate of 270 µl/min. Subsequently, liver organoids were cultured for the indicated time periods under static conditions and observed effects compared to statically cultured controls without perfusion.

Analysis of CYP3A4 metabolite formation. Liver organoids were cultured for 72h in absence or presence of LPS, respectively. Medium was exchanged every 24 hours. Subsequently, liver organoids were incubated for 6 h with serum-free hepatocyte culture medium containing Midazolam (Rotexmedica, Trittau, Germany), provided as an aqueous solution at 13.8 mM (5 mg/ml) and diluted to a final concentration of 3 µM. After protein precipitation and concentration, samples were analyzed using an LC-MS/MS system consisting of an ABSciex QTrap 4000 tandem mass spectrometer (Darmstadt, Germany) equipped with a Turbo V ion spray source and coupled to a LC-20 liquid chromatography system (Shimadzu, Jena, Germany). Separation was performed on a ZORBAX Eclipse XDBC18 column (4.6 × 150 mm, 5 µm) from Agilent (Böblingen, Germany) using a gradient program with 50 mM ammonium formate buffer plus 0.75% formic acid (eluent A) and acetonitrile (eluent B). The mass spectrometer was operated in scheduled multiple reaction monitoring (MRM) mode using the target transition *m/z* 342 to 324 for quantification of 1-OH-midazolam. Instrument control, data acquisition, and data evaluation were performed using Analyst software 1.6.2 (ABSciex, Darmstadt, Germany).

Immunofluorescence staining and CDF-DA assay. For staining of cells of the hepatic cell layer the sealing foil of the biochip (serving as cell substrate) was carefully removed with a scalpel. For staining of cells from the vascular layer the suspended membrane was similarly removed. Cells were then fixed with 4% paraformaldehyde for 10 min at room temperature (RT). Staining was done with antibodies against: MRP-2, PECAM-1 (Cell Signaling, Leiden, The Netherlands), von Willebrand factor, VE-Cadherin (BD Biosciences), ApoB (Santa Cruz, Heidelberg, Germany), ZO-1 (Life Technologies, Karlsruhe, Germany), CYP3A4 (Merck-Millipore, Schwalbach, Germany) CD163 (Biolegend, United Kingdom), CD197 (BD BioScience), CD68 (Santa Cruz Biotechnology, Heidelberg, Germany) and secondary antibodies goat-anti-mouse-Cy3, goat-anti-rabbit-Cy5 (Dianova, Hamburg, Germany), goat-anti-rabbit-AlexaFluor488 and DAPI (Life Technologies). Samples were embedded into fluorescent mounting medium (Dako, Hamburg, Germany). MRP-2 activity analysis was performed by incubation of HepaRG cell layers in serum free Williams E medium (GIBCO) containing 5 µM 5(6)-Carboxy -2′,7′-dichlorofluorescein diacetate (CD-FDA) (Sigma-Aldrich) at 37 °C for 15 min. Subsequently, imaging was performed on an AXIO Observer Z1 fluorescence microscope with Apotome 2 extension (Carl Zeiss AG, Jena, Germany). Image analysis was done with ImageJ2 software.

FACS analysis. Cells of the vascular or hepatic layer were separately detached and collected from the biochip using 4 mg/ml Lidocaine and 5 mM EDTA (Sigma Aldrich) in PBS (Lonza). Flow cytometric analysis of ECs was performed using antibodies CD54-AF647 and CD106-APC (Biolegend, Fell, Germany). Transmigrated primary monocytes were collected in the lower chamber of the biochip. Monocytes were stained with CD45-FITC antibody (Immunotools, Friesoythe, Germany). Viability of cells from the hepatic layer was assessed by staining with Annexin V (conjugated to APC, BD Bioscience) for apoptotic cells and 7AAD (BD Bioscience) for dead cells. Flow cytometry was performed on a BD FACS-Canto II (BD Biosciences, Germany) with FACSDiva software and analyzed using FlowJo X software (FlowJo LLC, Ashland, OR, USA).

Cytometric bead array (CBA). Supernatants were collected after indicated time periods and immediately frozen at −80 °C. Cytokines were detected using CBA assay (BD Biosciences) according to the manufacturer's protocol. Enhanced sensitivity flex set was used for measurement of TNFα and IL-1β release. Secretion of IL-6, IL-10, sICAM-1 and sVCAM-1 was analyzed using standard CBA flex sets. Analysis was performed on a BD FACS-Canto II cytometer with FACSDiva software. Data analysis was performed using FCAP Array V3 software (Softflow, Pecs, Hungary).

Lactate, Glucose, Albumin, Urea, ASAT, ALAT, GLDH and LDH measurements. The respective parameters were measured in cell culture supernatants using the Abbott Architect ci8200 Integrated System (Abbott Laboratories, Abbott Park, IL, USA) according to the manufacturer's protocol.

Peritoneal contamination and infection in mice. Severe sepsis was induced using a peritoneal contamination and infection model by administration of standardized fecal slurry as described previously[44] and approved by the local animal welfare committee (TLLV, 02-037/12). Female C57Bl/6 mice (aged 12–14 weeks, n = 55) undergoing sepsis were monitored and resuscitated for four days (25 µL/g B.W. balanced saline solution, twice a day, s.c.). Starting six hours following insult, mice underwent antibiotic rescue (meropenem, 25 µg/g B.W., twice a day for four days, s.c.). Overall survival rate (21 days, unfavorable outcome was only observed in between first 72 hours) accounted to 74%. At time points indicated randomly selected mice were removed (at least five animals/time points), deeply anaesthetized for subsequent preparation of liver tissue and plasma samples. Parameters of organ (dys)function were determined using a Fuji Dri Chem 3000i analyzer according manufacturer's instructions.

RNA was isolated from freshly frozen tissue (25–30mg) applying RNeasy Mini Kit (QIAGEN, Hilden Germany). Via reverse transcription 1µg RNA was used to convert the mRNA fraction into single strand cDNA (Thermo Scientific, Germany). Using Rotorgene Q System (QIAGEN, Hilden Germany) expression rate of

CYP3A11(fw: 5′-agc agg gat gga cct gg-3′; rv: 5′-cgg tag agg agc acc aa-3′) and Mrp2 (fw: 5′-aac ttg ggt tgc tcc atg a-3′; rv: 5′-cag gac cag gat ttt gga ttt-3′) were tested and normalized to GusB (fw: 5′-gaa acc cgc cgc ata tta c-3′; rv: 5′-ccc cag gtc tgc atc ata tt-3′) according to the method of Pfaffl[65]. All tests were performed according to manufacturer's instructions. In parallel, freshly frozen tissue was equally used to determine enzyme activity of CYP3A family using the ethylmorphine N-demethylation model reaction as previously described[66].

Statistics. For each experiment shown at least three independent experiments have been performed. Statistical analysis has been performed with GraphPad Prism 6.05 (GraphPad Software, La Jolla, CA, USA). For analysis of statistical significance student's t-test, one-way ANOVA with Dunnett's multiple comparisons or two-way ANOVA with Dunnett's multiple comparisons test have been used as indicated.

References

1. Bauer, M., Press, A. T. & Trauner, M. The liver in sepsis: patterns of response and injury. *Curr. Opin. Crit. Care* **19,** 123–7 (2013).
2. Recknagel, P. *et al.* Liver Dysfunction and Phosphatidylinositol-3-Kinase Signalling in Early Sepsis: Experimental Studies in Rodent Models of Peritonitis. *PLoS Med* **9,** 9–10 (2012).
3. Ring, a & Stremmel, W. The hepatic microvascular responses to sepsis. *Semin. Thromb. Hemost.* **26,** 589–94 (2000).
4. Seok, J. *et al.* Genomic responses in mouse models poorly mimic human inflammatory diseases. *Proc. Natl. Acad. Sci. USA* **110,** 3507–3512 (National Acad Sciences, 2013).
5. Takao, K. & Miyakawa, T. Genomic responses in mouse models greatly mimic human inflammatory diseases. *Proc Natl Acad Sci USA* **112,** 1401965111– (2014).
6. Bouwens, L., Baekeland, M., De Zanger, R. & Wisse, E. Quantitation, tissue distribution and proliferation kinetics of Kupffer cells in normal rat liver. *Hepatology* **6,** 718–722 (1986).
7. Seki, E. *et al.* TLR4 enhances TGF-beta signaling and hepatic fibrosis. *Nat Med* **13,** 1324–1332 (2007).
8. Kmiec, Z. & Kmieć, Z. Cooperation of liver cells in health and disease. *Adv Anat Embryol Cell Biol* **161,** III–XIII, 1–151 (2001).
9. Kordes, C., Sawitza, I., Haussinger, D. & Häussinger, D. Hepatic and pancreatic stellate cells in focus. *Biol Chem* **390,** 1003–1012 (2009).
10. Weiskirchen, R. & Tacke, F. Cellular and molecular functions of hepatic stellate cells in inflammatory responses and liver immunology. *Hepatobiliary Surg Nutr* **3,** 344–363 (2014).
11. Godoy, P. *et al.* Recent advances in 2D and 3D *in vitro* systems using primary hepatocytes, alternative hepatocyte sources and non-parenchymal liver cells and their use in investigating mechanisms of hepatotoxicity, cell signaling and ADME. *Arch Toxicol* **87,** 1315–1530 (2013).
12. LeCluyse, E. L., Witek, R. P., Andersen, M. E. & Powers, M. J. Organotypic liver culture models: Meeting current challenges in toxicity testing. *Crit. Rev. Toxicol.* **42,** 501–548 (2012).
13. Osuchowski, M. F., Craciun, F., Weixelbaumer, K. M., Duffy, E. R. & Remick, D. G. Sepsis chronically in MARS: systemic cytokine responses are always mixed regardless of the outcome, magnitude, or phase of sepsis. *J Immunol* **189,** 4648–4656 (2012).
14. Toh, Y.-C. C. *et al.* A microfluidic 3D hepatocyte chip for drug toxicity testing. *Lab Chip* **9,** 2026–2035 (2009).
15. Messner, S., Agarkova, I., Moritz, W. & Kelm, J. M. Multi-cell type human liver microtissues for hepatotoxicity testing. *Arch Toxicol* **87,** 209–213 (2013).
16. Wagner, I. *et al.* A dynamic multi-organ-chip for long-term cultivation and substance testing proven by 3D human liver and skin tissue co-culture. *Lab Chip* **13,** 3538–3547 (2013).
17. Rennert, K. *et al.* A microfluidically perfused three dimensional human liver model. *Biomaterials* **71,** 119–131 (2015).
18. Raasch, M. *et al.* Microfluidically supported biochip design for culture of endothelial cell layers with improved perfusion conditions. *Biofabrication* **7,** 15013 (2015).
19. Hotchkiss, R. S., Monneret, G. & Payen, D. Sepsis-induced immunosuppression: from cellular dysfunctions to immunotherapy. *Nat Rev Immunol* **13,** 862–874 (2013).
20. Cerec, V. *et al.* Transdifferentiation of hepatocyte-like cells from the human hepatoma HepaRG cell line through bipotent progenitor. *Hepatology* **45,** 957–967 (2007).
21. Aninat, C. *et al.* Catecholamines induce an inflammatory response in human hepatocytes. *Crit Care Med* **36,** 848–54 (2008).
22. Rubin, L. L. *et al.* A cell culture model of the blood-brain barrier. *J. Cell Biol.* **115,** 1725–1735 (1991).
23. Wake, K. Hepatic stellate cells: Three-dimensional structure, localization, heterogeneity and development. *Proc Jpn Acad Ser B Phys Biol Sci* **82,** 155–164 (2006).
24. Guillouzo, A. & Guguen-Guillouzo, C. Evolving concepts in liver tissue modeling and implications for *in vitro* toxicology. *Expert Opin. Drug Metab. Toxicol.* **4,** 1279–1294 (2008).
25. Klein, M. *et al.* A Systematic Comparison of the Impact of Inflammatory Signaling on Absorption, Distribution, Metabolism, and Excretion Gene Expression and Activity in Primary Human Hepatocytes and HepaRG Cells. *Drug Metab Dispos* **43,** 273–283 (2015).
26. Denis, C. V. Molecular and cellular biology of von Willebrand factor. *Int J Hematol* **75,** 3–8 (2002).
27. Privratsky, J. R., Newman, D. K. & Newman, P. J. PECAM-1: conflicts of interest in inflammation. *Life Sci* **87,** 69–82 (2010).
28. Khetani, S. R. & Bhatia, S. N. Microscale culture of human liver cells for drug development. *Nat. Biotechnol.* **26,** 120–6 (2008).
29. Luo, G., Guenthner, T., Gan, L. S. & Humphreys, W. G. CYP3A4 induction by xenobiotics: biochemistry, experimental methods and impact on drug discovery and development. *Curr Drug Metab* **5,** 483–505 (2004).
30. Moriya, N., Kataoka, H., Fujino, H., Nishikawa, J. & Kugawa, F. Different expression patterns of hepatic cytochrome P450 s during anaphylactic or lipopolysaccharide-induced inflammation. *Pharmazie* **69,** 1–6 (2014).
31. Levels, J. H. M., Lemaire, L. C. J. M., van den Ende, A. E., van Deventer, S. J. H. & van Lanschot, J. J. B. Lipid composition and lipopolysaccharide binding capacity of lipoproteins in plasma and lymph of patients with systemic inflammatory response syndrome and multiple organ failure. *Crit Care Med* **31,** 1647–1653 (2003).
32. Geier, A., Fickert, P. & Trauner, M. Mechanisms of disease: mechanisms and clinical implications of cholestasis in sepsis. *Nat Clin Pr. Gastroenterol Hepatol* **3,** 574–585 (2006).
33. Zamek-Gliszczynski, M. J. *et al.* Pharmacokinetics of 5 (and 6)-carboxy-2′,7′-dichlorofluorescein and its diacetate promoiety in the liver. *J. Pharmacol. Exp. Ther.* **304,** 801–9 (2003).
34. Aird, W. C. The role of the endothelium in severe sepsis and multiple organ dysfunction syndrome. *Blood* **101,** 3765–3777 (2003).
35. van Oosten, M., van de Bilt, E., van Berkel, T. J. & Kuiper, J. New scavenger receptor-like receptors for the binding of lipopolysaccharide to liver endothelial and Kupffer cells. *Infect Immun* **66,** 5107–5112 (1998).
36. Géraud, C. *et al.* Unique cell type-specific junctional complexes in vascular endothelium of human and rat liver sinusoids. *PLoS One* **7,** e34206 (2012).
37. Desai, T. R., Leeper, N. J., Hynes, K. L. & Gewertz, B. L. Interleukin-6 causes endothelial barrier dysfunction via the protein kinase C pathway. *J Surg Res* **104,** 118–123 (2002).
38. Kjaergaard, A. G., Dige, A., Krog, J., Tønnesen, E. & Wogensen, L. Soluble Adhesion Molecules Correlate with Surface Expression in an *In Vitro* Model of Endothelial Activation. *Basic & Clinical Pharmacology & Toxicology* **113,** 273–279 (2013).

39. Wang, H. E. *et al.* Inflammatory and endothelial activation biomarkers and risk of sepsis: a nested case-control study. *J Crit Care* **28,** 549–555 (2013).
40. Nomura, Y. *et al.* Phenotype for activated tissue macrophages in histiocytic necrotizing lymphadenitis. *Pathol. Int.* **59,** 631–5 (2009).
41. Mantovani, A., Sozzani, S., Locati, M., Allavena, P. & Sica, A. Macrophage polarization: Tumor-associated macrophages as a paradigm for polarized M2 mononuclear phagocytes. *Trends Immunol.* **23,** 549–555 (2002).
42. Gonnert, F. A. *et al.* Hepatic Fibrosis in a Long-term Murine Model of Sepsis. *Shock* **37,** 399–407 (2012).
43. Gonnert, F. A. *et al.* Characteristics of clinical sepsis reflected in a reliable and reproducible rodent sepsis model. *J. Surg. Res.* **170,** e123–34 (2011).
44. Otto, G. P. *et al.* Impact of antibiotic treatment intensity on long-term sepsis-associated kidney injury in a polymicrobial peritoneal contamination and infection model. *Nephron* **129,** 137–42 (2015).
45. Recknagel, P., Claus, R. A., Neugebauer, U., Bauer, M. & Gonnert, F. A. *In vivo* imaging of hepatic excretory function in the rat by fluorescence microscopy. *J Biophotonics* **5,** 571–81 (2012).
46. Aitken, A. E. & Morgan, E. T. Gene-specific effects of inflammatory cytokines on cytochrome P450 2C, 2B6 and 3A4 mRNA levels in human hepatocytes. *Drug Metab Dispos* **35,** 1687–1693 (2007).
47. Lekkou, A., Mouzaki, A., Siagris, D., Ravani, I. & Gogos, C. A. Serum lipid profile, cytokine production, and clinical outcome in patients with severe sepsis. *J. Crit. Care* **29,** 723–7 (2014).
48. Figueras-Aloy, J. *et al.* Serum soluble ICAM-1, VCAM-1, L-selectin, and P-selectin levels as markers of infection and their relation to clinical severity in neonatal sepsis. *Am J Perinatol* **24,** 331–338 (2007).
49. Billiar, T. R., Curran, R. D., Williams, D. L. & Kispert, P. H. Liver nonparenchymal cells are stimulated to provide interleukin 6 for induction of the hepatic acute-phase response in endotoxemia but not in remote localized inflammation. *Arch Surg* **127,** 31–37 (1992).
50. Harvey, S. A. K., Dangi, A., Tandon, A. & Gandhi, C. R. The transcriptomic response of rat hepatic stellate cells to endotoxin: implications for hepatic inflammation and immune regulation. *PLoS One* **8,** e82159 (2013).
51. Schildberger, A., Rossmanith, E., Eichhorn, T., Strassl, K. & Weber, V. Monocytes, peripheral blood mononuclear cells, and THP-1 cells exhibit different cytokine expression patterns following stimulation with lipopolysaccharide. *Mediators Inflamm.* **697972,** 697972 (2013).
52. Makó, V. *et al.* Proinflammatory activation pattern of human umbilical vein endothelial cells induced by IL-1β, TNF-α, and LPS. *Cytom. Part A* **77A,** 962–970 (2010).
53. Lawson, C. & Wolf, S. ICAM-1 signaling in endothelial cells. *Pharmacol. Rep.* **61,** 22–32 (2009).
54. Campion, S. N. *et al.* Hepatic Mrp4 induction following acetaminophen exposure is dependent on Kupffer cell function. *Am J Physiol Gastrointest Liver Physiol* **295,** G294–304 (2008).
55. Holt, M. P., Cheng, L. & Ju, C. Identification and characterization of infiltrating macrophages in acetaminophen-induced liver injury. *J Leukoc Biol* **84,** 1410–1421 (2008).
56. Tacke, F. & Zimmermann, H. W. Macrophage heterogeneity in liver injury and fibrosis. *J Hepatol* **60,** 1–17 (2014).
57. Porcheray, F. *et al.* Macrophage activation switching: An asset for the resolution of inflammation. *Clin. Exp. Immunol.* **142,** 481–489 (2005).
58. Murray, P. J. & Wynn, T. A. Protective and pathogenic functions of macrophage subsets. *Nat Rev Immunol* **11,** 723–737 (2011).
59. Shalova, I. N. *et al.* Human monocytes undergo functional re-programming during sepsis mediated by hypoxia-inducible factor-1alpha. *Immunity* **42,** 484–498 (2015).
60. Esch, M. B. *et al.* Multi-cellular 3D human primary liver cell culture elevates metabolic activity under fluidic flow. *Lab Chip* **15,** 2269–2277 (2015).
61. Prodanov, L. *et al.* Long-term maintenance of a microfluidic 3D human liver sinusoid. *Biotechnol. Bioeng.* **113,** 1–10 (2015).
62. Hotchkiss, R. S. & Opal, S. Immunotherapy for sepsis–a new approach against an ancient foe. *N Engl J Med* **363,** 87–89 (2010).
63. Gripon, P. *et al.* Infection of a human hepatoma cell line by hepatitis B virus. *Proc Natl Acad Sci USA* **99,** 15655–15660 (2002).
64. Jaffe, E. A., Nachman, R. L., Becker, C. G. & Minick, C. R. Culture of human endothelial cells derived from umbilical veins. Identification by morphologic and immunologic criteria. *J Clin Invest* **52,** 2745–56 (1973).
65. Pfaffl, M. W. A new mathematical model for relative quantification in real-time RT-PCR. *Nucleic Acids Res.* **29,** e45 (2001).
66. Klinger, W. & Müller, D. Ethylmorphine-N-demethylation by liver homogenate of newborn and adult rats; Enzyme kinetics and age course of Vmax and Km1. *Acta Biol. Med. Ger.* **36,** 1149–59 (1977).

Acknowledgements

We thank Torsten Mayr and Josef Ehgartner (Institute of Analytical Chemistry and Food Chemistry, Graz University of Technology, Graz, Austria) for providing oxygen sensors. We are grateful to the excellent technical work of Maria Franke, Margot Voigt and Daniela Remane. We thank the team of the Placenta Laboratory of the Jena University Hospital for supplying umbilical cords for HUVEC isolation. The authors would further like to acknowledge support of this work by 2011 VF 0005 grant of the Thüringer Aufbaubank. This work was further supported by the Federal Ministry of Education and Research (BMBF), Germany, FKZ: 01EO1002.

Author Contributions

M.G., K.R., B.G., E.W., J.D. and A.L. performed the experiments. F.T.P., M.K., R.A.C., M.B. and O.H. contributed reagents/materials/analysis tools. F.T.P., R.A.C., M.K. and A.S.M. analyzed the data. A.L., H.F., M.B. and R.A.C. wrote parts of the manuscript. O.H. and A.S.M. wrote the manuscript. R.A.C. and A.S.M. designed the study and supervised experiments.

Additional Information

Supplementary information accompanies this paper at http://www.nature.com/srep

Competing financial interests: The authors declare no competing financial interests.

How to cite this article: Gröger, M. *et al.* Monocyte-induced recovery of inflammation-associated hepatocellular dysfunction in a biochip-based human liver model. *Sci. Rep.* **6**, 21868; doi: 10.1038/srep21868 (2016).

Manuscript II – Supplementary information

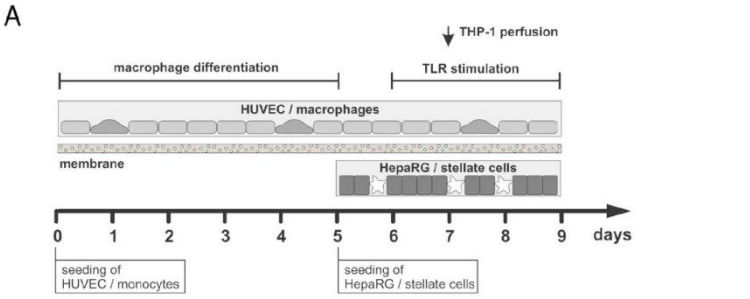

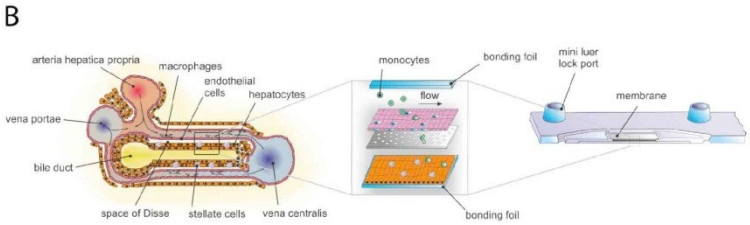

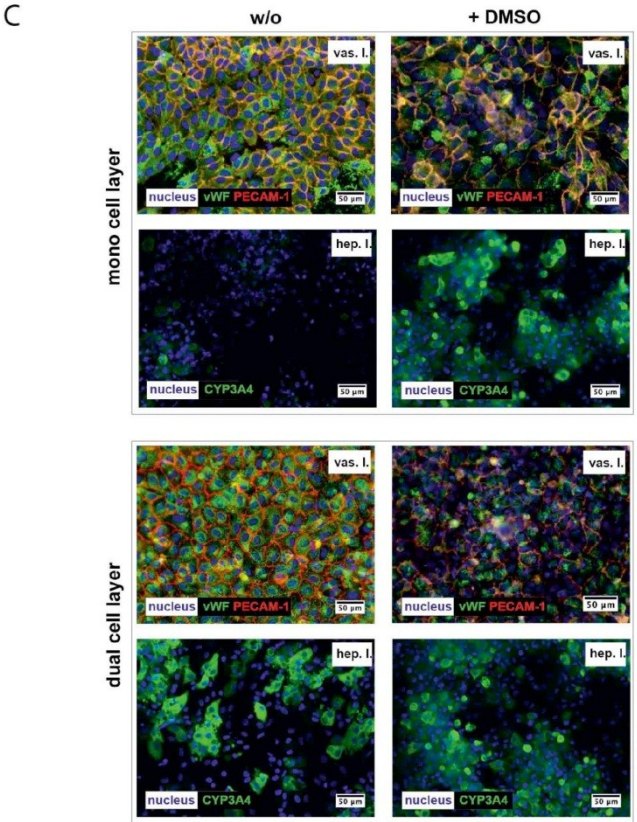

Supplementary Figure 1. A) Timeline of organoid assembly and experimental setting. B) Principle structure of the human sinusoid and abstracted implementation as tissue layers in the MOTiF biochip. C) Effects of DMSO addition on expression of von Willebrand Factor (vWF, green) and PECAM-1 (red) on vascular layers (vas. l.), and CYP3A4 on hepatic layers (hep. l.) in mono cell layer and dual cell layer culture. Representative data out of five independent experiments are shown. Nuclei are stained with DAPI (blue).

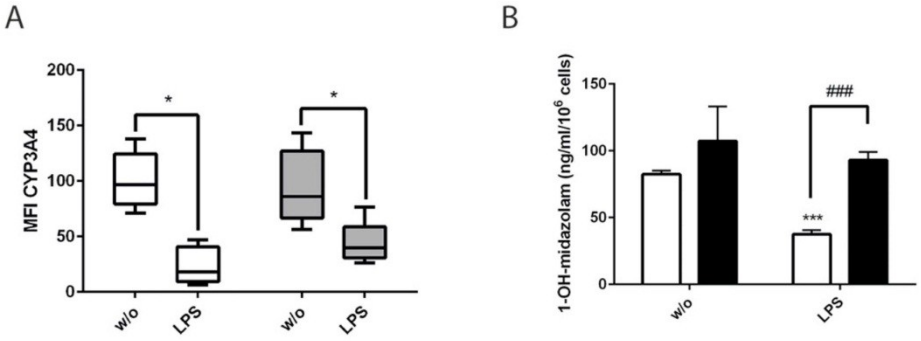

Supplementary Figure 2. A) Expression of CYP3A4 after 72 h of LPS treatment in mono-cell cultures of HepaRG cells (open bars) and HepaRG cells co-cultured with stellate cells (grey bars). Computational analyses of fluorescence intensities of at least 20 ROIs per condition and experiment (labeled as mean immunofluorescence intensity (MFI) of specific stainings of CYP3A4) of three independent experiments. B) Formation rate of 1-OH-midazolam in HepaRG mono-cell cultures (open bars) and in liver organoids (black bars) of three independent experiments. Statistical significance was calculated compared to untreated control (* $p < 0.05$, *** $p < 0.01$) or between indicated conditions (## $p < 0.01$, ## $p < 0.001$) using student's t-test.

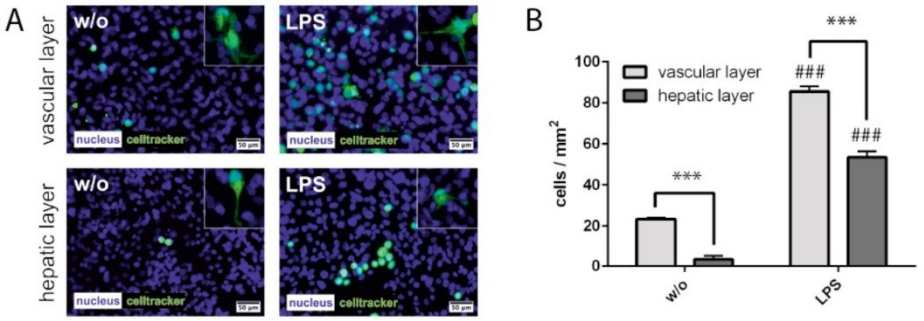

Supplementary Figure 3. A) Flow-based adhesion and migration assay of THP-1 monocytes stained with Celltracker® Green at the vascular and hepatic layer of liver organoids in absence (w/o) of LPS or liver organoids 24 h pre-stimulated with LPS. Nuclei are stained with DAPI (blue). Representative data out of three independent experiments are shown. B) Number of adhesive and transmigrated THP-1 monocytes at the vascular or hepatic layer 48 h post monocyte perfusion. Statistical significance was calculated between indicated conditions (*** $p < 0.001$) or compared to the corresponding condition without LPS treatment (### $p < 0.001$) using student's t-test. Results of three independent experiments are shown.

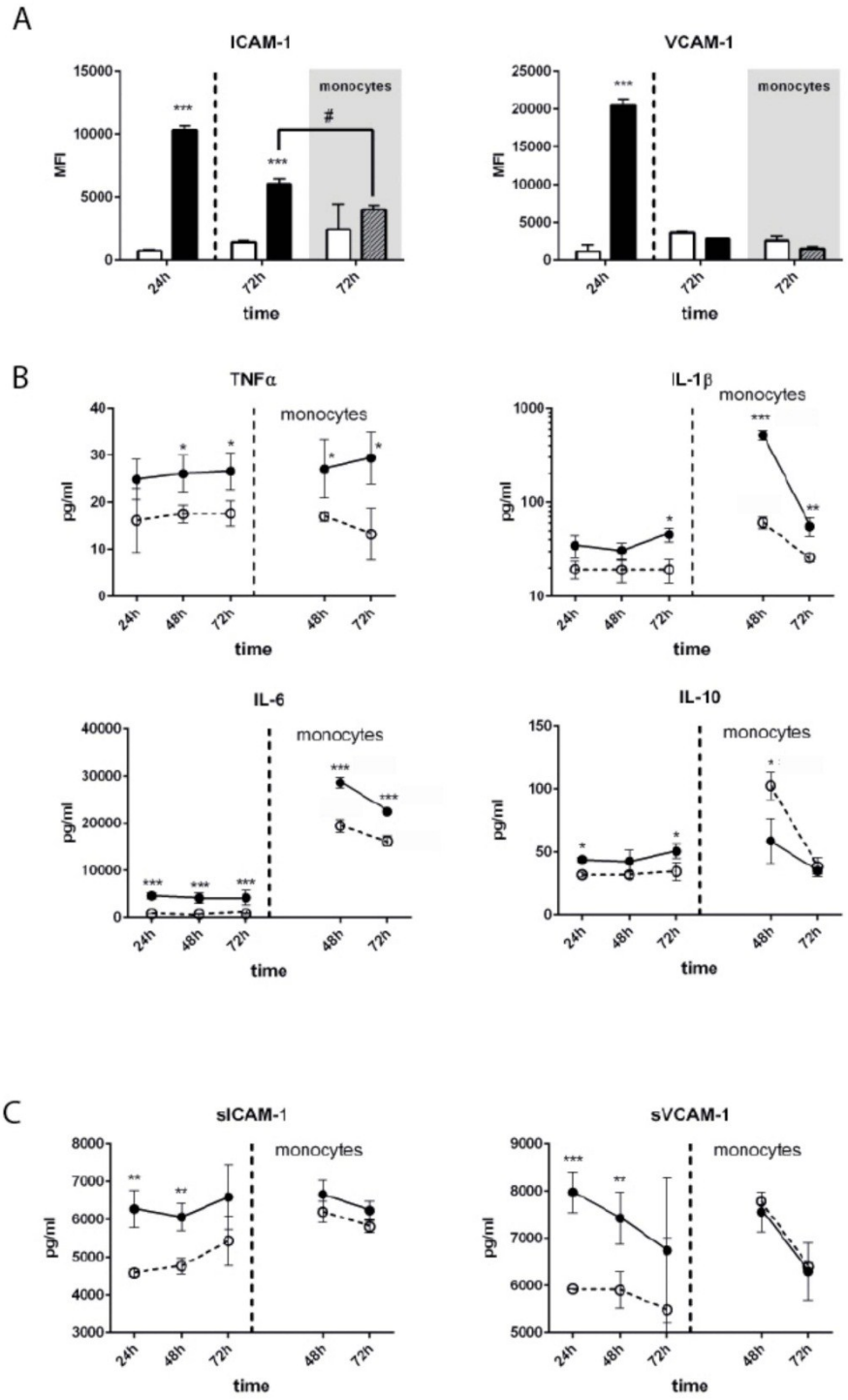
A
ICAM-1
VCAM-1
MFI
monocytes
time
B
TNFα
IL-1β
IL-6
IL-10
pg/ml
C
sICAM-1
sVCAM-1

Supplementary Figure 4. A) Expression of endothelial cell adhesion molecules (CAMs) and release of soluble CAMs and cytokines by THP-1 monocytes. A) Surface expression of CAMs of untreated (open bars) and LPS-treated liver organoids (black bars) after 24 h and 72 h without THP-1 monocyte perfusion (white background) and with THP-1 monocyte perfusion (grey background). Flow cytometric analyses of mean fluorescence intensities (MFI) of fluorescence-labeled antibodies directed against endothelial ICAM and VCAM, respectively. Statistical significance was calculated between untreated and LPS treated liver organoids of identical time points (*** $p < 0.001$) or between indicated conditions (# $p < 0.05$) using student's t-test. B) CBA assay of released sICAM and sVCAM in response to THP-1 perfusion and adhesion. C) Secretion of IL-1β, IL-6, TNFα and IL-10 in response to THP-1 perfusion and adhesion. Liver organoids were untreated (dashed line) or stimulated with LPS (solid line), without THP-1 monocyte perfusion (left from vertical dashed line) or with THP-1 monocyte perfusion (right from vertical dashed line, monocytes). A-C) Statistical significance was calculated between untreated and LPS-treated liver organoids of identical time points and perfusion conditions (* $p < 0.05$, ** $p < 0.01$, *** $p < 0.001$) using student's t-test. Results of three independent experiments are shown. B-C) Data of liver organoids without monocyte perfusion are identical to data used in Fig. 4.

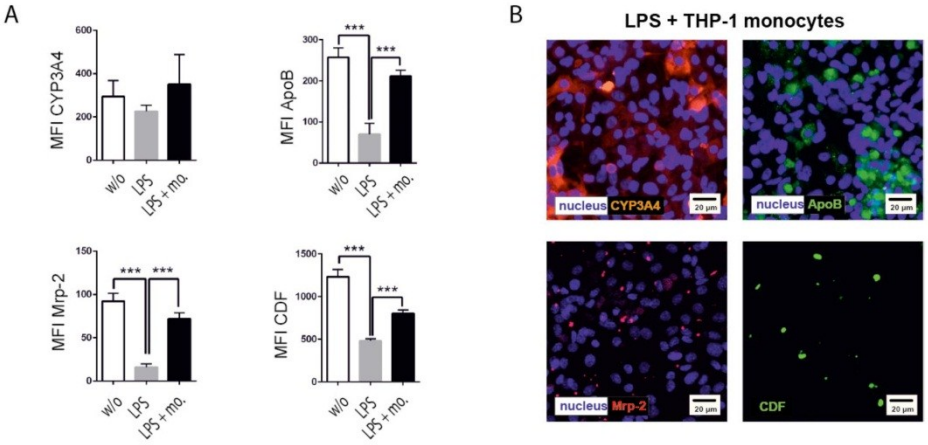

Supplementary Figure 5 A) Computational analyses of fluorescence intensities of hepatocyte proteins without stimulation (w/o) and in presence of 100 ng/ml LPS (LPS) or 100 ng LPS and THP-1 monocytes (LPS + mo.) of at least 20 ROI per tested condition (labeled as mean immunofluorescence intensity (MFI) of specific staining of the respective protein) of three independent experiments using random field analysis of the hepatic layer. Statistical significance was calculated between indicated conditions using student's t-test (* $p < 0.05$, ** $p < 0.01$, $p < 0.001$). B) Liver organoids treated with LPS in presence of invading THP-1 monocytes. Immunostainings of the hepatic layer for CYP3A4 (red), ApoB (green), MRP-2 (red) and detection of CDF secretion (green). Nuclei are stained with DAPI (blue). Representative results of three independent experiments are shown.

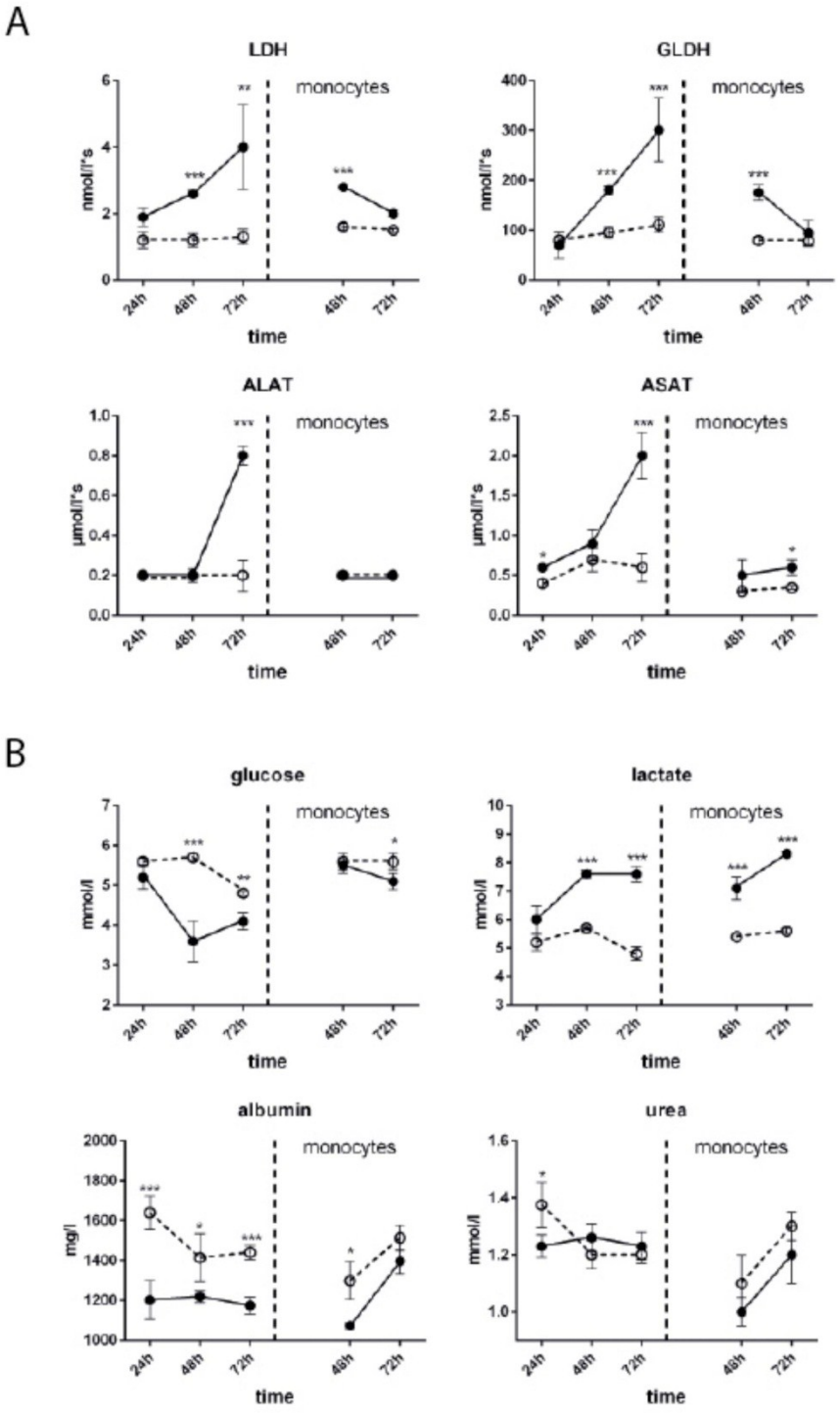
A
LDH
monocytes
nmol/l*s
time
GLDH
monocytes
nmol/l*s
time
ALAT
monocytes
µmol/l*s
time
ASAT
monocytes
µmol/l*s
time
B
glucose
monocytes
mmol/l
time
lactate
monocytes
mmol/l
time
albumin
monocytes
mg/l
time
urea
monocytes
mmol/l
time
24h
48h
72h

Supplementary Figure 6 A-B) Release of intracellular enzymes and metabolic activity of the liver organoid. Liver organoids were untreated (dashed line) or stimulated with LPS (solid line), without monocyte perfusion (left from vertical dashed line) or with THP-1 monocyte perfusion (monocytes, right from vertical dashed line). A) Release of lactate-dehydrogenase (LDH), glutamate-dehydrogenase (GLDH), aspartate-transaminase (ASAT) and alanine-transaminase (ALAT). B) Changes in glucose, lactate, albumin and urea levels. Statistical significance was calculated compared to untreated control (* $p < 0.05$, ** $p < 0.01$, *** $p < 0.001$) at the corresponding time points with similar perfusion conditions using student's t-test. A-B) Data of liver organoids without monocyte perfusion are identical to data used in Fig. 6.

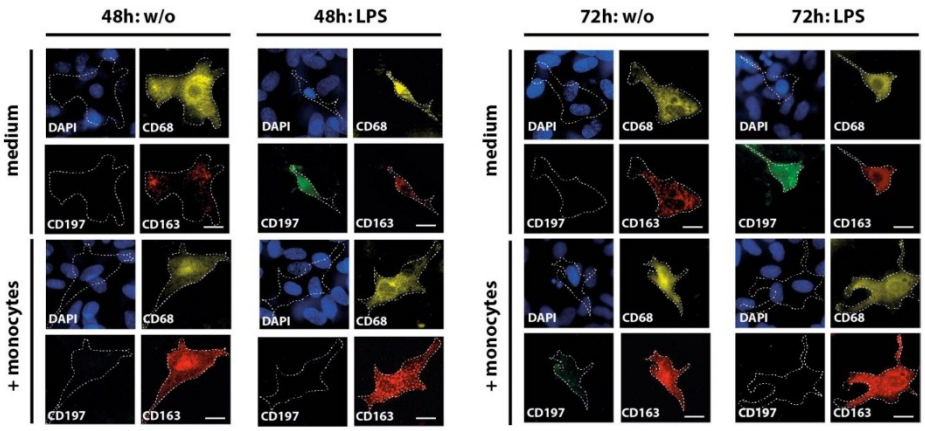

Supplementary Figure 7. Liver organoids were cultured for 48 h or 72 h. Untreated (w/o) or LPS-stimulated (LPS) organoids were perfused with medium (medium) or medium containing primary monocytes (+ monocytes). Macrophages residing in the vascular layer of the liver organoid were immunostained for macrophage marker protein CD68 (yellow), M1-polarization marker protein CD197 (green) and M2-polarization marker protein CD163 (red). Nuclei were stained with DAPI (blue). Cell borders are indicated by dashed lines. Scale bar 10µm.

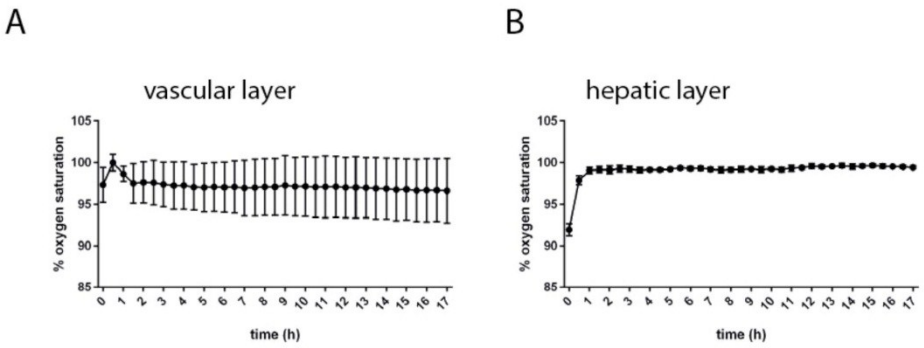

Supplementary Figure 8. A-B) Oxygen level in the A) vascular and B) hepatic chamber within MOTiF biochips during liver organoid culture. A 100% oxygen saturation corresponds to 20,942 % atmospheric O_2. Shown is the mean of percent oxygen saturation of three independent measurements with respective standard deviation.

3.3 Manuscript III

Preservation of cell structure, metabolism and biotransformation activity of liver-on-chip organ models by hypothermic storage

---

Gröger M, Dinger J, Kiehntopf M, Peter FT, Rauen U, Mosig AS

Published in:
Advanced Healthcare Materials, 2018, 7(2).

Cryopreservation is a valuable tool to maintain the viability and function of explanted organs, i.e. for liver transplantation. For the first time we here describe a method for hypothermal storage (4 °C) of a microphysiological human liver model for up to two days. Evaluation of five different formulated solutions revealed best results for an adapted derivative of the TiProtec® solution complemented with PEG, iron chelators and a balanced composition of physiological ions (including Ca^{2+}, Cl^{-}, Mg^{2+} and K^{+}). This solution was shown to preserve the morphology, metabolism and immune response of liver-on-a-chip models after cold storage. No alterations of cell function were found for barrier integrity (VEC staining), hepatocyte-specific bile canaliculi function (5 (and 6)-carboxy-2′,7′-dichlorofluorescein (CDF) secretion rate) and CYP3A4 activity (midazolam turnover) after storage, compared to fresh models. Furthermore, immune cell activity in response to LPS stimulation was fully maintained as proven by the release of pro-inflammatory cytokines and its effect on metabolic alterations in hepatocytes. Taken together, this new approach showed feasibility of hypothermal storage for the preservation complex biochip-based liver tissues. The novel storage protocol will allow a broader use of these microphysiological models, i.e. in routine drug testing, and contribute to foster its application as a real alternative to animal experimentation.

FULL PAPER

Hypothermal Storage

ADVANCED HEALTHCARE MATERIALS

www.advhealthmat.de

Preservation of Cell Structure, Metabolism, and Biotransformation Activity of Liver-On-Chip Organ Models by Hypothermic Storage

*Marko Gröger, Julia Dinger, Michael Kiehntopf, Frank T. Peters, Ursula Rauen, and Alexander S. Mosig**

The liver is a central organ in the metabolization of nutrition, endogenous and exogenous substances, and xenobiotic drugs. The emerging organ-on-chip technology has paved the way to model essential liver functions as well as certain aspects of liver disease in vitro in liver-on-chip models. However, a broader use of this technology in biomedical research is limited by a lack of protocols that enable the short-term preservation of preassembled liver-on-chip models for stocking or delivery to researchers outside the bioengineering community. For the first time, this study tested the ability of hypothermic storage of liver-on-chip models to preserve cell viability, tissue morphology, metabolism and biotransformation activity. In a systematic study with different preservation solutions, liver-on-chip function can be preserved for up to 2 d using a derivative of the tissue preservation solution TiProtec, containing high chloride ion concentrations and the iron chelators LK614 and deferoxamine, supplemented with polyethylene glycol (PEG). Hypothermic storage in this solution represents a promising method to preserve liver-on-chip function for at least 2 d and allows an easier access to liver-on-chip technology and its versatile and flexible use in biomedical research.

1. Introduction

The liver is a central organ in the metabolization of carbohydrates, lipids, and proteins from nutrition, biotransformation of drugs, and detoxification of xenobiotics. The organ is composed of non-parenchymal cells (endothelial cells, Kupffer cells, and stellate cells) and hepatocytes that are separated from the endothelial lining by the space of Disse.

The emerging organ-on-chip technology has paved the way to model liver metabolism in vitro. Liver-on-chip models create new possibilities for biomedical research, i.e., modeling molecular and cellular aspects of diseases, and are valuable tools in the development of novel tailored treatment strategies.[1–3] We recently introduced a novel 3D liver-on-chip model that reflects essential aspects of the micro-physiological conditions and the metabolism of the human liver in vitro.[4] Biochips were used to coculture human cells in two layers separated by a porous membrane mimicking the space of Disse. In the upper cell layer that forms the vascular compartment of the liver-on-chip model, human umbilical vein endothelial cells (HUVECs) were cocultured with human monocyte-derived macrophages. A second layer at the opposite side of the membrane is composed of HepaRG hepatocytes cocultured with LX-2 stellate cells. Microfluidic perfusion of the liver model allows the supply with nutrition and the removal of catabolic waste products, thus enabling enhanced metabolic activity and in vivo-like metabolism of biochip-embedded artificial liver tissues for up the 7 d of culture.[4] However, a broad use of organ-on-chip models in biomedical research and drug screening outside tissue engineering laboratories requires optimized storage protocols to enable, i.e., shipment of standardized and preassembled organ models to end users.

Hypothermic storage is widely used for preservation of cell, tissue, or organ function.[5–10] Cold storage in special preservation solutions limits the metabolic activity and avoids the adverse effects of shortage in oxygen and nutrition availability in the surrounding medium, i.e., energy deficiency and subsequent cell injury.[6,7,11] The traditional preservation solutions used in transplantation medicine, such as University of Wisconsin solution (UW) and histidine–tryptophan–ketoglutarate solution (HTK), are adapted to the intracellular ion composition and possess a low chloride content and impermeants to avoid cell swelling during cold storage and a high buffering capacity to avoid acidosis during ischemia.[5,12] However, they

M. Gröger, Dr. A. S. Mosig
Center for Sepsis Control and Care
Jena University Hospital
07747 Jena, Germany
E-mail: alexander.mosig@med.uni-jena.de
Dr. J. Dinger, Dr. F. T. Peters
Institute of Forensic Medicine
Jena University Hospital
07747 Jena, Germany
Dr. M. Kiehntopf
Institute of Clinical Chemistry and Laboratory Diagnostics
Jena University Hospital
07747 Jena, Germany
Prof. U. Rauen
Institut für Physiologische Chemie
Universitätsklinikum Essen
45112 Essen, Germany
The ORCID identification number(s) for the author(s) of this article can be found under https://doi.org/10.1002/adhm.201700616.

DOI: 10.1002/adhm.201700616

ADVANCED SCIENCE NEWS
www.advancedsciencenews.com

ADVANCED HEALTHCARE MATERIALS
www.advhealthmat.de

were developed in the sixties and seventies of the last century and some concepts have changed since. Thus, it has been shown that hypothermia can also elicit cell injury in its own right and that this cell injury is not mediated by cell swelling but by an iron-dependent formation of reactive oxygen species.[13] Especially endothelial cells proved to be very sensitive to this iron-dependent hypothermic injury, but also hepatocytes, kidney cells and many other cell types are affected.[14] This hypothermic injury has been shown to display apoptotic features and is primarily mediated by a cold-induced increase in cytosolic redox-active iron ions followed by a mitochondrial permeability transition.[14,15] Thus, it can be inhibited by membrane-permeable iron chelators. In addition, a second-line hypothermic injury appears to occur in several cell types: This appears to be mediated by chloride ions in rat hepatocytes, but not in human hepatocytes.[16,17] While chloride-poor solutions protect rat hepatocytes during cold storage,[16] chloride-rich solutions proved to be superior for human hepatocytes,[17] for the storage of isolated blood vessels,[18] for aortic endothelial cells,[14] and for the maintenance of the microcirculation of cold-stored rat livers.[19] These results and the finding of a relatively high toxicity of the traditional organ preservation solutions[20] prompted the development of a new organ preservation solution.[19] As the needs of isolated cells and smaller tissue samples during cold storage differ from the need of whole organs (e.g., lower requirement of buffering capacity due to altered cell to storage solution ratio), a derivative of this organ preservation solution Custodiol-N was optimized for the hypothermic storage of blood vessels or smaller tissue samples.[18] This solution, TiProtec, which is an *N*-acetylhistidine-buffered, chloride-rich solution containing the iron chelators deferoxamine and LK614 did not only improve the hypothermic storage of porcine[18] and human[21] blood vessels, but also proved superior to existing solutions for the cold storage of human hepatocytes,[17] when used in a modification with a higher concentration of deferoxamine. For the cold storage of rat hepatocytes in suspension, however, a chloride-poor variant of the latter solution yielded the best results.[17,22]

In the present study, we have tested these three variants of the cell/tissue preservation solution and two additional, not yet published variants, for the hypothermic storage of liver-on-chip models, that consist of bioengineered liver tissue, composed of four different cell types and embedded in microfluidically perfused biochips.[23,24]

In the first part of the study we tested the individual impact of chloride ion concentrations, addition of dextran or polyethylene glycol (PEG) and iron chelators in the tissue preservation solution on cell viability, morphology, and maintenance of typical cell type markers. The most promising variants were then characterized for their ability to preserve cellular morphology, metabolism, biotransformation rate, and 5(6)-carboxy-2′,7′-dichlorofluorescein (CDF) secretion activity in microfluidically perfused liver-on-chip models.

2. Results

The individual preservation capacity of the five storage solutions was first analyzed for cocultures of HUVECs with macrophages and HepaRG with LX-2 cells under static culture conditions. The storage solutions used were the vascular preservation solution TiProtec (termed low_Defer solution), a previously used derivative of it with a higher concentration of the iron chelator deferoxamine[17] (termed standard), a chloride-poor variant of the standard cell preservation solution in which the organic anion lactobionate was used as substitute for most of the chloride ions (termed low_Cl^- solution), a variant of the standard cell preservation solution supplemented with dextran 40 000, a macromolecular additive which has been shown to enhance hypothermic lung storage,[25] here designated dextran solution, and a variant in which PEG (average m.w. 35 000) was used as macromolecular alternative to dextran (termed PEG solution). After cold storage in these different preservation solutions for 2 and 6 d and subsequent rewarming for 24 h HUVEC/macrophage cocultures showed a reduction in the total cellular protein compared to fresh cell cultures. After 6 d, this reduction in cellular protein was similar in the different preservation solutions, except for storage in dextran and PEG solutions. For HepaRG/LX-2 cultures, we observed a reduction of the cellular protein content only after 6 d of hypothermic storage in solutions low_Cl^- and low_Defer, indicating that HUVEC/macrophage cell cultures are more sensitive to hypothermic storage than HepaRG/LX-2 cell cultures (**Figure 1**). This idea is also supported by the observation, that the percentage of attached viable cells after 6 d storage of HepaRG/LX-2 cells is only reduced in solutions low_Cl^- and low_Defer (Figure 1). In contrast, HUVEC/macrophage cell cultures already showed a significantly decreased Alamar blue reduction (viability) after 2 d storage, except for PEG solution. After 6 d of hypothermic storage, however, we observed conversion rates (cell viabilities) lower than 50% of all HUVEC/macrophages irrespective of the selected storage solution (Figure 1).

A morphological analysis of the cocultures with bright-field microscopy revealed comparable results. After 2 d of storage the cellular morphology and confluence of the cell layers was similar to untreated controls. However, after 6 d of storage a cell detachment of HUVECs and macrophages was observed in all storage solutions. Further, typical cell islands of hepatocyte-like cells of differentiated HepaRG cells[26] were lost after 6 d hypothermic storage due to cell detachment (Figure S2, Supporting Information).

Based on these data, in particular viability rates and total protein content after reculture, we excluded solutions standard, low_Cl^-, and low_Defer from further characterization and analyzed only the maintenance of typical cell markers in cell layers stored for 2 and 6 d for storage in dextran or PEG solutions. The adherence junction protein vascular endothelial cadherin (VE cadherin) was found expressed in all HUVEC/macrophage cocultures stored in dextran and PEG solutions for up to 6 d. However, we observed a diminished preservation of the macrophage marker protein CD68 after 6 d storage in dextran and PEG solution, indicating macrophage detachment. In HepaRG/LX-2 cell layers preservation of CYP3A4, the major P450 cytochrome enzyme responsible for biotransformation of more than 50% of prescribed drugs[27] was found decreased after 2 d of storage in dextran solution and after 6 d storage in both solutions. Due to the complex morphology of LX-2 stellate cells, a precise determination of the cell numbers in coculture with

ADVANCED SCIENCE NEWS
www.advancedsciencenews.com

ADVANCED HEALTHCARE MATERIALS
www.advhealthmat.de

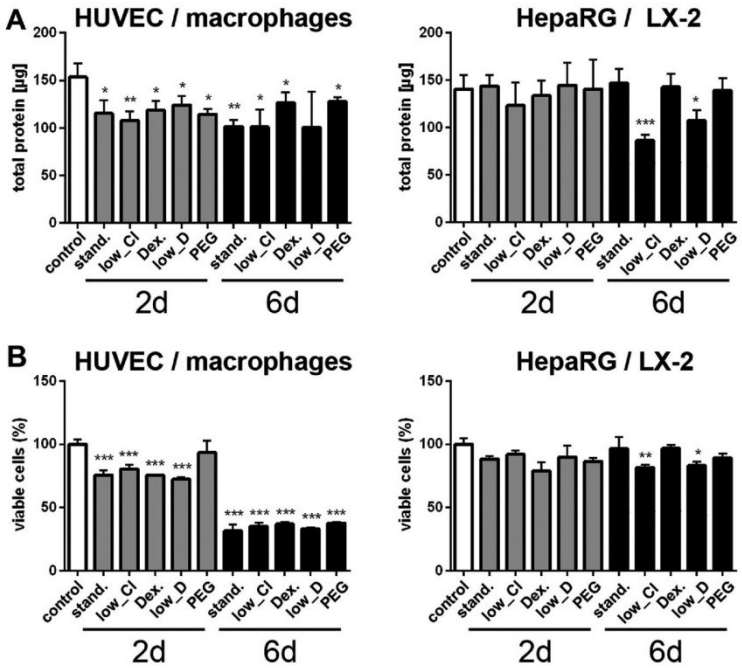

Figure 1. Hypothermic storage of cocultures under static conditions in cell culture dishes. A) Total cellular protein content and B) percentage of viable cells of HUVEC/macrophage and HepaRG/LX-2 cell cultures. Cell cultures without storage (marked as control) are compared to cell cultures after hypothermic storage for 2 and 6 d in the respective storage solutions and 24 h reculture. One-way ANOVA with Dunnett's multiple comparisons test; $*p < 0.05$, $**p < 0.01$, $***p < 0.001$ compared to control; $n = 5$ (standard solution (stand.), dextran solution (Dex.), low_Defer solution (low_D)).

HepaRG was not possible. We therefore measured the expression level of smooth muscle actin (SMA), a marker of LX-2 stellate cells. SMA expression levels were found decreased after 2 d storage in dextran solution, and 6 d storage in both, dextran as well as PEG solution (**Figure 2**).

HepaRG cells form self-organized functional bile canaliculi-like structures through which they secret bile acids.[2,28] The release of the fluorescent dye CDF into bile canaliculi was measured as surrogate for bile secretion.[29] In this assay, we focused on the accumulation of CDF and determined the number of functionally active bile canaliculi. We observed a full preservation of CDF secretion and active bile canaliculi after 2 d storage in both dextran and PEG solution. Hypothermic storage of cell layers in both solutions however, markedly reduced CDF secretion through active bile canaliculi after 6 d (**Figure 3**).

Based on the CDF secretion data, we have not considered a hypothermic storage of liver-on-chip models beyond 2 d. Immunofluorescence staining of VE-cadherin and CD68 in HUVEC/macrophage layers in liver-on-chip models revealed a diminished preservation of these cell marker proteins after 6 d hypothermic storage. Also, the maintenance of CYP3A4 and SMA was found decreased in HepaRG/LX-2 cell layers stored under these conditions. In contrast, maintenance of cell marker proteins VE-cadherin, CD68, CYP3A4, and SMA was not diminished in liver-on-chip models stored for 2 d in dextran or PEG solutions (**Figure 4**). Similar results were obtained for preservation of the multidrug resistance-associated protein-2 (MRP-2), a hepatic transporter protein, that defines the apical membrane of polarized hepatocytes.[30] MRP-2 is expressed at the bile canaliculi and acts as major transporter protein for the secretion of bile acids.[31] Our analysis demonstrates that during hypothermic storage of liver-on-chip models MRP-2 protein expression and structural organization of bile canaliculi lined with this transporter protein are preserved in dextran and PEG solution (Figure 4G).

We further analyzed the preservation of metabolic capabilities of liver-on-chip models during hypothermic storage. Therefore, synthesis and secretion of albumin and urea were measured during recultivation under perfusion conditions every 24 h for up to 3 d and compared to fresh liver-on-chip models. The synthesis rate of albumin and urea was comparable between fresh and stored liver-on-chip models (in both solutions). Also, the consumption of glucose and formation of lactate was similar. Furthermore, the release of hepatocyte-specific intracellular enzymes aspartate-transaminase (ASAT), alanine-transaminase (ALAT), and glutamate-dehydrogenase (GLDH) was not influenced by hypothermic storage. However, we observed an increased release of the intracellular enzyme

ADVANCED SCIENCE NEWS
www.advancedsciencenews.com

ADVANCED HEALTHCARE MATERIALS
www.advhealthmat.de

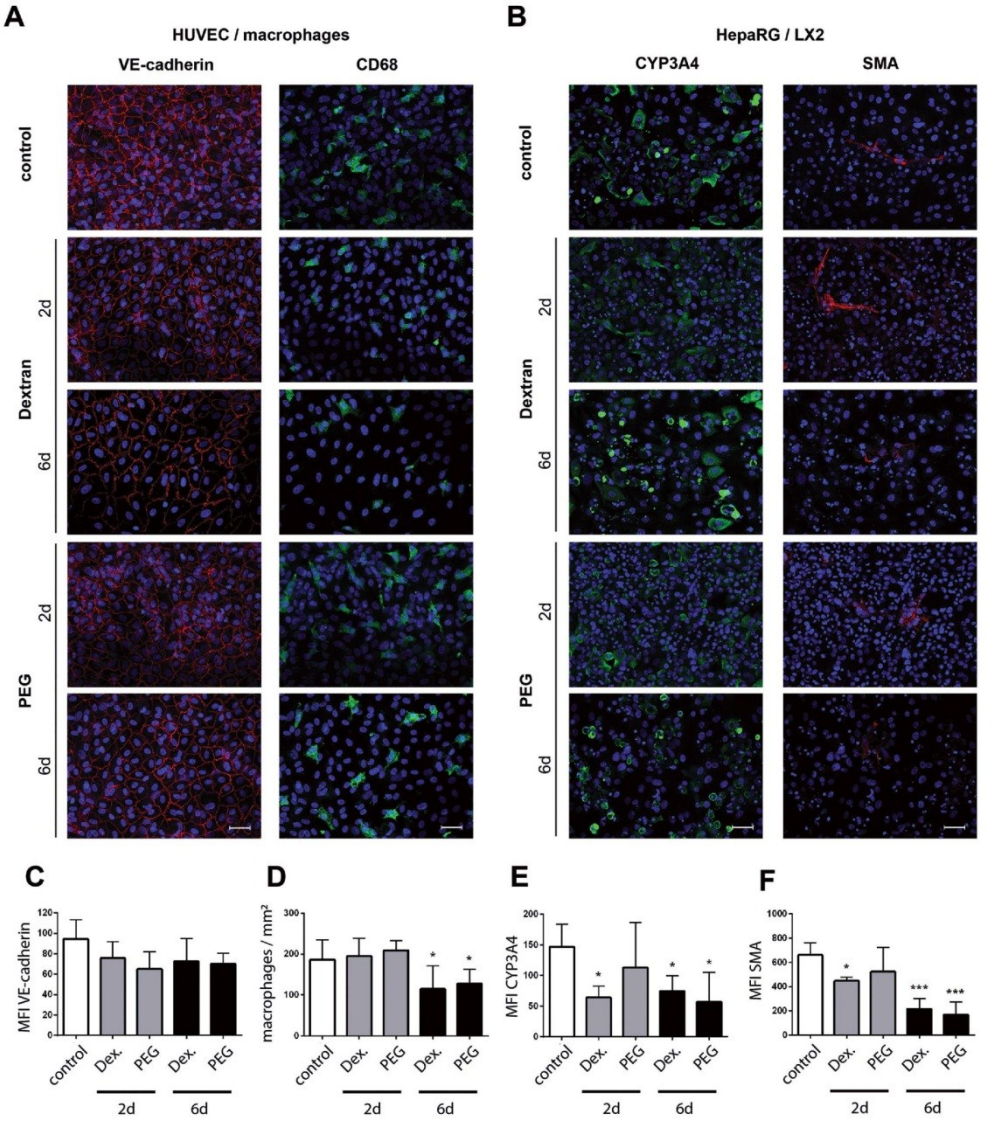

Figure 2. Immunofluorescence staining of cell cultures under static conditions. A) Endothelial adherence junction protein VE-cadherin (red) and macrophage marker protein CD68 (green) in HUVEC/macrophage cocultures. B) CYP3A4 (green) expression in hepatocytes and SMA expression (red) in LX-2 cells of HepaRG/LX-2 cocultures. Representative images of three independent experiments. Scale bar 50 µm. C–F) Quantification of the mean fluorescence intensity (MFI) for the expression of C) VE-cadherin, D) number of macrophages mm^{-2}, E) MFI of CYP3A4, and F) SMA. One-way ANOVA with Dunnett's multiple comparisons test; $^{*}p < 0.05$, $^{***}p < 0.001$ compared to control; $n = 3$, at least three regions of interest per experiment were analyzed. Cell cultures without storage (termed control) and hypothermic storage in solutions dextran (Dex.) or PEG for 2 and 6 d followed by 24 h reculture.

ADVANCED SCIENCE NEWS
www.advancedsciencenews.com

ADVANCED HEALTHCARE MATERIALS
www.advhealthmat.de

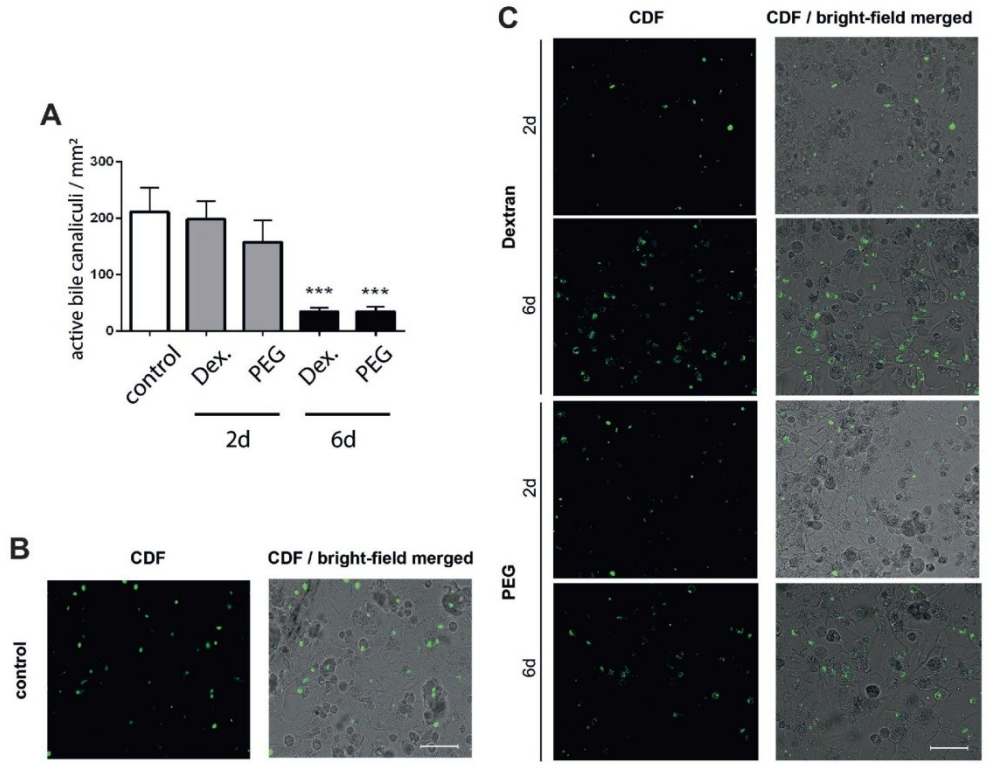

Figure 3. CDF secretion assay of HepaRG/LX-2 cell layers without storage (termed control) and after hypothermic storage in dextran (Dex.) and PEG solutions for 2 and 6 d followed by 24 h reculture. A) Quantification of active bile canaliculi mm^{-2} secreting CDF. One-way ANOVA with Dunnett's multiple comparisons test; $^{***}p < 0.001$ compared to control; $n = 3$, at least three regions of interest per experiment were analyzed. B,C) Representative images of three independent experiments from B) control and C) stored HepaRG/LX-2 cell layers. Impaired CDF secretion results in intracellular dye accumulation visible as fuzzy green staining within the cytosol. CDF (green) and merged with bright-field images. Scale bar 50 µm.

lactate-dehydrogenase (LDH) during the first 24 h of culture after storage. Still, LDH release was not found significantly increased in the further course of culture up to 3 d compared to untreated controls (**Figure 5**). Thus, our observations indicate an increased cell death of non-parenchymal cells in the initial phase of cell culture after storage. To further elucidate the biotransformation ability of stored liver-on-chip models, we characterized the enzyme activity of CYP3A4 through measurement of the biotransformation rate of midazolam to 1-hydroxy-midazolam[32] and the enzyme activity of CYP2C9 by formation of 4-hydroxy-diclofenac from diclofenac.[33] Interestingly, we observed no significant differences in the biotransformation rate involving these two major CYP enzymes (Figure 5).

We have recently reported that inflammation-associated liver dysfunction can be emulated by stimulation of Toll-like receptor-4 with its agonist lipopolysaccharide (LPS) in our liver-on-chip model.[2] We next studied the impact of hypothermic storage on the responsiveness of liver-on-chip models upon LPS stimulation and characterized its effect on cell viability and metabolic activity. In fresh livers-on-chip LPS stimulation resulted in a reduction of albumin and urea secretion, increased lactate formation and the release of ASAT, ALAT, GLDH, and LDH which is in line with previous reports.[2] Similar results for albumin and urea formation and ASAT, ALAT, and GLDH release were obtained in livers-on-chip stored for 2 d in dextran or PEG solutions. We also observed differences for LDH release 24 h after LPS treatment. However, at later time points LDH release in preserved liver-on-chip was not significantly increased by LPS treatment compared to untreated controls. Further, liver-on-chip models stored in dextran solution were not responsive to LPS stimulation in the formation of lactate, but liver models stored in PEG solution were found responsive to LPS. We confirmed a preservation of the LPS responsiveness of liver-on-chip stored in PEG solution when regarding CDF secretion. Liver-on-chip stored in dextran solution however, showed reduced CDF secretion activity already without LPS stimulation and no significant additional decline was observed after LPS treatment (**Figure 6**).

ADVANCED SCIENCE NEWS
www.advancedsciencenews.com

ADVANCED HEALTHCARE MATERIALS
www.advhealthmat.de

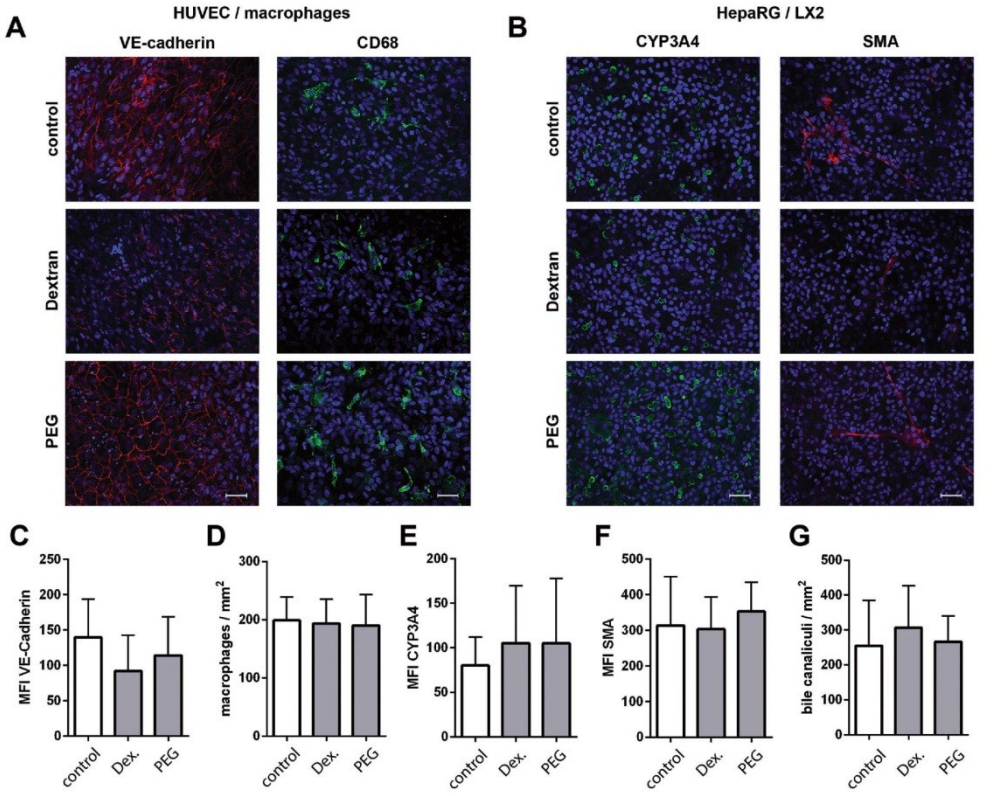

Figure 4. Immunofluorescence staining of cell layers in liver-on-chip models. Immunofluorescence images of A) endothelial adherence junction protein VE-cadherin (red) and macrophage marker protein CD68 (green) in HUVEC/macrophage cell layers. B) CYP3A4 (green) expression in hepatocytes and SMA expression (red) in LX-2 cells of HepaRG/LX-2 cell layers. Representative images of three independent experiments. Scale bar 50 µm. C–G) Quantification of the mean fluorescence intensity (MFI) for C) VE-cadherin, D) number of macrophages mm^{-2}, E) MFI of CYP3A4, and F) SMA. G) Number bile canaliculi lined with MRP-2 mm^{-2} of liver-on-chip models without storage (control) and hypothermic storage of 2 d in dextran or PEG solution followed by 24 h reculture under static conditions and 72 h perfusion. $n = 3$, at least three regions of interest per experiment were analyzed.

We observed no significant differences in the total number of macrophages present in the vascular layer of stored liver-on-chip models without stimulation or stimulation with LPS compared to the respective controls without storage (Figure S3, Supporting Information).

We next analyzed the expression of the macrophage marker proteins CD68 and CD163 in macrophages residing in the endothelial cell layer of liver-on-chip after storage. We found no significant changes in the expression level of both proteins compared to liver-on-chip without storage. However, after storage we observed a significant filopodia formation and elongation of macrophages without any additional stimulation. Treatment with LPS also mediated a significant elongation of the macrophages and the formation of filopodia by these cells, independent whether liver-on-chip was stored or freshly stimulated (**Figure 7**). As elongation and filopodia formation are considered typical markers of macrophages in a proinflammatory activation stage,[34] we next measured the release of the cytokines interleukin (IL) IL-1β, tumor necrosis factor (TNF), IL-6, and IL-10 of stored liver-on-chip models in response to LPS stimulation. The release of TNF by liver-on-chip stored in dextran or PEG solution was comparable to TNF release by tissues without storage (Figure 7). For the release of IL-1β and IL-6 we also observed similar trends for cytokine levels after storage in dextran or PEG solution for up to 72 h of LPS stimulation. However, in non-stimulated liver-on-chip we found an increased release of IL-1β and IL-10 already in non-stimulated liver-on-chip stored in dextran solution.

3. Discussion

We here tested different up-to-date cold storage solutions for their ability to preserve liver-on-chip models by hypothermic

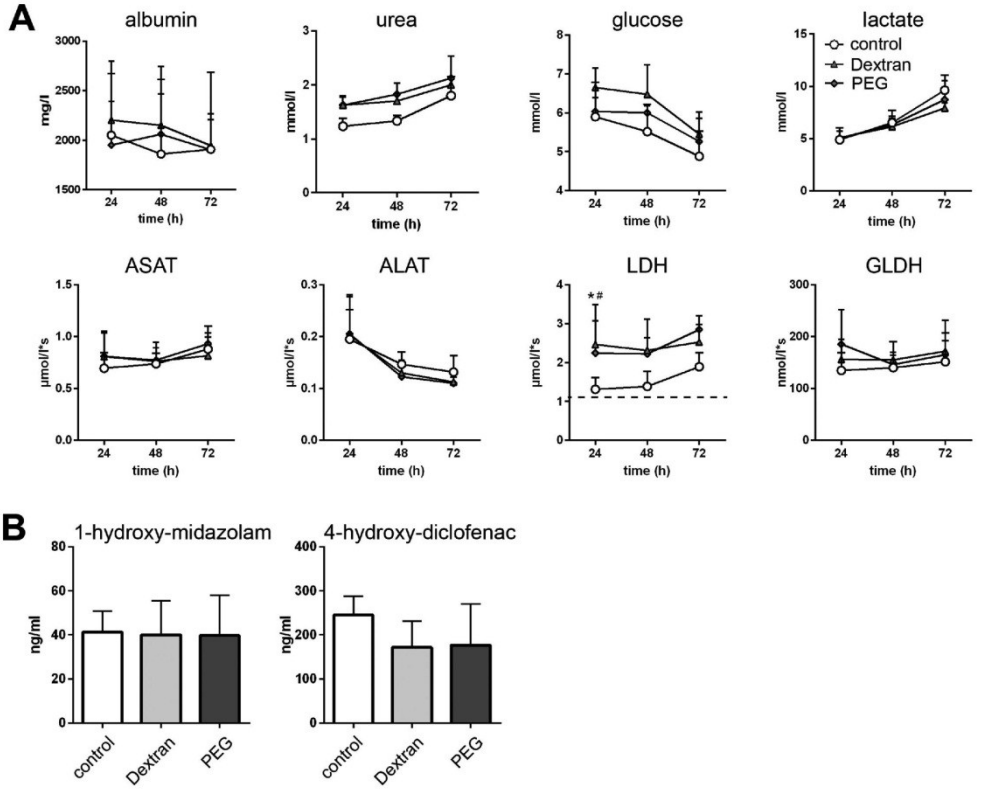

Figure 5. Metabolic activity, release of intracellular hepatic enzymes and biotransformation rate of liver-on-chip models after 2 d storage and subsequent reculture. A) Formation of albumin and urea, concentration of glucose and lactate in the perfusion medium, and release of intracellular enzymes ASAT, ALAT, LDH, GLDH for up to 72 h. Parameters of liver-on-chip models without storage (control, open circles) compared to storage in dextran solution (gray filled triangles) and PEG solution (gray filled diamonds). Dashed line for LDH marks basal enzyme activity in perfusion medium. Two-way ANOVA with Dunnett's multiple comparisons test; $^{*}p < 0.05$ for dextran solution compared to control, $^{\#}p < 0.05$ for PEG compared to control, $n = 5$. B) Biotransformation rate of midazolam and diclofenac to its metabolites 1-hydroxy-midazolam and 4-hydroxy-diclofenac, respectively.

storage. To the best of our knowledge, this is the first study that systematically addresses the storage of organ-on-chip models. The storage solutions used were all based on the same basic principles, the principles of the tissue preservation solution TiProtec and the organ preservation solution Custodiol-N, thus allowing to attribute differing preservation results of the variants to single ingredients/features.

The basic features of the parent solution and of all variants used here are the use of *N*-acetylhistidine as buffering system and a pH of 7.0. *N*-Acetylhistidine was used as buffer as it shows far lower toxicity then the buffers histidine or phosphate that are used in other preservation solutions in high concentrations.[18,35] The pH was adjusted to 7.0 as a mild acidosis has been reported to protect against several types of cell injury, including hypoxic or energy deficiency injury.[36] In addition, glycine and the related amino acid alanine were added to the storage solutions because of their known protection against hypoxic injury and against injury elicited by energy deficiency.[36,37] These two small amino acids have been shown to prevent hypoxia-induced sodium ion influx and plasma membrane pore formation.[37,38] Furthermore, aspartate and α-ketoglutarate were added to provide intermediates of the citric acid cycle, whereas glucose was added as substrate for the highly glycolytic endothelial cells.[39] A low concentration of phosphate was added to allow resynthesis of ATP and sucrose serves as impermeant. The iron chelators deferoxamine, a strong, but hydrophilic hexadentate chelator, and LK614, a new lipophilic hydroxamic acid derivative,[18] were used to inhibit iron-dependent hypothermic injury. Previous studies had shown that the combination of the poorly membrane-permeable chelator deferoxamine with low concentrations of LK614 enhanced preservation of endothelial cells and hepatocytes during hypothermic storage.[18] Solutions based on the combination of these principles, i.e., Custodiol-N and precursors

ADVANCED SCIENCE NEWS
www.advancedsciencenews.com

ADVANCED HEALTHCARE MATERIALS
www.advhealthmat.de

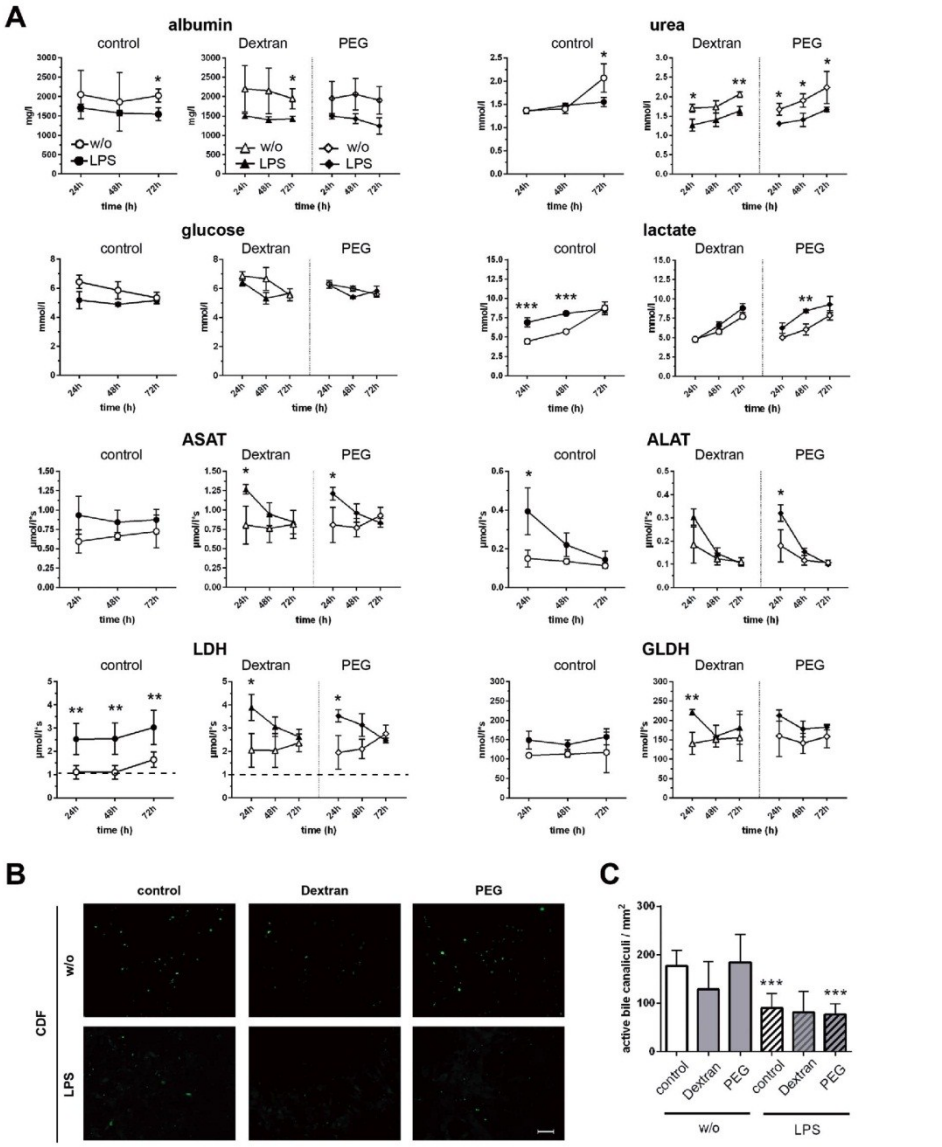

Figure 6. Metabolic activity, release of intracellular hepatic enzymes, and secretion of CDF in liver-on-chip models stimulated with LPS. A) Formation of albumin and urea, concentration of glucose and lactate in the perfusion medium, and release of intracellular enzymes ASAT, ALAT, LDH, GLDH for up to 72 h. Parameters of liver-on-chip without storage (circles) and stored in dextran solution (triangles) or PEG solution (diamonds) untreated (open symbols) or stimulated with LPS (filled symbols) during reculture ($n = 5$). Dashed line for LDH marks basal enzyme activity in perfusion medium. One-way ANOVA with Dunnett's multiple comparisons test; $^{*}p < 0.05$, $^{**}p < 0.01$, $^{***}p < 0.001$ compared to control; $n = 5$. B,C) CDF (green) secretion assay without storage (control) and liver-on-chip models stored in dextran or PEG solution for 2 d. B) Representative images of three independent experiments. Scale bar 50 µm. C) Quantification of the number of active bile canaliculi mm^{-2} secreting CDF. Two-way ANOVA with Dunnett's multiple comparisons test; $^{*}p < 0.05$, $^{**}p < 0.01$, $^{***}p < 0.001$ compared to condition without LPS stimulation; $n = 3$, at least three regions of interest per experiment were analyzed.

ADVANCED SCIENCE NEWS
www.advancedsciencenews.com

ADVANCED HEALTHCARE MATERIALS
www.advhealthmat.de

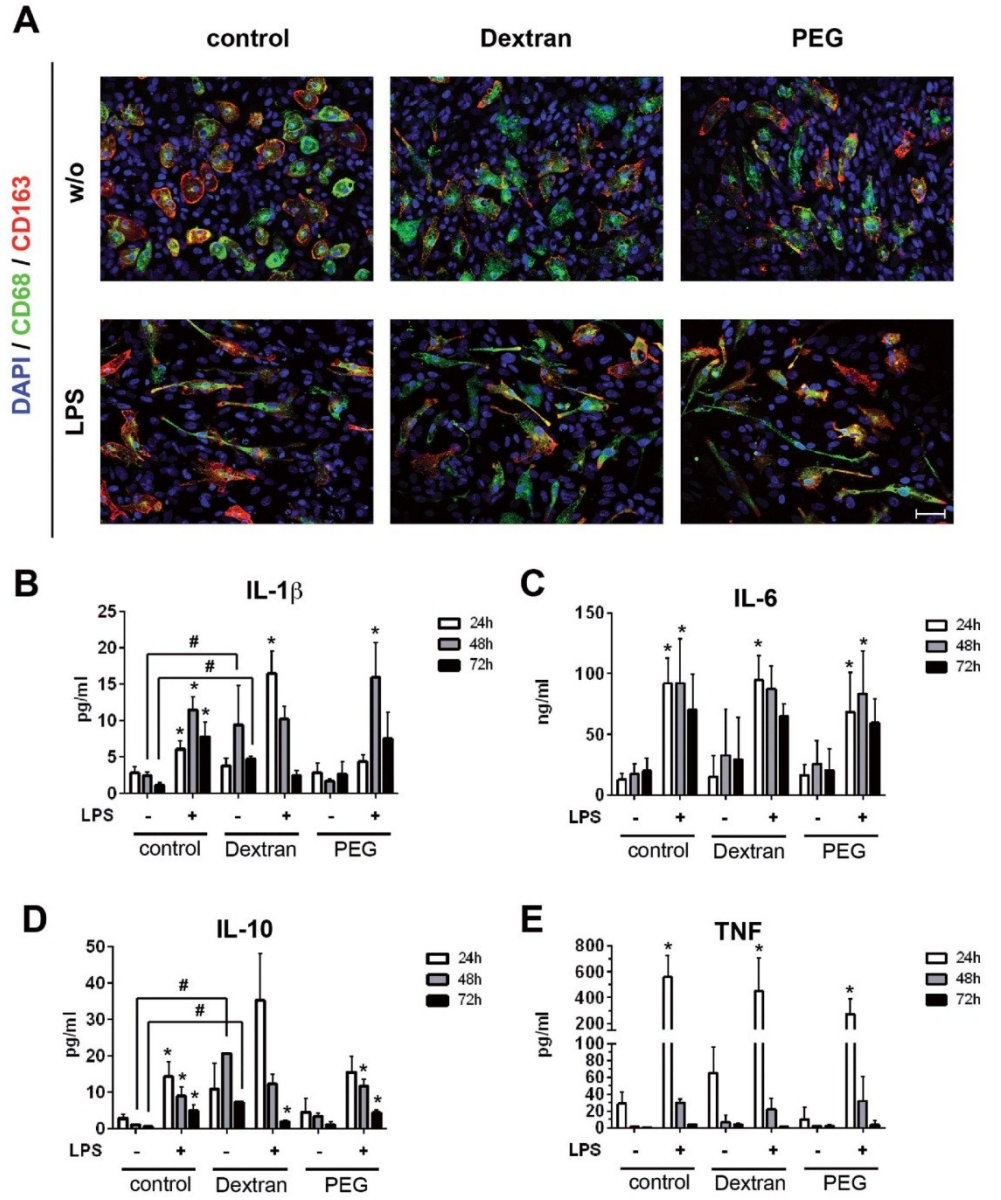

Figure 7. Immune response to LPS in liver-on-chip models without storage (control) and after storage in dextran or PEG solution. A) Expression of macrophage marker proteins CD68 (green) and CD163 (red) without stimulation (w/o) and LPS stimulation (LPS). Representative images of three independent experiments are shown. Scale bar 50 µm. B–E) Release of IL-1β, TNF, IL-6, and IL-10. Two-way ANOVA with Dunnett's multiple comparisons test; $^{\#}p < 0.05$ between indicated conditions; $^{*}p < 0.05$ compared to unstimulated samples at the same time point and storage condition, $n = 3$.

and TiProtec and its variants, have been shown to be protective during cold storage of different cell types and tissues.[17,18,21,22]

The individual storage solutions used in the current study differed in the concentrations of chloride (low_Cl^-) and the iron chelator deferoxamine (low_Defer) and the addition of macromolecular additives (dextran or PEG solutions). The reasoning behind the variation of the chloride concentration is that chloride ion concentrations above 40–50 mmol L^{-1} impaired survival of isolated rat hepatocytes after cold storage,[16] while chloride-rich solutions have been shown to yield a significantly better endothelial cell survival[18] and a better survival of human hepatocytes after cold storage.[17] To test the effect of the chloride ion concentration during hypothermic storage of the liver-on-chip models—small models of liver tissue composed of four different cell types, for which the overall chloride effect could not be predicted—the impermeant anion lactobionate was used in storage solution low_Cl^- to largely substitute chloride ions as described previously.[22,40]

In the first part of our study that consisted in the characterization of the functionality of separately stored "vascular" (HUVEC/macrophage) and "hepatic" (HepaRG/LX-2) cell layers under static culture conditions, especially HUVEC/macrophage cell cultures were found vulnerable to hypothermic storage. The observed differences in the amount of the total protein content and the number of viable cells of HUVEC/macrophage cocultures after 6 d storage can be explained by presence of dead/apoptotic cells that still stick to the membrane. These cells will contribute to the measurement of the total protein content but do not metabolize Resazurin in the viability assay. The high sensitivity of endothelial cells toward storage injury is in line with previous reports in cellular systems as well as during organ preservation.[14,19] In our experiments storage in solution low_Cl^-, that contained the low concentration of chloride ions, resulted in a reduced endothelial/macrophage viability and protein content. A similar inferiority of the chloride-poor solution low_Cl^- compared to its counterpart the chloride-rich standard solution was observed for HepaRG/LX-2 cell layers. Our data thus indicate that high chloride concentrations in the storage solutions are beneficial for hypothermic storage of both cell layers. This is in line with the recent reports showing that chloride-rich solutions yield a significantly better survival of endothelial cells and human hepatocytes after cold storage,[17,18] but contradict classical concepts of organ preservation.[5] The substitution of chloride by lactobionate is seen as one of the important principles of the organ preservation solution University of Wisconsin solution and a chloride influx during hypothermic storage followed by cell swelling has for decades been regarded as a major injurious mechanism during cold storage.[5,6] In isolated liver endothelial cells and in cultured rat hepatocytes, however, such a cold-induced influx of chloride could not be confirmed.[14]

Low_Defer solution contained the original deferoxamine concentration of TiProtec, i.e., 0.08 mmol L^{-1}. Deferoxamine concentrations in this range had proven optimal for the storage of isolated vessels while the requirement for optimal preservation of isolated cells appeared to be higher, i.e., in the range of 1 mmol L^{-1} deferoxamine when used as single chelator or 0.5 mmol L^{-1} when used in combination with LK614.[17] Therefore, we here tested preservation of cocultures with the original deferoxamine concentration of TiProtec (low_Defer) and the higher concentration described for isolated cells (0.5 mmol L^{-1} deferoxamine in its direct counterpart the standard solution), which showed a clearcut advantage of the solution with the higher deferoxamine concentration in the HepaRG/LX-2 cell layers—confirming the previous results with cultured cells.[17]

Cold storage of porcine lungs in Custodiol-N could be improved by the addition of 50 g L^{-1} dextran 40 000.[25] This additive has also been used for the cold perfusion of porcine kidneys.[41,42] Functional studies in the cold-stored lungs indicated less edema formation and better oxygenation after addition of dextran to Custodiol-N.[25] To test whether dextran also possesses beneficial effects on the storage of cocultures/simplified liver-on-chip models dextran 40 000 was added to dextran storage solution in the same concentration that has previously been used successfully as additive to the parent preservation solution Custodiol-N, i.e., 50 g L^{-1}.[25,42] An alternative to dextran is PEG[43] that has been described long ago to decrease lipid peroxidation, to prevent hepatocyte cell swelling and protects the cell cytoskeleton during cold storage and that has also been suggested to build a protective layer on the cellular surface.[43,44] Thus, 50 g L^{-1} PEG 35 000 was added to the storage solution (PEG) in a concentration of 50 g L^{-1}—i.e., in the same concentration (in g L^{-1}, which, for the macromolecules is likely to be the more relevant value with regard to colloidosmotic pressure) as dextran and in a concentration that has been shown to exert protection in preliminary cold storage experiments in other cell types (B. Akyildiz, U. Rauen, unpublished results)—and tested for its potential beneficial effects on the preservation of cell viability and maintenance of liver-on-chip function. Both solutions with macromolecular additives (dextran and PEG solutions) proved to be superior to their counterpart without these additives (standard solution) with regard to the maintenance of total protein content in endothelial/macrophage cocultures, without further differences observed. Therefore, these two solutions with macromolecular additives were then used for the storage of liver-on-chip models.

The PEG storage solution that contained PEG 35 000 demonstrated the best performance in its ability to preserve structural and functional features of liver-on-chip models. Especially expression of cell type marker proteins was better preserved after storage in PEG solution. This observation is in agreement with the previous reports on protective effects on the cytoskeleton and on cellular membranes.[43] Interestingly, however, only minor differences between dextran and PEG storage solutions were found for the preservation of hepatocyte metabolism. Here, we observed comparable performance of fresh and stored liver-on-chip models for up to 3 d.

Although release of liver-specific cell death markers such as ALAT, ASAT, and GLDH were comparable between fresh and stored liver-on-chip models, a significant increase of the unspecific cell death marker LDH was observed. As hepatocyte viability, metabolism and the rate of drug biotransformation were not affected by storage, this finding might indicate an increased cell death of non-parenchymal cells.

In our liver model stimulation with LPS was shown to impair hepatocyte metabolism and CDF secretion due to macrophage activation with inflammation and consecutive hepatocellular dysfunction.[2] A comparable immune response was

ADVANCED SCIENCE NEWS
www.advancedsciencenews.com

ADVANCED HEALTHCARE MATERIALS
www.advhealthmat.de

found for liver models stored the dextran solution as well as the PEG solution upon LPS stimulation. As the immune response to LPS is mainly related to macrophage function, the increased LDH release within first 24 h after storage is not attributed to dying macrophages but suggests the death of endothelial cells. This finding was confirmed by similar macrophage counts and comparable expression levels of macrophages marker proteins in liver-on-chip after storage in dextran and PEG solution and stimulation with LPS. Macrophages in stored liver-on-chip also showed full responsiveness to LPS stimulation as seen by the rendering of their morphology to a more elongated shape with increased filopodia formation and the release of cytokines. However, a change in macrophage morphology was also seen after storage in dextran and PEG solution without LPS stimulation. This observation might indicate a preactivation of macrophages in the endothelial cell layer due to storage conditions. However, this could only be confirmed by the release of IL-1β and IL-10 of liver-on-chips stored in dextran but not PEG storage solution.

Although 2 d of cold storage are sufficient for shipping of liver-on-chip models, longer cold storage times are desirable, especially with regard to providing a stock of ready-to-use liver-on-chip models. For isolated hepatocytes, storage times of 7 d are already possible.[22] However, mitochondrial function/ATP generation might be compromised in cells after prolonged cold storage.[45,46] Further analysis of these limitations is likely to identify additional targets for intervention, thus allowing to further improve cold preservation and extend cold preservation periods.

4. Conclusions

A broad application of organ-on-chip technology relies on the ability to store preassembled organ models, i.e., for shipment to end users. We here demonstrate for the first time, that hypothermic storage enables preservation of cell viability, morphological structure, metabolism, and biotransformation activity of liver-on-chip models for up to 2 d. In our study, a combination of high molecular weight PEG with storage solutions containing high chloride ion concentrations and iron chelators LK614 and deferoxamine was the most suitable formulation for liver-on-chip preservation. However, additional studies are required to further optimize current storage protocols for liver-on-chip models (especially in order to further prolong storage periods), but also for the specific requirements of other organ-on-chip models, such as kidney-, lung-, or gut-on-chip to enable an efficient long-term preservation. Hypothermic storage of organ-on-chip models will thereby offer an easier and more flexible way to access organ-on-chip technology, i.e., to replace animal experimentation in biomedical screening studies.

5. Experimental Section

Biochips: MOTiF biochips were made from polystyrol (PS) and obtained from microfluidic ChipShop GmbH (Jena, Germany). Biochips were manufactured as previously described by injection molding.[24] The upper chamber of the biochip has a height of 700 µm, the lower chamber's height is 400 µm. Afferent and efferent channels have a width of 0.8 mm and 2 mm, respectively. The height of these channels measures 0.6 and 0.4 mm, respectively. The upper chamber including the channel system has a total medium volume of 220 µL. The lower chamber including the channel system has a filling volume of 120 µL. A 12 µm thick polyethylene terephthalate (PET) membrane with a pore diameter of 8 µm and a pore density of 1×10^5 pores cm^{-2} (TRAKETCH Sabeu, Radeberg, Germany) was integrated. At the suspended membrane, an area of 1.1 cm^2 is available for cell culture. Chips and channel structures were sealed on top and bottom side with an extruded 140 µm thick PS film using a low-temperature proprietary bonding method. Gas permeable silicon tubing was used for perfusion, allowing oxygen equilibration during experimentation. In addition, the biochips were characterized by a high rediffusion of oxygen through the PS bulk material and 140 µm thin PS sealing films. Ramping structures were introduced into the chip bulk to avoid unfavorable flow conditions and trapping of stationary air bubbles. Bubble formation was further reduced by oxygen plasma treatment for hydrophilization of the whole chip surface and use of equilibrated perfusion medium that was stirred overnight under perfusion conditions before use.

Cell Culture: HepaRG cells were obtained from Biopredic International (Rennes, France). LX-2 stellate cells were kindly provided by Ralf Weiskirchen (Institute of Molecular Pathobiochemistry, Experimental Gene Therapy and Clinical Chemistry, RWTH University Hospital Aachen, Germany). HUVECs were isolated and cultured as previously described.[47] Primary blood mononuclear cells were isolated from healthy donors by Ficoll density gradient centrifugation and seeded in 6-well plates with a density of 1×10^6 cm^{-2} in X-VIVO 15 (Lonza, Cologne, Germany) supplemented with 10% autologous human serum (v/v), 10 ng mL^{-1} GM-CSF (PeproTech, Hamburg, Germany), 10 ng mL^{-1} M-CSF (PeproTech), and 100 U mL^{-1} penicillin/100 µg mL^{-1} streptomycin mixture (Pen/Strep) (Thermo Fisher, Darmstadt, Germany). GM-CSF and M-CSF were added to induce and enhance macrophage polarization. After 1 h incubation cells were washed twice with X-VIVO 15 medium and cultivated for 72 h before detachment.

Liver-On-Chip Assembly: Liver-on-chip models were assembled as described.[23] Briefly, HUVECs were seeded with a density of 1.5×10^5 cm^{-2} in the upper chamber of a sterilized biochip in EC medium (Promocell, Heidelberg, Germany). After 48 h of culture macrophages were seeded on top of the confluent HUVEC cell layer with a density of 5×10^4 cm^{-2} in M199 medium (Life Technologies) supplemented with 10% (v/v) fetal calf serum (FCS, Life Technologies), 10% (v/v) autologous serum, 680×10^{-6} M L-glutamine (Sigma-Aldrich), 25 µg mL^{-1} heparin (Sigma-Aldrich), 7.5 µg mL^{-1} endothelial mitogen (Thermo Fisher), 5 µg mL^{-1} ascorbic acid (Sigma-Aldrich), 10 ng mL^{-1} GM-CSF, 10 ng mL^{-1} M-CSF, and Pen/Strep. After 72 h of static culture and daily medium exchange, a mixture of HepaRG (3×10^5 cm^{-2}) and LX-2 cells (1×10^4/cm^2) was seeded in the bottom chamber of the biochip and cultured in Williams' medium E (Biochrom, Berlin, Germany) containing 10% (v/v) FCS (GIBCO), 5 µg mL^{-1} insulin (Sigma-Aldrich), 2×10^{-3} M glutamine (GIBCO), 5×10^{-5} M hydrocortisone-hemisuccinate (Sigma-Aldrich), and Pen/Strep. The ports of each biochip were enclosed and the whole liver model cultured upside down for 24 h under static conditions. Thereafter, the fully assembled liver-on-chip model was used in experimental series as described. Liver-on-chip models were perfused with a flow rate of 50 µl min^{-1} (shear stress: 0.07 Pa) in the upper chamber with M199 medium. The bottom chamber was kept under static culture and Williams' medium E exchanged every 24 h.

For stimulation with LPS stimulation cells were treated with 100 ng mL^{-1} LPS (Sigma-Aldrich, Taufkirchen, Germany) and medium exchanged every 24 h for fresh medium with 100 ng mL^{-1} LPS for a total incubation time of up to 72 h. Cells were cultured in a humidified cell incubator at 5% CO_2 and 37 °C.

Preparation of Storage Solutions: The compositions of the storage solutions are given in **Table 1**. Chemicals used for the preparation of the solutions were obtained from Sigma-Aldrich, Merck (Darmstadt, Germany), Fluka (Munich, Germany), Acros Organics (Geel, Belgium), Applichem (Darmstadt, Germany), or Carl Roth (Karlsruhe, Germany)

ADVANCED SCIENCE NEWS
www.advancedsciencenews.com

ADVANCED HEALTHCARE MATERIALS
www.advhealthmat.de

Table 1. Composition of storage solutions. All concentrations are given in [mmol L^{-1}] unless otherwise stated.

Solutions	Standard	Low_Cl^-	Dextran	Low_Defer	PEG
Deferoxamine	0.5	0.5	0.5	0.08	0.5
LK 614	0.02	0.02	0.02	0.02	0.02
Dextran 40 000	–	–	1.25	–	–
PEG 35 000	–	–	–	–	1.43
Cl^-	103.1	8.1	103.1	103.1	103.1
Lactobionate	–	95	–	–	–
α-Ketoglutarate	2	2	2	2	2
Aspartate	5	5	5	5	5
$H_2PO_4^-$	1	1	1	1	1
Na^+	16	16	16	16	16
K^+	93	93	93	93	93
Mg^{2+}	8	8	8	8	8
Ca^{2+}	0.05	0.05	0.05	0.05	0.05
N-Acetylhistidine	30	30	30	30	30
Glycine	10	10	10	10	10
Alanine	5	5	5	5	5
Tryptophan	2	2	2	2	2
Sucrose	20	20	20	20	20
Glucose	10	10	10	10	10
pH	7.0	7.0	7.0	7.0	7.0

unless stated otherwise. LK614 and *N*-acetylhistidine were kindly provided by Dr. F. Köhler Chemie (Bensheim, Germany).

Hypothermic Storage: The study was performed in a blinded design: storage solution labeling was blinded to all experimentators involved in experimental handling and data acquisition. For storage, cell cultures in dishes or liver-on-chip models were washed twice with warm (25 °C) Dulbecco's phosphate buffered saline (PBS) (Biochrom, Berlin, Germany) and incubated within the indicated storage solution at 25 °C. Cells cultured in dishes or biochips were immediately transferred to cold storage and kept protected from light at 4 °C for indicated time periods. After storage cell layers were washed with chilled (10 °C) PBS. Subsequently, PBS was exchanged for indicated cell culture media and cells cultured for additional 24 h at 37 °C and 5% CO_2 under static culture conditions to allow firm cell attachment. All solutions were free from endotoxin and contaminating microorganisms, and used under sterile conditions (Figure S1, Supporting Information).

Determination of Protein Content: Cells were lysed with 0.1% Triton X-100 in PBS for 20 min at 4 °C. Subsequently, the solution was centrifuged for 20 min with 10 000 × *g* at 4 °C and the supernatants stored at −80 °C for later analysis. Whole protein concentration was determined using the Pierce BCA protein assay kit (Thermo Fisher) according to the manufacturer's protocol.

Cell Viability Assay: Cell layers were washed once with PBS (with Ca^{2+} and Mg^{2+}) and incubated with 250 µl of respective serum-free culture media including 25 µl AlamarBlue Cell Viability Reagent (Thermo Fisher). Cell layers were kept for 2 h at 37 °C in the medium and the supernatant subsequently removed. The resorufin formation by intracellular redox reaction (surrogate of cell viability) was measured by extinction measurement at a wavelength of 570 nm.

Analysis of 1-Hydroxy-Midazolam and 4-Hydroxy-Diclofenac Formation: Liver-on-chip models were cultured for 72 h in the absence or presence of LPS and medium was exchanged every 24 h. Subsequently, liver-on-chip models were incubated 6 h with serum-free hepatocyte culture medium containing 3×10^{-6} M midazolam (Rotexmedica, Trittau, Germany) and 10×10^{-6} M diclofenac (Sigma-Aldrich). After protein precipitation and concentration, samples were analyzed using an LC–MS/MS system consisting of an QTrap 4000 tandem mass spectrometer (AB Sciex, Darmstadt, Germany) equipped with a Turbo V ion spray source and coupled to a LC-20 liquid chromatography system (Shimadzu, Jena, Germany). Separation was performed on a ZORBAX Eclipse XDBC18 column (4.6 × 150 mm, particle size 5 µm) (Agilent, Böblingen, Germany) using a gradient program with 50×10^{-3} M ammonium formate buffer plus 0.75% formic acid (eluent A) and acetonitrile (eluent B). The mass spectrometer was operated in scheduled multiple reaction monitoring (MRM) mode using the target transition *m/z* 342–324 for quantification of 1-hydroxy-midazolam (metabolite formation as surrogate of Cyp3A4 activity) and *m/z* 310–266 for quantification of 4-hydroxy-diclofenac (metabolite formation as surrogate of Cyp2C9 activity). Instrument control, data acquisition, and data evaluation were performed using Analyst software 1.6.2 (AB Sciex).

Viability and Metabolic Liver Parameters: ASAT, ALAT, GLDH, LDH, and lactate, glucose, urea, and albumin, were measured in cell culture supernatants (Williams' medium E containing 10% human autologous serum) of conventional cell cultures or liver-on-chip using the Abbott Architect ci8200 Integrated System (Abbott Laboratories, Abbott Park, IL, USA) according to the manufacturer's protocol. Basel levels of the perfusion medium containing 10% FCS was <0.1 µmol L^{-1} s^{-1} ASAT, <0.08 µmol L^{-1} s^{-1} ALAT, 1.25 µmol L^{-1} s^{-1} LDH, <50 nmol L^{-1} s^{-1} GLDH, <0.6 mmol L^{-1} urea, 8.0 mmol L^{-1} glucose, 1.5 mmol L^{-1} lactate, and 50 mg L^{-1} albumin.

Immunofluorescence Staining: Cells were fixed with 10% paraformaldehyde for 10 min at room temperature. Subsequently, cells were permeabilized and unspecific binding sites blocked with PBS including 0.1% saponin and 3% goat serum. For staining, the following antibodies were used: primary antibodies: MRP-2 (Cell Signaling, Leiden, Netherlands), SMA (Dako, Hamburg, Germany), Cyp3A4 (Merck-Millipore, Schwalbach, Germany), CD68 (BD Biosciences), CD163 (Biolegend, United Kingdom), VE-cadherin (BD Bioscience); secondary antibodies: goat-anti mouse-Cy3 (Invitrogen, Karlsruhe, Germany), goat-anti-rabbit-AF488 (Invitrogen), AF647-Phalloidin (Thermo Fisher), and

DAPI (Invitrogen). Samples were embedded in fluorescent mounting medium (Dako) and imaged with an AxioObserver Z1 fluorescence microscope equipped with an ApoTome-2 (Carl Zeiss AG, Jena, Germany).

5(6)-Carboxy-2′,7′-Dichlorofluorescein (CDF) Assay: The hepatic cell layers were incubated with 3×10^{-6} M 5(6)-carboxy-2′,7′-dichlorofluorescein-diacetate (CDF-DA) in serum- and phenolred-free Williams' medium E for 30 min at 37 °C. Subsequently, the solution was removed and the hepatic cell layer was immediately analyzed for specific secretion of CDF through bile canaliculi formed between the hepatocytes by fluorescence imaging with an AxioObserver Z1 fluorescence microscope with an ApoTome-2 (Carl Zeiss AG).

Cytometric Bead Array (CBA): Supernatants of the upper chamber containing endothelial cells and macrophages were collected after indicated time periods and immediately frozen at −80 °C. Cytokines were detected using CBA assay (BD Biosciences) according to the manufacturer's protocol. Enhanced sensitivity flex set was used for measurement of TNF, IL-10 and IL-1β release. Secretion of IL-6 was analyzed using standard CBA flex sets. Analysis was performed on a BD FACS-Canto II cytometer with FACSDiva software and data quantified using the FCAP Array V3 software (Softflow, Pecs, Hungary).

Statistics: For each experiment shown, at least three independent experiments were performed. Statistical analysis was performed with GraphPad Prism 6.05 (GraphPad Software, La Jolla, CA, USA). For analysis of statistical significance one-way ANOVA with Dunnett's multiple comparisons or two-way ANOVA with Dunnett's multiple comparisons test have been used as indicated. A p-value <0.05 was considered statistically significant. Data presentation shows the mean ± standard deviation (SD).

Supporting Information

Supporting Information is available from the Wiley Online Library or from the author.

Acknowledgements

The authors are grateful to the excellent technical work of Melanie Ulrich and Cora Richert. This work was supported by the Federal Ministry of Education and Research, Germany (FKZ: 01EO1002).

Conflicts of Interest

U.R. is a scientific consultant of Dr. F. Köhler Chemie, Germany. She is one of the inventors of the organ preservation solution Custodiol-N and the tissue preservation solution TiProtec. The company Dr. F. Köhler Chemie holds patents on these solutions; however, the design, performance, data interpretation, and manuscript writing were under the complete control of the authors and have never been influenced by the company.

Keywords

endothelial cells, hepatocytes, hypothermic storage, liver-on-chip, LPS

Received: May 15, 2017
Revised: July 31, 2017
Published online:

[1] A. S. Mosig, *Future Sci. OA* **2016**, https://doi.org/10.4155/fsoa-2016-0038.
[2] M. Groger, K. Rennert, B. Giszas, E. Weiss, J. Dinger, H. Funke, M. Kiehntopf, F. T. Peters, A. Lupp, M. Bauer, R. A. Claus, O. Huber, A. S. Mosig, *Sci. Rep.* **2016**, *6*, 21868.
[3] A. T. Press, A. Traeger, C. Pietsch, A. Mosig, M. Wagner, M. G. Clemens, N. Jbeily, N. Koch, M. Gottschaldt, N. Beziere, V. Ermolayev, V. Ntziachristos, J. Popp, M. M. Kessels, B. Qualmann, U. S. Schubert, M. Bauer, *Nat. Commun.* **2014**, *5*, 5565.
[4] K. Rennert, S. Steinborn, M. Groeger, B. Ungerboeck, A.-M. Jank, J. Ehgartner, S. Nietzsche, J. Dinger, M. Kiehntopf, H. Funke, F. T. Peters, A. Lupp, C. Gaertner, T. Mayr, M. Bauer, O. Huber, A. S. Mosig, *Biomaterials* **2015**, *71*, 119.
[5] F. O. Belzer, J. H. Southard, *Transplantation* **1988**, *45*, 673.
[6] P. W. Hochachka, *Science* **1986**, *231*, 234.
[7] P. A. Clavien, P. R. Harvey, S. M. Strasberg, *Transplantation* **1992**, *53*, 957.
[8] J. D. Blankensteijn, O. T. Terpstra, *Hepatology* **1991**, *13*, 1235.
[9] L. Hunt, D. L. Hacker, F. Grosjean, M. De Jesus, L. Uebersax, M. Jordan, F. M. Wurm, *Biotechnol. Bioeng.* **2005**, *89*, 157.
[10] H. Wise, P. W. Abel, D. Cawkill, *J. Biomol. Screen.* **2009**, *14*, 716.
[11] E. E. Guibert, A. Y. Petrenko, C. L. Balaban, A. Y. Somov, J. V. Rodriguez, B. J. Fuller, *Transfus. Med. Hemother.* **2011**, *38*, 125.
[12] R. Sumimoto, N. Kamada, N. V. Jamieson, Y. Fukuda, K. Dohi, *Transplantation* **1991**, *51*, 589.
[13] U. Rauen, B. Polzar, H. Stephan, H. G. Mannherz, H. de Groot, *FASEB J.* **1999**, *13*, 155.
[14] U. Rauen, H. de Groot, *J. Invest. Med.* **2004**, *52*, 299.
[15] U. Rauen, F. Petrat, T. Li, H. De Groot, *FASEB J.* **2000**, *14*, 1953.
[16] U. Rauen, U. Kerkweg, H. de Groot, *Cryobiology* **2007**, *54*, 77.
[17] G. Pless, I. M. Sauer, U. Rauen, *Cell Transplant.* **2012**, *21*, 23.
[18] T. Wille, H. de Groot, U. Rauen, *J. Vasc. Surg.* **2008**, *47*, 422.
[19] C. D. Fingas, S. Wu, Y. Gu, J. Wohlschlaeger, A. Scherag, U. Dahmen, A. Paul, H. de Groot, U. Rauen, *Liver Transplant.* **2011**, *17*, 650.
[20] U. Rauen, H. de Groot, *Cryobiology* **2008**, *56*, 88.
[21] S. Garbe, B. Zatschler, B. Muller, P. Dieterich, A. Ebner, U. Rauen, K. Matschke, A. Deussen, *J. Vasc. Surg.* **2011**, *53*, 1063.
[22] G. Pless-Petig, B. B. Singer, U. Rauen, *PLoS One* **2012**, *7*, e40444.
[23] K. Rennert, S. Steinborn, M. Groger, B. Ungerbock, A. M. Jank, J. Ehgartner, S. Nietzsche, J. Dinger, M. Kiehntopf, H. Funke, F. T. Peters, A. Lupp, C. Gartner, T. Mayr, M. Bauer, O. Huber, A. S. Mosig, *Biomaterials* **2015**, *71*, 119.
[24] M. Raasch, K. Rennert, T. Jahn, S. Peters, T. Henkel, O. Huber, I. Schulz, H. Becker, S. Lorkowski, H. Funke, A. Mosig, *Biofabrication* **2015**, *7*, 015013.
[25] N. Pizanis, A. Petrov, J. Heckmann, I. Wiswedel, J. Wohlschlager, H. de Groot, H. Jakob, U. Rauen, M. Kamler, *J. Heart Lung Transplant.* **2012**, *31*, 310.
[26] A. Guillouzo, A. Corlu, C. Aninat, D. Glaise, F. Morel, C. Guguen-Guillouzo, *Chem. Biol. Interact.* **2007**, *168*, 66.
[27] G. Luo, T. Guenthner, L. S. Gan, W. G. Humphreys, *Curr. Drug Metab.* **2004**, *5*, 483.
[28] A. Guillouzo, C. Guguen-Guillouzo, *Expert Opin. Drug Metab. Toxicol.* **2008**, *4*, 1279.
[29] M. J. Zamek-Gliszczynski, H. Xiong, N. J. Patel, R. Z. Turncliff, G. M. Pollack, K. L. Brouwer, *J. Pharmacol. Exp. Ther.* **2003**, *304*, 801.
[30] G. Jedlitschky, U. Hoffmann, H. K. Kroemer, *Expert Opin. Drug Metab. Toxicol.* **2006**, *2*, 351.
[31] G. A. Kullak-Ublick, G. B. Baretton, M. Oswald, E. L. Renner, G. Paumgartner, U. Beuers, *Hepatol. Res.* **2002**, *23*, 78.
[32] I. F. Sevrioukova, T. L. Poulos, *Proc. Natl. Acad. Sci. USA* **2017**, *114*, 486.
[33] W. Tang, *Curr. Drug Metab.* **2003**, *4*, 319.
[34] P. Pelegrin, A. Surprenant, *EMBO J.* **2009**, *28*, 2114.
[35] U. Rauen, S. Klempt, H. de Groot, *Cell. Mol. Life Sci.* **2007**, *64*, 192.
[36] Y. Nishimura, L. H. Romer, J. J. Lemasters, *Hepatology* **1998**, *27*, 1039.

[37] R. Carini, G. Bellomo, M. Grazia De Cesaris, E. Albano, *Hepatology* **1997**, *26*, 107.
[38] A. Frank, U. Rauen, H. de Groot, *J. Hepatol.* **2000**, *32*, 58.
[39] S. Mertens, T. Noll, R. Spahr, A. Krutzfeldt, H. M. Piper, *Am. J. Physiol.* **1990**, *258*, 689.
[40] R. Sumimoto, K. Dohi, T. Urushihara, N. V. Jamieson, H. Ito, K. Sumimoto, Y. Fukuda, *Transplantation* **1992**, *53*, 1206.
[41] D. Candinas, F. Largiader, U. Binswanger, D. E. Sutherland, R. Schlumpf, *Transplant Int.* **1996**, *9*, 32.
[42] A. Gallinat, B. Luer, S. Swoboda, U. Rauen, A. Paul, T. Minor, *Cryobiology* **2013**, *66*, 131.
[43] J. E. Mack, J. A. Kerr, P. K. Vreugdenhil, F. O. Belzer, J. H. Southard, *Cryobiology* **1991**, *28*, 1.
[44] H. Ben Abdennebi, J. P. Steghens, A. Hadj-Aissa, A. Barbieux, S. Ramella-Virieux, C. Gharib, O. Boillot, *Transplant Int.* **2002**, *15*, 348.
[45] A. Bienholz, B. Walter, G. Pless-Petig, H. Guberina, A. Kribben, O. Witzke, U. Rauen, *PLoS One* **2017**, *12*, e0180553.
[46] B. Walter, B. Knoop, U. Rauen, *Transplant Int.* **2016**, *29*, 31.
[47] E. A. Jaffe, R. L. Nachman, C. G. Becker, C. R. Minick, *J. Clin. Invest.* **1973**, *52*, 2745.

Manuscript III - Supplementary information

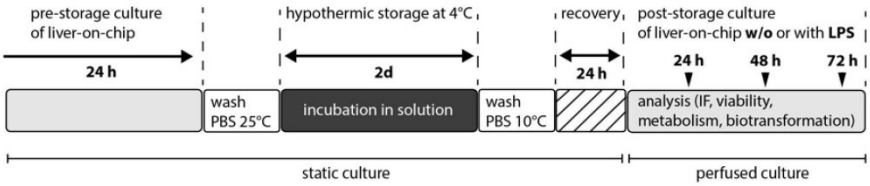

Supplementary Figure 1. *Scheme of liver-on-chip storage and analysis of treatment effects. Liver-on-chip were first cultured under static conditions (static culture), washed with PBS adjusted to 25°C, filled with the indicated solution and hypothermically stored as described. After storage liver-on-chip were washed with 10°C PBS and cultured for another 24 h under static conditions with the described media to allow recovery and firm attachment of cells to the membrane (recovery). Subsequently, liver-on-chip were perfused with 50 µl/min endothelial medium (perfused culture) and morphological and functional analysis performed every 24 h (vertical arrows mark to analysis time points; IF: immunofluorescence). The impact of 100 ng/ml lipopolysaccharide stimulation (LPS, present throughout the perfusion period) was compared to untreated controls (w/o).*

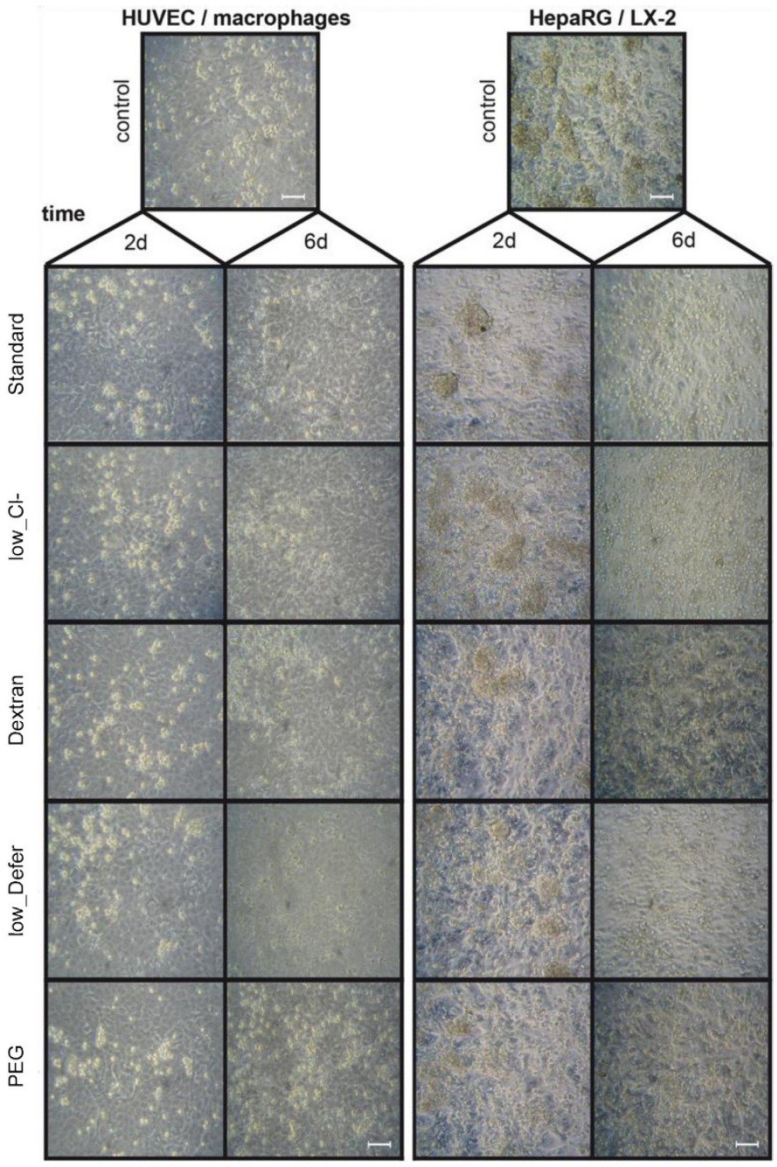

Supplementary Figure 2. *Bright field images of HUVEC/macrophage and HepaRG/LX-2 cell layers after storage and subsequent culture for 24 h under static conditions. Cell cultures without storage (termed control) and after hypothermic storage for 2 days (2d) and 6 days (6d) in the respective storage solutions and*

subsequent reculture. Representative images of three independent experiments. Scale bar 100 µm.

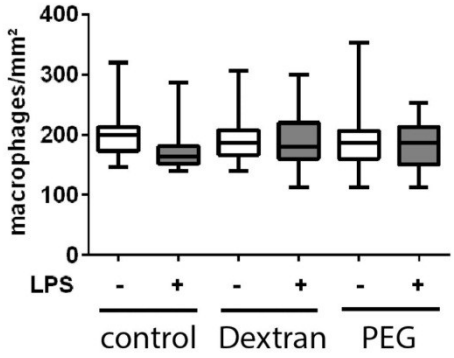

Supplementary Figure 3. *Immune response to LPS in liver-on-chip models without storage (control) and after storage in Dextran or PEG solution. Macrophage cell counts. (n=3, 5 regions of interest per experiment were analysed).*

4 DISCUSSION

For this thesis, a microphysiological human liver-on-a-chip was established to study mechanisms of liver inflammation under *in vivo*-like conditions. Still, emulation of the human physiology is a major challenge in pre-clinical research, which intensifies the need for new *in vitro* tools to overcome the limitations of available applications, i.e. animal experimentation. This tendency is reinforced by the ongoing and controversial debate about the use of *in vivo* models limiting their applicability for purposes of translational medicine (Seok et al. 2013, Takao and Miyakawa 2015, Warren et al. 2015). Murine models display a complex physiology with desirable organ-interactions creating a beneficial tool to study diseases and their impact on the entire organism. However, their interspecies differences e.g. in the immune system reduce the transferability of the obtained results to humans (Mestas and Hughes 2004). To overcome these issues microphysiological models are a promising approach to increase the relevance of *in vitro* experimentation by reverse engineering of human organs (Ingber 2016). This organ-on-a-chip concept possesses the potential to emulate complex physiological processes, thereby getting closer to mimic the function of human organs *ex vivo*.

4.1 Liver-on-a-chip - complexity matters

The concept of our microphysiological *in vitro* liver model is inspired by the structure of the human liver sinusoid. In this thesis, it was realized by the use of a perfused vascular cell layer, containing HUVECs and macrophages, physiologically protecting the HepaRG and LX-2 cells from shear stress. A porous membrane, already used for co-culture of ECs with hepatocytes (Kang et al. 2013, Bale et al. 2016), served as cell substrate providing the space of Disse between the endothelial lining and the parenchyma (Kang et al. 2017). This cellular arrangement and the vascular perfusion enabled intercellular communication, stable oxygenation, optimal supply with nutrients and efficient removal of cellular waste products.

4.1.1 Biochip design and technical variables

The passive support of the static hepatic chamber in our model creates a low media to cell ratio, which is considered to be an important parameter of microphysiological systems (Wikswo 2014). A non-physiological high media to cell ratio increases the

dilution of secreted paracrine signaling molecules (Faley et al. 2008) and metabolites of biotransformation (Bale et al. 2015b). With a rate of approximately 0,4 nl/cell in the bottom co-culture chamber of HepaRG and LX-2 cells the characterized liver-on-a-chip is suitable for efficient intercellular signaling as well as investigation of accumulating CYP-associated metabolites like 1-OH-midazolam and 4-hydroxy-diclofenac. Furthermore, the limited amount of cell culture media restricts the availability of nutrients like glucose, which is supposed to induce insulin resistance and to affect CYP-activity of primary human hepatocytes (Davidson et al. 2016). Additionally, our system allows variable adjustment of the perfused media and the associated oxygen saturation in the bottom chamber.

As already mentioned translucent PDMS is commonly used for manufacturing biochip devices but it exhibits unspecific binding properties (Toepke and Beebe 2006, van Meer et al. 2017). Van Midwoud and colleagues determined a reduced recovery of testosterone and 7-hydroxycoumarin in PDMS devices, whereas the viability of HepG2 liver cells was almost similar compared to PS and cyclic olefin copolymer (COC) (van Midwoud et al. 2012). To avoid potential alterations regarding an unspecific binding of liver metabolites, the chosen material of the Multi Organ Tissue Flow (MOTiF) biochip was, dependent on its application, PS or COC. Integration of luminescence-emitting sensor spots allowed continuous online-measurement of oxygen saturation in the media within the respective chambers of each biochip. It was observed that microfluidic devices made of PS have higher oxygen permeance than COC-based platforms (Byrne et al. 2014). Similar results were obtained by oxygen measurements under static conditions in our liver biochips. The PS-based devices showed a constant diffusion of oxygen into the media, whereas the oxygen saturation of the COC biochip decreased below 5 % after 1 h in the statically cultured hepatic chamber. Additionally, these hypoxic conditions were associated with ATP depletion in our model, a known characteristic of ischemic injury (Dagher 2000). This was confirmed by calculation of a high ADP/ATP ratio, indicating hepatic cell apoptosis. After application of low perfusion rates in the bottom chamber (1-10 µl/min) we could prove that cellular oxygen consumption can be used as a surrogate for metabolic activity of the hepatocytes. Therefore, the integrated sensor spots represent a valuable addition to allow the establishment of models of liver zonation *in vitro*.

4.1.2 Vascular perfusion as a critical parameter for endothelial and hepatocyte cell function

In vitro, the application of vascular perfusion enables the removal of cellular debris and metabolic products thereby avoiding their harmful accumulation. Furthermore, shear stress led to morphological adaption and cytoskeletal remodeling of HUVEC cell layers (Raasch et al. 2016). In contrast, estimation of physiological shear rates affecting hepatocytes *in vivo* is almost impossible and needs to be evaluated carefully for *in vitro* applications. Whereas very low shear stress (4.7×10^{-5} dyn/cm²) enhanced CYP activity in 2D-hepatocyte cultures (Rashidi et al. 2016), an increase (>1.4 dyn/cm²) resulted in continuous alteration of albumin synthesis and finally cellular detachment at 20 dyn/cm² (Tanaka et al. 2006). In this thesis it was proven that perfusion of HUVEC/macrophage layers, acting as a supportive cellular barrier, with 50 µl/min (0.5 dyn/cm²) is sufficient to maintain the function of the static HepaRG/LX-2 chamber for up to 96 h. Prodanov et al. (2016), who used a comparable liver-on-a-chip with 1 µl/min of vascular perfusion and two distinct cell layers, reported an increased albumin and urea secretion compared to static conditions during a four week culture period. They claimed that the improved hepatic function originates from a better nutrient supply and clearance of metabolites (Prodanov et al. 2016). We observed similar effects in our liver-on-a-chip model regarding albumin- and urea synthesis. However, our results indicate an enhanced CYP3A4 activity under perfused conditions compared to static culture after 96 h. This is contrary to the measurements of Prodanov and colleagues who used primary human hepatocytes and could be explained by the varying CYP3A4 expression of HepaRG cells dependent on their differentiation status (Kanebratt and Andersson 2008). Additionally, Prodanov et al. (2016) measured the enzyme activity of CYP3A4 after seven days compared to four days in our model. Therefore, it is necessary to verify CYP3A4 function after prolonged culture and investigate additional phase I as well as phase II enzymes in our liver-on-a-chip. This is further supported by the results of Du et al. (2017) who used primary murine cells in a biochip-based liver model and applied a vascular perfusion of 0.1 dyn/cm². The authors observed no shear stress-dependent changes of urea synthesis, but an increased CYP1A2 and CYP2D6 activity after 24 h of culture (Du et al. 2017). The discussed liver-on-a-chip models as well as our model apply a vascularization strategy. Hence, specific media for endothelial and epithelial cells can be used according to their requirements.

4.1.3 Cellular diversity - the key to hepatic micro-physiology

Despite the technical and exogenous control of the microenvironment, cellular composition is a critical element to emulate hepatic tissue and related function. To date, there is no reported human liver-on-a-chip that contains primary LSECs, KCs, hepatocytes and HSCs in a single device. This might be related to their demanding culture protocols. The use of cell lines has several advantages, like almost unlimited cell availability, better reproducibility, cost-effectiveness and a stable cellular phenotype. Furthermore, limited availability of primary cells is associated with their isolation from patients who suffer from diseases and get particular medication, which increases experimental variance. Therefore, we used in the described liver-on-a-chip model the established LX-2 and HepaRG cell lines as surrogates for HSCs and primary hepatocytes, respectively. Furthermore, freshly isolated HUVECs mimic the endothelial lining of the liver sinusoid that is interspersed with surrogates of KCs emulated by monocyte-derived macrophages. *In vitro,* LSECs rapidly dedifferentiate accompanied by the loss of fenestration as well as increasing expression of CD31 on the cell surface (Ford et al. 2015), which is contrary to their mature phenotype (Poisson et al. 2017). HUVECs up-regulate CD31 during perfusion (Raasch et al. 2016) and show differences regarding transendothelial migration of monocytes compared to LSECs (Zimmermann et al. 2015). Although the HUVECs formed a functional vascular barrier in our liver-on-a-chip, it needs to be assessed if LSEC are a possible surrogate in future studies. Therefore, investigation of specific differentiation markers (e.g. CD31) and functional characteristics (e.g. fenestration, scavenger function) is necessary to identify differences regarding the ability of HUVECs and LSECs to mimic the physiology of the hepatic vasculature in our model. The maintenance of hepatocyte polarization is a critical indicator for their metabolic activity. Guillouzo et al. (1993) postulated that hepatic function *in vitro* is influenced by three major regulators: 1) paracrine signaling, 2) cell-cell contacts and 3) interaction with ECM. Although we did not implement any exogenous ECM, microfluidic models developed by other researchers used a collagen matrix for long term stabilization of primary hepatocytes (McCarty et al. 2015, Prodanov et al. 2016). Nonetheless, albumin synthesis, urea secretion and bile canaliculi formation was shown to be stabilized in co-culture with ECs, which can produce ECM (Kim et al. 2012). Spheroids containing hepatocytes and stellate cells were further able to form a

fibronectin capsule, which was not observed in mono-culture approaches without HSCs (Thomas et al. 2005). These results favor the assumption that the HUVECs or LX-2 cells in our model contribute to endogenous production of ECM and functional stabilization of the cellular microenvironment. Nonetheless, the presence of ECM needs to be verified by immunofluorescence staining of the respective proteins. Additionally, implementation of exogenous ECM is necessary to determine the impact on possible long term maintenance of the liver-on-a-chip beyond four days.

Another important characteristic of the liver model is the complex microenvironment, which is maintained by interactions and close contacts of all cell types. Krause et al. (2009) determined that incubation of hepatocytes with HSC-conditioned media and their co-culture in direct contact with primary murine HSCs led to a higher phosphoenolpyruvate carboxykinase 1 activity. Although, we could not confirm the observations of Krause and colleagues regarding CYP3A4 expression of HepaRG co-cultured with LX-2, the fully assembled liver-on-a-chip increased the albumin and urea synthesis as well as the CYP3A4 expression significantly. Furthermore, hepatocyte growth factor (HGF) is secreted by LX-2 cells (Yu et al. 2013) as well as HUVECs (Toyoda et al. 2012) and is discussed as a critical mitogen for hepatocytes (Michalopoulos 2007). Du and colleagues reported an enhanced production of HGF by NPCs in co-culture with primary murine hepatocytes with a cellular arrangement comparable to our model (Du et al. 2017). This was associated with a higher CYP-activity and albumin secretion, which fits to the observations in our human liver-on-a-chip. Although we did not systematically investigate the influence of direct cell contacts and added no exogenous HGF to the media, our results indicate that an increased complexity (number of different cell types) is directly affiliated with enhanced hepatic function.

Taken together, our hepatic model enables co-culture of the four main cell types of the liver, thereby creating an organotypic, self-maintained physiological micro-environment. Therefore, this liver-on-a-chip could be a suitable *in vitro* tool to emulate the complex hepatic microphysiology in a reproducible manner. Although we detected elongated bile canaliculi between the hepatocytes, which were also observed in murine (Li et al. 2010) and human tissues (Nies et al. 2001), substitution of the HepaRG cells with primary human hepatocytes is necessary to identify cell type-specific drawbacks of our approach and assess the stabilizing effect of the complex microenvironment regarding the metabolic capabilities of our liver-on-a-chip.

4.2 Inflammation-on-a-chip – a suitable tool for translational medicine?

Inflammation-associated hepatic dysfunction is characterized by interplay of various factors, namely immune cell recruitment, cytokine signaling and interaction of hepatocytes with NPCs (Adams et al. 2010). The explanatory power of conventional *in vitro* liver models used for studying inflammation is restricted by the lack of certain hepatic cell types, by the use of exogenous application of cytokines or a combination of both (Klein et al. 2015, Zhou et al. 2015, Rose et al. 2016). Although, those applications might be useful for addressing cell type-specific effects, they hardly reflect the complex microphysiology and cellular interaction during hepatic inflammation. Our established human liver-on-a-chip model was successfully characterized by its response to TLR-mediated inflammatory dysfunction. In addition to the four cell types previously integrated, we were able to introduce circulating monocytes, which were protective against liver damage. Thus, our results indicate that the improved microphysiology of the human liver-on-a-chip is associated with a specific response to PAMPs, mimicking some aspects of hepatic inflammation.

4.2.1 TLR-mediated liver dysfunction in a micro-physiological liver-on-a-chip

To prove the applicability of our liver-on-a-chip model for studying inflammation we investigated the immune reaction after simulation of the receptors TLR-1/2, 4 and 9, respectively. All TLR-agonists analyzed require MyD88-dependent signaling and lead to activation of NF-κB (Mencin et al. 2009). In contrast, we observed a specific cytokine profile dependent on the individual activated TLR receptor. Human hepatocytes for example do not contribute to cytokine production after TLR-9 stimulation (Bröring et al. 2012), which indicates a specific contribution of different cells types to TLR-mediated signaling. Nevertheless, we did not examine the individual contribution of the different cell types to the total amount of secreted cytokines. Importantly, in contrast to other models our liver-on-a-chip does not rely on exogenous addition of cytokines, which creates a beneficial, self-contained release and interaction of the inflammatory mediators.

4.2.1.1 Hepatocytes as inflammatory targets

Stimulations of our liver model with LPS, PAM3CSK4 and ODN-2006 resulted in

cholestasis-like hepatocellular dysfunction (reduced MRP-2 expression and CDF release) and diminished ApoB expression. Similar results were determined in patients suffering from systemic inflammatory response syndrome who showed decreased concentrations of ApoB in lymph and blood plasma (Levels et al. 2003). Furthermore, there is evidence that patients with cholestasis in sepsis have increased bilirubin levels in the serum, which is related to a disturbance in canalicular bile excretion via MRP-2 (Nesseler et al. 2012, Bhogal and Sanyal 2013). Another important characteristic of our inflammation-on-a-chip model was the elevation of glutamate dehydrogenase (GLDH), alanine aminotransferase (ALAT) and aspartate aminotransferase (ASAT) after 72 h LPS treatment. An increased serum concentration of ALAT is another clinical indicator associated with liver failure during sepsis (Bakker et al. 2004). Elevated ASAT and ALAT levels in the PCI mouse model of our collaborators also confirmed this.

In contrast to our expectations, CYP3A4 protein expression and activity was not affected by LPS stimulation (100 ng/ml) in our inflammation-on-a-chip model. This is contrary to results from human hepatocytes stimulated with a 100-fold higher concentration of LPS (10 µg/ml) (Aitken and Morgan 2007). Although they determined a fold change of CYP3A4 mRNA below 0.05 compared to control after 24 h, expression on the protein level was only reduced to approximately 50 % (40 h stimulation) and slightly recovered over time. This might be related to a cellular desensitization after continuous LPS exposure, which was observed in LSECs and hepatocytes by a down-regulation of TLR-signaling (Uhrig et al. 2005, Scott et al. 2009). The stabilizing effect of the microphysiological environment in association with a LPS tolerance might contribute to an improved hepatic metabolism in our inflammation-on-a-chip model. This assumption is supported by the minor recovery of CYP3A11 (homolog of human CYP3A4) observed after 72 h on the mRNA- and the metabolic level in the PCI mouse model of our collaborators.

4.2.1.2 Sinusoidal activation and recruitment of immune cells

Despite the presence of immunomodulatory KCs in the liver sinusoids, active recruitment of immune cells to the inflamed endothelium is an important regulator of the hepatic homeostasis (Shi and Pamer 2011). Static *in vitro* models lack the option of perfusion, which makes it impossible to study mechanisms of circulating leucocytes in a physiological manner. We could prove that perfused monocytes are actively recruited to the vascular endothelium in our model. Additionally, LPS

treatment led to an increased amount of adherent monocytes as well as transmigration into the hepatic cell layer. Interestingly, this process was associated with a recovery of TLR-mediated dysfunction after 72 h. Du et al. (2017) investigated that neutrophil recruitment after LPS treatment is directly correlated to the complexity of their liver-on-a-chip model. The presence of ECs, KCs, hepatocytes and HSCs resulted in an increased amount of adherent neutrophils. However, they did not investigate the effect of the invading immune cells in regard to the function of their model (Du et al. 2017).

Leucocytes are attracted to the activated vascular endothelium by the interaction of different adhesion molecules and their respective ligand, i.e. ICAM-1 and VCAM-1 with integrin αL/β2 und integrin α4/β1 (Blankenberg et al. 2003). It was shown that the expression of ICAM-1 is rapidly increased after LPS stimulation in macrophages and ECs (Leeuwenberg et al. 1992, Bernatchez et al. 1997). We determined that both adhesion molecules were up-regulated after 24 h of LPS incubation, thereby causing the activation of the vascular endothelium. Increased expression of those surface proteins was also observed in mono-cultures of primary human LSECs after treatment with TNF and IFN-γ (Bruns et al. 2015). Although we used HUVECs in our model the results indicate the mechanistic capability of these cells regarding monocyte recruitment. Additionally, integration of circulating monocytes cells increased the shedding of ICAM-1 and VCAM-1, which are discussed as potential clinical biomarkers for sepsis patients (Kjaergaard et al. 2016).

Interestingly, Beattie and colleagues determined a functional cellular adaptation of liver-resident macrophages to their microenvironment (Beattie et al. 2016). In their study a loss of yolk sac-derived macrophages in mice led to replacement of the KCs by monocytes originating from the bone marrow. Although, the populations were distinguishable by differentially expressed genes, the response to LPS and their phagocytic activity were comparable. This might be important considering the use of HUVECs and monocyte-derived macrophages as surrogates for LSECs and KCs in our inflammation-on-a-chip. The enhanced hepatic microphysiology of our model might contribute to a functional adaptation of these cells, which could be critical for the evaluation of obtained results regarding pathophysiological mechanisms during liver inflammation.

4.2.2 Monocyte-macrophage interaction during hepatic inflammation

After evaluation of the monocyte recruitment mechanisms in our liver-on-a-chip we investigated their influence on the tissue-resident macrophages. It was reported that circulating monocytes compete for free niches from perished macrophages during inflammation (Guilliams and Scott 2017) and contribute to the course of hepatic inflammation in dependence of the recruited subtype (Brempelis and Crispe 2016). LPS stimulation triggered formation of filopodia and morphological elongation of the adherent immune cells in our liver-on-a-chip, indicating an activated phenotype (M1 polarization). We confirmed the presence of a M1-polarization state by determination of an increased expression of the chemokine receptor CD197 (CCR7) as well as an increased secretion of IL-6 and TNF compared to the control, which is in line with other studies (Mantovani et al. 2002, Martinez and Gordon 2014). Upon monocyte recruitment to the site of inflammation, we observed a shift towards an anti-inflammatory macrophage phenotype (M2) known to mediate tissue regeneration in the liver (Tacke and Zimmermann 2014). This was verified by a recovery of albumin and urea synthesis as well as maintenance of the vascular barrier integrity. Van den Bossche et al. (2016) have provided evidence that activated human M1-polarized macrophages are not able to repolarize back to M2. Although we did not examine this process, the higher number of recruited monocytes after LPS-treatment fosters the assumption that M1 macrophages might be replaced rather than transitioned back to M2. Due to the continuous transition of described macrophage markers (Mantovani et al. 2002, Martinez and Gordon 2014) it would be difficult to identify a time-dependent polarization shift in our liver-on-a-chip by immunofluorescence staining. However, an evaluation of the total amount of macrophages before and after LPS treatment, combined with a tracking of stained, perfused monocytes could give more support to prove the replacement assumption.

During human sepsis hepatic injury and recovery is balanced by a cascade of pro- and anti-inflammatory cytokines (Yan et al. 2014). We observed that circulating monocytes contributed significantly to an initial burst of the investigated cytokines 24 h after their perfusion (LPS conditions). Prolonged LPS exposure led to a decrease of IL-6, TNF and IL-1β concentration, which might be related to the excessive release of IL-10, a known suppressor of LPS-induced synthesis of the mentioned cytokines in human peripheral blood mononuclear cells (Wang et al.

1994). Further, IL-10 mediates a decreased NLRP3 inflammasome activation in macrophages (Ip et al. 2017) subsequently preventing maturation of IL-1β (Lopez-Castejon and Brough 2011). Shalova and colleagues demonstrated that isolated monocytes from septic patients displayed a pro-inflammatory gene expression profile but were tolerant towards LPS stimulation. Nonetheless, they were able to induce angiogenesis of HUVECs, which supports the observed recovery of VEC in our liver-on-a-chip model. Additionally, they suggested that hypoxia-inducible factor-1α (HiF-1α) is involved in the switch of monocytes to an immunosuppressive phenotype (Shalova et al. 2015). Those immunologically repressed monocytes might also contribute to the resolution by clearance of LPS, thereby preventing the induction of M1-macrophage polarization through specific TLR-signaling (Martinez and Gordon 2014). Additionally, this was confirmed by the results of Ramachandran et al. (2012) who showed that phagocytic activity is associated with transition to a restorative phenotype of monocyte-derived macrophages in mice due to enhanced ERK-signaling. An evaluation of the phagocytic activity of the macrophages in our liver-on-a-chip in addition to the analysis of CD197, CD163 and the release pro- and anti-inflammatory cytokines would verify the assumed polarization states and give more information about the involved mechanisms of hepatic regeneration.

We did not investigate all assumed mechanisms in detail, but our observations regarding cytokine release, macrophage transition and hepatic tissue repair are in agreement with the results from other studies discussed. In this context, HiF-1α and the enhanced LPS-clearance by a restorative macrophage phenotype transition might be possible mediators for inflammatory resolution and need to be investigated in follow-up experiments.

4.3 Novel hypothermal preservation strategy for liver-on-a-chip models

For the first time we showed the applicability of cold storage to preserve our liver-on-a-chip model for up to two days. Cellular integrity, arrangement and function of the microphysiological hepatic *in vitro* model were almost similar to fresh assembled devices after a short recovery time. Based on the TiProtec® and Custodiol-N preservation solutions we tested five different formulations and evaluated critical components regarding their effects on cell viability, morphology and function after hypothermal preservation.

4.3.1 Basic components of cold storage solutions

All storage solutions in this study share some key characteristics to improve the outcome of liver-on-a-chip preservation based on previous reports. The pH was adjusted to 7.0 in all of the applied storage solutions. In contrast to the physiological pH of 7.4, it was reported that mild acidosis is protective to preserve vitality and mitochondrial membrane potential of ECs (Wille et al. 2008). The cytotoxic histidine was replaced by N-acetylhistidine due to its lower toxicity and similar buffering capacity (Rauen et al. 2007b). To further support the energetic metabolism of the cells a mixture of different substances was added to prevent metabolic alterations. Whereas phosphate is necessary for the synthesis of ATP, addition of glucose stabilized the glycolytic activity of ECs (Mertens et al. 1990). Aspartate and α-ketoglutarate were supplemented to support the cellular energy management associated with the citrate cycle (Wu et al. 2009). Based on previous reports from a modified HTK solution, which already comprised tryptophan, the amino acids alanine and glycine were added. In combination with sucrose these two substrates were able to prevent hepatocyte cell death after cold storage (Pless-Petig et al. 2012). Mechanistically, alanine and glycine contribute to a reduction of plasma membrane permeability during hypoxia (Frank et al. 2000, Petrat et al. 2012). Carini and colleagues further revealed that glycine prevents excessive accumulation of sodium in hepatocytes after hypothermic storage (Carini et al. 2000). In summary, a variety of beneficial effects were reported for all discussed ingredients during recovery of cold-preserved cells. Therefore, we included these additives as the basis for all our storage solutions

4.3.2 Iron chelators and chloride – critical elements for cold storage of liver cells

To specify the impact of additional storage solution components we tested five different derivates of our basic solution with minimal adjustments. In a first approach we assessed the outcome after hypothermal preservation regarding morphology, viability and protein content of the individual cell layers (vascular and hepatic) for two and six days. Overall, HUVECs and macrophages were more sensitive to cold storage resulting in a decreased viability and protein content at both investigated time points. In contrast, only minor impairments of the HepaRG/LX-2 cell layers were observed in lowCl^- and low_Defer solutions after six days.

The lowCl^- storage solution is characterized by a chloride concentration of 8.1 mM and the addition of lactobionate. This was tested due to the fact that low chloride

concentrations (5 mM) had a beneficial effect on cold-stored murine hepatocytes (Rauen et al. 2007a). Their study revealed that substitution with lactobionate in a modified Krebs-Henseleit buffer prevented iron-independent impairment of these cells. Similar observations were made by Pless-Petig et al. (2012) who observed an increased cell death of primary murine hepatocytes in a chloride-rich (103.1 mM) cold storage buffer. Surprisingly, the same concentration led to a better hypothermal preservation of human hepatocytes after rewarming, which indicates species-dependent differences (Pless et al. 2012). Although HepaRG and LX-2 are human cell lines, high concentrations of chloride favored long term storage (six days) in our experiments. Further, the protective effect of high chloride concentrations on the viability of porcine aortic segments (Wille et al. 2008) could not be demonstrated in cold storage of HUVEC/macrophage cell layers.

The addition of iron chelators to preservatives is critical for the maintenance of cell function and viability of various cell types as well as tissues (Rauen et al. 2007a, Wille et al. 2008, Arthur et al. 2013). Therefore, we added a combination of 0.02 mmol/l LK614 and 0.5 mmol/l deferoxamine to all storage solutions, which was reported to improve the recovery after hypothermal preservation of blood vessels (Wille et al. 2008) and human hepatocytes (Pless et al. 2012). Nonetheless, high concentrations of iron chelators are supposed to be cytotoxic (Chaston and Des Richardson 2003). In this regard, it was investigated if lower concentrations of deferoxamine (0.08 mmol/l), initially used for the TiProtec® solution, are sufficient to preserve the distinct cell layers of our model. In contrast, our results indicate that low concentrations of deferoxamine (compared to the standard solution) significantly reduce viability and protein content of the hepatic cells after six days of cold storage. This observation could simply be the result of concentration-dependent chelation efficiency, reported for deferoxamine (Richardson et al. 1994). Due to the limited amount of storage solution (~250 µl/Well) an exchange during long-term preservation (>2 days) might improve the outcome of the low_Defer derivative. Nevertheless, we excluded the lowCl^- and low_Defer solutions after the determined cellular impairment during six days of storage compared to the other three hypothermal preservatives.

4.3.3 Dextran and PEG enhance liver-on-a-chip storage

Although the standard solution displayed almost similar outcome for the preservation of the hepatic cells, cold storage of HUVECs and macrophages was enhanced after addition of dextran and PEG (higher total protein content after six days storage).

Therefore, we excluded the standard solution in our study regarding the maintenance of functional cellular markers.

Storage of the hepatic cell layer for six days in either PEG or Dextran solution revealed a significant decrease in CYP3A4 expression and number of functional bile canaliculi. Although, viability and protein content were not affected these results indicate dedifferentiation of the HepaRG, losing their hepatocyte-like phenotype, which is essential for marker stabilization (Cerec et al. 2007). Furthermore, the amount of CD68-positive macrophages as well as the smooth muscle actin (LX-2 marker) expression decreased. Therefore, we excluded the long-term storage (six days) in the analysis of hypothermal liver-on-a-chip preservation. In a final set of experiments we examined the influence of the macromolecular additives PEG and dextran regarding the outcome of cold-stored, fully assembled liver-on-a-chip models in respect of functional and morphological markers as well as the inflammatory responsiveness after LPS treatment.

Dextran has a molecular weight of 40,000 and was successfully used for hypothermal preservation of different organs i.e. lung (Pizanis et al. 2012), kidney (Gallinat et al. 2013) and liver (Cheng et al. 2005). PEG, on the other hand, improved cold storage of hepatocytes by decreasing lipid peroxidation, thereby contributing to stabilization of cellular membrane integrity (Mack et al. 1991, Puts et al. 2015). Furthermore, PEG is supposed to prevent osmotic cell swelling and acting as a scavenger for free radicals, two important requirements for cold storage of cells in general (Shi and Xue 2016). The addition of either PEG or dextran to the standard preservation solution resulted in a full recovery of all cell type specific cell markers determined by immuno-fluorescence. Further, metabolism of diclofenac and midazolam, as surrogates for CYP3A4 and CYP2C9 activity, as well as the function of bile canaliculi were fully restored after two days of hypothermal preservation. This is in line with improved endothelial morphology and higher bile flow in rat livers after cold storage with PEG or dextran, respectively (Cheng et al. 2005, Abbas et al. 2010). Apart from the LDH release, which can be explained by the slight viability decrease of the HUVEC/macrophage layer after two days, the hepatic cell death markers ALAT, ASAT and GLDH were not increased after storage. Additionally, albumin and urea synthesis were maintained and comparable to fresh liver-on-a-chip models, independent of the applied solution.

We identified tissue-resident macrophages as important regulators of inflammation and hepatocellular dysfunction in our inflammation-on-a-chip model. Therefore, it was

tested whether cold storage itself or additives, such as glycine (Petrat et al. 2012), affect the outcome of TLR-mediated immune reaction. Overall, we observed only slight differences between fresh and stored liver-on-a-chip models after LPS stimulation. The tissue-resident macrophages showed an activated morphology (filopodia elongation) accompanied by increased cytokine release and impaired hepatocyte function. Nonetheless, storage in solution supplemented with dextran led to higher IL-1β and IL-10 secretion. Although the morphology of the macrophages was comparable to the PEG derivative, the reduced viability of the HUVEC/macrophage layer might lead to an accumulation of DAMPs. As a result, this could slightly activate the macrophages in the liver-on-a-chip model, a commonly observed event in cold-stored liver grafts (Abu-Amara et al. 2010).

Taken together, our results indicate that the standard solution supplemented with PEG (35 kDa) was the most suitable formulation for liver-on-a-chip preservation for up to two days. Although this might be sufficient for fast and local distribution, it needs to be evaluated if the storage period can be prolonged, as cold storage of hepatocytes and vascular cells was reported for at least seven days (Wille et al. 2008, Pless et al. 2012). Possible strategies would be the continuous exchange of the preservative to prevent accumulation of ROS and decreased efficiency of iron chelators over time.

5 CONCLUSION

The developed MOTiF-biochip design allows the integration of the four major liver cell types, thereby creating a complex, organotypic microenvironment. Perfusion of the vascular layer, which acts as a physiological barrier for the hepatic parenchyma, is necessary for the effective supply with nutrients and removal of accumulating metabolic waste products. The interaction and communication of all cell types improves the polarization of hepatocytes resulting in an enhanced metabolization rate better resembling the *in vivo* situation, compared to conventional cell cultures. We cultured hepatic cell lines (HepaRG and LX-2) together with freshly isolated primary cells (HUVECs and monocytes/macrophages) in our liver-on-a-chip to grant reproducibility and cost-effectiveness. Although our approach is associated with functional alterations of the respective cell types, the restricted availability as well as donor-specific variances of primary liver cells and tissue decreases their applicability for the establishment of microphysiological models. Nonetheless, the partial replacement of individual cell types is necessary to verify the functional benefits and identify drawbacks of the concept. Induction of TLR-mediated inflammation in the liver-on-a-chip model revealed pathophysiological similarities to human sepsis and mouse models. Thus, it would be interesting to compare the effect of isolated TLR-agonists with living bacteria in our model and assess the course of hepatic inflammation after a complex infection. Targeting the polarization state of monocyte-derived macrophages, circulating monocytes are critical regulators of hepatocellular recovery in the liver-on-a-chip. In this context, the anti-inflammatory cytokine IL-10 was identified as a potential key mediator of immune tolerance and tissue regeneration. However, further studies are needed to confirm the role of IL-10 and its involvement in molecular signaling pathways required for liver regeneration after acute inflammation. Additionally, it would be of interest to investigate the perfusion of classical ($CD14^{++}/CD16^{-}$) and non-classical ($CD14^{+}/CD16^{++}$) monocyte subtypes in the liver-on-a-chip, respectively. This could provide information about a specific recruitment of subsets and related transition of phenotypes during hepatic inflammation. To improve the availability of our liver-on-a-chip model also for external cooperating researchers we established a cold storage protocol for two days in a modified preservation solution. PEG, iron chelators and a high chloride concentration were identified as essential components to maintain the hepatic microstructure and

inflammatory responsiveness of the liver-on-a-chip. To enable storage beyond two days and eradicate limitations of the presented method detailed follow-up studies are necessary. Possible strategies would be repeated exchange of the preservative during cold storage and individualized storage solutions for the respective cell layers.

Due to the separated compartments in our biochip, it would be possible to connect different microphysiological organs as self-contained modules through vascular circulation. Thus, the organ-specific tissue is separated from the vasculature and allows the application of individualized cell culture medium. The opportunity of variable, modular interconnection offers new possibilities to study systemic organ interaction, i.e. gut-liver axis, *in vitro*. This would be useful for detailed drug screening studies (oral or intravenous application) and can be combined with disease models to evaluate their therapeutic effect.

Taken together, our biochip-based, human liver model allows the investigation of inflammatory hepatic dysfunction in a complex microphysiological environment. This new technology will help to close the gap between static *in vitro* and *in vivo* models to improve the outcome in translational research in the future.

A REFERENCES

Abbas R, Kombu RS, Dignam D, Gunning W, Stulberg JJ, Brunengraber H, Sanabria JR. 2010. Polyethylene glycol modified-albumin enhances the cold preservation properties of University of Wisconsin solution in rat liver and a hepatocyte cell line. J Surg Res, 164(1):95–104.

Abraham E, Laterre P-F, Garg R, Levy H, Talwar D, Trzaskoma BL, Francois B, Guy JS, Bruckmann M, Rea-Neto A, Rossaint R, Perrotin D, Sablotzki A, Arkins N, Utterback BG, Macias WL. 2005. Drotrecogin alfa (activated) for adults with severe sepsis and a low risk of death. N Engl J Med, 353(13):1332–1341.

Abu-Amara M, Yang SY, Tapuria N, Fuller B, Davidson B, Seifalian A. 2010. Liver ischemia/reperfusion injury: processes in inflammatory networks-a review. Liver Transpl, 16(9):1016–1032.

Adams DH, Ju C, Ramaiah SK, Uetrecht J, Jaeschke H. 2010. Mechanisms of immune-mediated liver injury. Toxicol Sci, 115(2):307–321.

Aitken AE, Morgan ET. 2007. Gene-specific effects of inflammatory cytokines on cytochrome P450 2C, 2B6 and 3A4 mRNA levels in human hepatocytes. Drug Metab Dispos, 35(9):1687–1693.

Arthur PG, Niu X-W, Huang W-H, Deboer B, Lai CT, Rossi E, Joseph J, Jeffrey GP. 2013. Desferrioxamine in warm reperfusion media decreases liver injury aggravated by cold storage. World J Gastroenterol, 19(5):673–681.

Bakker J, Grover R, McLuckie A, Holzapfel L, Andersson J, Lodato R, Watson D, Grossman S, Donaldson J, Takala J. 2004. Administration of the nitric oxide synthase inhibitor NG-methyl-L-arginine hydrochloride (546C88) by intravenous infusion for up to 72 hours can promote the resolution of shock in patients with severe sepsis: results of a randomized, double-blind, placebo-controlled multicenter study (study no. 144-002). Crit Care Med, 32(1):1–12.

Bale SS, Geerts S, Jindal R, Yarmush ML. 2016. Isolation and co-culture of rat parenchymal and non-parenchymal liver cells to evaluate cellular interactions and response. Scientific reports, 6:25329.

Bale SS, Golberg I, Jindal R, McCarty WJ, Luitje M, Hegde M, Bhushan A, Usta OB, Yarmush ML. 2015a. Long-term coculture strategies for primary hepatocytes and liver sinusoidal endothelial cells. Tissue Eng Part C Methods, 21(4):413–422.

Bale SS, Sridharan GV, Golberg I, Prodanov L, McCarty WJ, Usta OB, Jindal R, Yarmush ML. 2015. A novel low-volume two-chamber microfabricated platform for evaluating drug metabolism and toxicity. Technology (Singap World Sci), 3(4):155–162.

Barros MHM, Hauck F, Dreyer JH, Kempkes B, Niedobitek G. 2013. Macrophage polarisation: an immunohistochemical approach for identifying M1 and M2 macrophages. PLoS One, 8(11):e80908.

Beattie L, Sawtell A, Mann J, Frame TCM, Teal B, Labastida Rivera F de, Brown N, Walwyn-Brown K, Moore JWJ, MacDonald S, Lim E-K, Dalton JE, Engwerda CR, MacDonald KP, Kaye PM. 2016. Bone marrow-derived and resident liver macrophages display unique transcriptomic signatures but similar biological functions. J Hepatol, 65(4):758–768.

Bernatchez SF, Atkinson MR, Parks PJ. 1997. Expression of intercellular adhesion molecule-1 on macrophages in vitro as a marker of activation. Biomaterials, 18(20): 1371–1378.

Bhogal HK, Sanyal AJ. 2013. The molecular pathogenesis of cholestasis in sepsis. Front Biosci (Elite Ed), 5:87–96.

Blankenberg S, Barbaux S, Tiret L. 2003. Adhesion molecules and atherosclerosis. Atherosclerosis, 170(2):191–203.

Blankensteijn JD, Terpstra OT. 1991. Liver preservation. The past and the future. Hepatology, 13(6):1235–1250.

Brehm MA, Racki WJ, Leif J, Burzenski L, Hosur V, Wetmore A, Gott B, Herlihy M, Ignotz R, Dunn R, Shultz LD, Greiner DL. 2012. Engraftment of human HSCs in nonirradiated newborn NOD-scid IL2rgamma null mice is enhanced by transgenic expression of membrane-bound human SCF. Blood, 119(12):2778–2788.

Brempelis KJ, Crispe IN. 2016. Infiltrating monocytes in liver injury and repair. Clin Transl Immunology, 5(11):e113.

Bröring R, Lutterbeck M, Kleinehr K, Paul A, Gerken G, Schlaak JF. 2012. Toll-like receptor-activated primary human hepatocytes produce inflammatory cytokines and different types of interferon, resulting in HCV suppression in a co-culture model. Z Gastroenterol, 50(08).

Brun-Buisson C, Meshaka P, Pinton P, Vallet B. 2004. EPISEPSIS: a reappraisal of the epidemiology and outcome of severe sepsis in French intensive care units. Intensive Care Med, 30(4):580–588.

Bruns T, Zimmermann HW, Pachnio A, Li K-K, Trivedi PJ, Reynolds G, Hubscher S, Stamataki Z, Badenhorst PW, Weston CJ, Moss PA, Adams DH. 2015. CMV infection of human sinusoidal endothelium regulates hepatic T cell recruitment and activation. J Hepatol, 63(1):38–49.

Brunt EM, Gouw ASH, Hubscher SG, Tiniakos DG, Bedossa P, Burt AD, Callea F, Clouston AD, Dienes HP, Goodman ZD, Roberts EA, Roskams T, Terracciano L, Torbenson MS, Wanless IR. 2014. Pathology of the liver sinusoids. Histopathology, 64(7):907–920.

Byrne MB, Leslie MT, Gaskins HR, Kenis PJA. 2014. Methods to study the tumor microenvironment under controlled oxygen conditions. Trends Biotechnol, 32(11):556–563.

Carini R, Cesaris MG de, Splendore R, Bagnati M, Bellomo G, Albano E. 2000. Alterations of Na+ homeostasis in hepatocyte reoxygenation injury. Biochimica et Biophysica Acta (BBA) - Molecular Basis of Disease, 1500(3):297–305.

Cerec V, Glaise D, Garnier D, Morosan S, Turlin B, Drenou B, Gripon P, Kremsdorf D, Guguen-Guillouzo C, Corlu A. 2007. Transdifferentiation of hepatocyte-like cells from the human hepatoma HepaRG cell line through bipotent progenitor. Hepatology, 45(4):957–967.

Chaston TB, Des Richardson R. 2003. Iron chelators for the treatment of iron overload disease: relationship between structure, redox activity, and toxicity. Am J Hematol, 73(3):200–210.Chen Y, Wong PP, Sjeklocha L, Steer CJ, Sahin MB. 2012. Mature hepatocytes exhibit unexpected plasticity by direct dedifferentiation into liver progenitor cells in culture. Hepatology, 55(2):563–574.

Cheng Y, Liu Y-F, Cheng D-H, Li B-F, Zhao N. 2005. Evaluation of CMU-1 preservation solutions using an isolated perfused rat liver model. WJG, 11(16):2522.

Coppeta JR, Mescher MJ, Isenberg BC, Spencer AJ, Kim ES, Lever AR, Mulhern TJ, Prantil-Baun R, Comolli JC, Borenstein JT. 2016. A portable and reconfigurable multi-organ platform for drug development with onboard microfluidic flow control. Lab Chip, 17(1):134–144.

Coulouarn C, Corlu A, Glaise D, Guénon I, Thorgeirsson SS, Clément B. 2012. Hepatocyte-stellate cell cross-talk in the liver engenders a permissive inflammatory microenvironment that drives progression in hepatocellular carcinoma. Cancer Res, 72(10):2533–2542.

Dagher PC. 2000. Modeling ischemia in vitro: selective depletion of adenine and guanine nucleotide pools. Am J Physiol, Cell Physiol, 279(4):C1270-7.

Davidson MD, Ballinger KR, Khetani SR. 2016. Long-term exposure to abnormal glucose levels alters drug metabolism pathways and insulin sensitivity in primary human hepatocytes. Sci Rep, 6:28178.

Dejager L, Pinheiro I, Dejonckheere E, Libert C. 2011. Cecal ligation and puncture: the gold standard model for polymicrobial sepsis? Trends Microbiol, 19(4):198–208.

Deleve LD, Wang X, Guo Y. 2008. Sinusoidal endothelial cells prevent rat stellate cell activation and promote reversion to quiescence. Hepatology, 48(3):920–930.

Du Y, Li N, Yang H, Luo C, Gong Y, Tong C, Gao Y, Lu S, Long M. 2017. Mimicking liver sinusoidal structures and functions using a 3D-configured microfluidic chip. Lab Chip, 17(5):782–794.

Duffield JS, Forbes SJ, Constandinou CM, Clay S, Partolina M, Vuthoori S, Wu S, Lang R, Iredale JP. 2005. Selective depletion of macrophages reveals distinct, opposing roles during liver injury and repair. J. Clin. Invest., 115(1):56–65.

Edwards S, Lalor PF, Nash GB, Rainger GE, Adams DH. 2005. Lymphocyte traffic through sinusoidal endothelial cells is regulated by hepatocytes. Hepatology, 41(3): 451–459.

Efron PA, Mohr AM, Moore FA, Moldawer LL. 2015. The future of murine sepsis and trauma research models. J Leukoc Biol, 98(6):945–952.

Elferink MGL, Olinga P, Draaisma AL, Merema MT, Faber KN, Slooff MJH, Meijer DKF, Groothuis GMM. 2004. LPS-induced downregulation of MRP2 and BSEP in human liver is due to a posttranscriptional process. Am J Physiol Gastrointest Liver Physiol, 287(5):G1008–16.

Falasca L, Bergamini A, Serafino A, Balabaud C, Dini L. 1996. Human Kupffer cell recognition and phagocytosis of apoptotic peripheral blood lymphocytes. Exp Cell Res, 224(1):152–162.

Faley S, Seale K, Hughey J, Schaffer DK, VanCompernolle S, McKinney B, Baudenbacher F, Unutmaz D, Wikswo JP. 2008. Microfluidic platform for real-time signaling analysis of multiple single T cells in parallel. Lab Chip, 8(10):1700–1712.

Fink MP. 2014. Animal models of sepsis. Virulence, 5(1):143–153.

Fleischmann C, Thomas-Rueddel DO, Hartmann M, Hartog CS, Welte T, Heublein S, Dennler U, Reinhart K. 2016. Hospital Incidence and Mortality Rates of Sepsis. Dtsch Arztebl Int, 113(10):159–166.Frank A, Rauen U, Groot H de. 2000. Protection by glycine against hypoxic injury of rat hepatocytes: inhibition of ion fluxes through nonspecific leaks. J Hepatol, 32(1):58–66.

Ford AJ, Jain G, Rajagopalan P. 2015. Designing a fibrotic microenvironment to investigate changes in human liver sinusoidal endothelial cell function. Acta Biomater, 24:220–227.

Gallinat A, Lüer B, Swoboda S, Rauen U, Paul A, Minor T. 2013. Use of the new preservation solution Custodiol-N supplemented with dextran for hypothermic machine perfusion of the kidney. Cryobiology, 66(2):131–135.

Garbe S, Zatschler B, Müller B, Dieterich P, Ebner A, Rauen U, Matschke K, Deussen A. 2011. Preservation of human artery function following prolonged cold storage with a new solution. J Vasc Surg, 53(4):1063–1070.

Godoy P, Hewitt NJ, Albrecht U, Andersen ME, Ansari N, Bhattacharya S, Bode JG, Bolleyn J, Borner C, Bottger J, Braeuning A, Budinsky RA, Burkhardt B, Cameron NR, Camussi G, Cho C-S, Choi Y-J, Craig Rowlands J, Dahmen U, Damm G, Dirsch O, Donato MT, Dong J, Dooley S, Drasdo D, Eakins R, Ferreira KS, Fonsato V, Fraczek J, Gebhardt R, Gibson A, Glanemann M, Goldring CEP, Gomez-Lechon MJ, Groothuis GMM, Gustavsson L, Guyot C, Hallifax D, Hammad S, Hayward A, Haussinger D, Hellerbrand C, Hewitt P, Hoehme S, Holzhutter H-G, Houston JB, Hrach J, Ito K, Jaeschke H, Keitel V, Kelm JM, Kevin Park B, Kordes C, Kullak-Ublick GA, LeCluyse EL, Lu P, Luebke-Wheeler J, Lutz A, Maltman DJ, Matz-Soja M, McMullen P, Merfort I, Messner S, Meyer C, Mwinyi J, Naisbitt DJ, Nussler AK, Olinga P, Pampaloni F, Pi J, Pluta L, Przyborski SA, Ramachandran A, Rogiers V, Rowe C, Schelcher C, Schmich K, Schwarz M, Singh B, Stelzer EHK, Stieger B, Stober R, Sugiyama Y, Tetta C, Thasler WE, Vanhaecke T, Vinken M, Weiss TS, Widera A, Woods CG, Xu JJ, Yarborough KM, Hengstler JG. 2013. Recent advances in 2D and 3D in vitro systems using primary hepatocytes, alternative hepatocyte sources and non-parenchymal liver cells and their use in investigating mechanisms of hepatotoxicity, cell signaling and ADME. Arch Toxicol, 87(8):1315–1530.

Guibert EE, Petrenko AY, Balaban CL, Somov AY, Rodriguez JV, Fuller BJ. 2011. Organ Preservation: Current Concepts and New Strategies for the Next Decade. Transfus Med Hemother, 38(2):125–142.

Guilliams M, Scott CL. 2017. Does niche competition determine the origin of tissue-resident macrophages? Nat Rev Immunol, 17(7):451–460.

Guillouzo A, Morel F, Fardel O, Meunier B. 1993. Use of human hepatocyte cultures for drug metabolism studies. Toxicology, 82(1-3):209–219.

Hart NA 't, van der Plaats A, Faber A, Leuvenink HGD, Olinga P, Wiersema-Buist J, Verkerke GJ, Rakhorst G, Ploeg RJ. 2005. Oxygenation during hypothermic rat liver preservation: an in vitro slice study to demonstrate beneficial or toxic oxygenation effects. Liver Transpl, 11(11):1403–1411.

Ingber DE. 2016. Reverse Engineering Human Pathophysiology with Organs-on-Chips. Cell, 164(6):1105–1109.

Ip WKE, Hoshi N, Shouval DS, Snapper S, Medzhitov R. 2017. Anti-inflammatory effect of IL-10 mediated by metabolic reprogramming of macrophages. Science, 356(6337):513–519.

Iredale JP. 2007. Models of liver fibrosis: exploring the dynamic nature of inflammation and repair in a solid organ. J Clin Invest, 117(3):539–548.

Ishibashi H, Nakamura M, Komori A, Migita K, Shimoda S. 2009. Liver architecture, cell function, and disease. Semin Immunopathol, 31(3):399–409.

Jain A, Barrile R, van der Meer AD, Mammoto A, Mammoto T, Ceunynck K de, Aisiku O, Otieno MA, Louden CS, Hamilton GA, Flaumenhaft R, Ingber DE. 2018. Primary Human Lung Alveolus-on-a-chip Model of Intravascular Thrombosis for Assessment of Therapeutics. Clin Pharmacol Ther. 103(2):332–340.

Kanebratt KP, Andersson TB. 2008. Evaluation of HepaRG cells as an in vitro model for human drug metabolism studies. Drug Metab Dispos, 36(7):1444–1452.

Kang Y, Rawat S, Duchemin N, Bouchard M, Noh M. 2017. Human Liver Sinusoid on a Chip for Hepatitis B Virus Replication Study. Micromachines, 8(1):27.

Kang YBA, Sodunke TR, Lamontagne J, Cirillo J, Rajiv C, Bouchard MJ, Noh M. 2015. Liver sinusoid on a chip: Long-term layered co-culture of primary rat hepatocytes and endothelial cells in microfluidic platforms. Biotechnol Bioeng, 112(12):2571–2582.

Kang YBA, Rawat S, Cirillo J, Bouchard M, Noh HM. 2013. Layered long-term co-culture of hepatocytes and endothelial cells on a transwell membrane: toward engineering the liver sinusoid. Biofabrication, 5(4):45008.

Kim HJ, Li H, Collins JJ, Ingber DE. 2016. Contributions of microbiome and mechanical deformation to intestinal bacterial overgrowth and inflammation in a human gut-on-a-chip. Proc Natl Acad Sci USA, 113(1):E7–15.

Kim K, Ohashi K, Utoh R, Kano K, Okano T. 2012. Preserved liver-specific functions of hepatocytes in 3D co-culture with endothelial cell sheets. Biomaterials, 33(5):1406–1413.

Kimura S, Ozaki KS, Ueki S, Zhang M, Yokota S, Stolz DB, Geller DA, Murase N. 2016. Contribution of alloantigens to hepatic ischemia/reperfusion injury: Roles of natural killer cells and innate immune recognition of nonself. Liver Transpl, 22(1):80–90.

Kingsley SMK, Bhat BV. 2016. Differential Paradigms in Animal Models of Sepsis. Curr Infect Dis Rep, 18(9):26.

Kjaergaard AG, Dige A, Nielsen JS, Tønnesen E, Krog J. 2016. The use of the soluble adhesion molecules sE-selectin, sICAM-1, sVCAM-1, sPECAM-1 and their ligands CD11a and CD49d as diagnostic and prognostic biomarkers in septic and critically ill non-septic ICU patients. APMIS, 124(10):846–855.

Klein M, Thomas M, Hofmann U, Seehofer D, Damm G, Zanger UM. 2015. A systematic comparison of the impact of inflammatory signaling on absorption, distribution, metabolism, and excretion gene expression and activity in primary human hepatocytes and HepaRG cells. Drug Metab Dispos, 43(2):273–283.

Kozlova I, Khalid Y, Roomans GM. 2003. Preservation of mouse liver tissue during cold storage in experimental solutions assessed by x-ray microanalysis. Liver Transpl, 9(3):268–278.

Krause P, Saghatolislam F, Koenig S, Unthan-Fechner K, Probst I. 2009. Maintaining hepatocyte differentiation in vitro through co-culture with hepatic stellate cells. In Vitro Cell Dev Biol Anim, 45(5-6):205–212.

Krenkel O, Tacke F. 2017. Liver macrophages in tissue homeostasis and disease. Nat Rev Immunol, 17:306–321.

Le Moine O, Louis H, Demols A, Desalle F, Demoor F, Quertinmont E, Goldman M, Deviere J. 2000. Cold liver ischemia-reperfusion injury critically depends on liver T cells and is improved by donor pretreatment with interleukin 10 in mice. Hepatology, 31(6):1266–1274.

Leclerc E, Sakai Y, Fujii T. 2003. Cell Culture in 3-Dimensional Microfluidic Structure of PDMS (polydimethylsiloxane). Biomedical Microdevices, 5(2):109–114.

LeCluyse EL, Witek RP, Andersen ME, Powers MJ. 2012. Organotypic liver culture models: meeting current challenges in toxicity testing. Crit Rev Toxicol, 42(6):501–548.

Leeuwenberg JF, Smeets EF, Neefjes JJ, Shaffer MA, Cinek T, Jeunhomme TM, Ahern TJ, Buurman WA. 1992. E-selectin and intercellular adhesion molecule-1 are released by activated human endothelial cells in vitro. Immunology, 77(4):543–549.

Levels JHM, Lemaire LCJM, van den Ende AE, van Deventer SJH, van Lanschot JJB. 2003. Lipid composition and lipopolysaccharide binding capacity of lipoproteins in plasma and lymph of patients with systemic inflammatory response syndrome and multiple organ failure. Crit Care Med, 31(6):1647–1653.

Li M, Wang W, Soroka CJ, Mennone A, Harry K, Weinman EJ, Boyer JL. 2010. NHERF-1 binds to Mrp2 and regulates hepatic Mrp2 expression and function. J Biol Chem, 285(25):19299–19307.

Lopez-Castejon G, Brough D. 2011. Understanding the mechanism of IL-1β secretion. Cytokine Growth Factor Rev, 22(4):189–195.

Lu Y-C, Yeh W-C, Ohashi PS. 2008. LPS/TLR4 signal transduction pathway. Cytokine, 42(2):145–151.

Mack JE, Kerr JA, Vreugdenhil PK, Belzer FO, Southard JH. 1991. Effect of polyethylene glycol on lipid peroxidation in cold-stored rat hepatocytes. Cryobiology, 28(1):1–7.

Mantovani A, Sica A, Sozzani S, Allavena P, Vecchi A, Locati M. 2004. The chemokine system in diverse forms of macrophage activation and polarization. Trends Immunol, 25(12):677–686.

Mantovani A, Sozzani S, Locati M, Allavena P, Sica A. 2002. Macrophage polarization: tumor-associated macrophages as a paradigm for polarized M2 mononuclear phagocytes. Trends Immunol, 23(11):549–555.

Martinez FO, Gordon S. 2014. The M1 and M2 paradigm of macrophage activation: time for reassessment. F1000Prime Rep, 6:13.

Marx U, Andersson TB, Bahinski A, Beilmann M, Beken S, Cassee FR, Cirit M, Daneshian M, Fitzpatrick S, Frey O, Gaertner C, Giese C, Griffith L, Hartung T, Heringa MB, Hoeng J, Jong WH de, Kojima H, Kuehnl J, Leist M, Luch A, Maschmeyer I, Sakharov D, Sips AJAM, Steger-Hartmann T, Tagle DA, Tonevitsky A, Tralau T, Tsyb S, van de Stolpe A, Vandebriel R, Vulto P, Wang J, Wiest J, Rodenburg M, Roth A. 2016. Biology-inspired microphysiological system approaches to solve the prediction dilemma of substance testing. ALTEX, 33(3):272–321.

Maschmeyer I, Hasenberg T, Jaenicke A, Lindner M, Lorenz AK, Zech J, Garbe L-A, Sonntag F, Hayden P, Ayehunie S, Lauster R, Marx U, Materne E-M. 2015. Chip-based human liver-intestine and liver-skin co-cultures--A first step toward systemic repeated dose substance testing in vitro. Eur J Pharm Biopharm, 95(Pt A):77–87.

Materne E-M, Maschmeyer I, Lorenz AK, Horland R, Schimek KMS, Busek M, Sonntag F, Lauster R, Marx U. 2015. The multi-organ chip--a microfluidic platform for long-term multi-tissue coculture. J Vis Exp (98):e52526.

McCarty WJ, Prodanov L, Bale SS, Bhushan A, Jindal R, Yarmush ML, Usta OB. 2015. Layer-by-layer Collagen Deposition in Microfluidic Devices for Microtissue Stabilization. J Vis Exp (103):e53078.

McCarty WJ, Usta OB, Luitje M, Bale SS, Bhushan A, Hegde M, Golberg I, Jindal R, Yarmush ML. 2014. A novel ultrathin collagen nanolayer assembly for 3-D microtissue engineering: Layer-by-layer collagen deposition for long-term stable microfluidic hepatocyte culture. Technology (Singap World Sci), 2(1):67–74.

Mencin A, Kluwe J, Schwabe RF. 2009. Toll-like receptors as targets in chronic liver diseases. Gut, 58(5):704–720.

Mertens S, Noll T, Spahr R, Krützfeldt A, Piper HM. 1990. Energetic response of coronary endothelial cells to hypoxia. Am J Physiol, 258(3 Pt 2): H689–94.

Mestas J, Hughes CCW. 2004. Of mice and not men: differences between mouse and human immunology. J Immunol, 172(5):2731–2738.

Meyvantsson I, Beebe DJ. 2008. Cell culture models in microfluidic systems. Annu Rev Anal Chem (Palo Alto Calif), 1:423–449.

Michalopoulos GK. 2007. Liver regeneration. J Cell Physiol, 213(2):286–300.

Nesseler N, Launey Y, Aninat C, Morel F, Mallédant Y, Seguin P. 2012. Clinical review: The liver in sepsis. Crit Care, 16(5):235.

Nies AT, König J, Pfannschmidt M, Klar E, Hofmann WJ, Keppler D. 2001. Expression of the multidrug resistance proteins MRP2 and MRP3 in human hepatocellular carcinoma. Int J Cancer, 94(4):492–499.

Nishimura Y, Romer LH, Lemasters JJ. 1998. Mitochondrial dysfunction and cytoskeletal disruption during chemical hypoxia to cultured rat hepatic sinusoidal endothelial cells: the pH paradox and cytoprotection by glucose, acidotic pH, and glycine. Hepatology, 27(4):1039–1049.

O'Callaghan JM, Morgan RD, Knight SR, Morris PJ. 2014. The effect of preservation solutions for storage of liver allografts on transplant outcomes: a systematic review and meta-analysis. Ann Surg, 260(1):46–55.

Ono K, Nishitani C, Mitsuzawa H, Shimizu T, Sano H, Suzuki H, Kodama T, Fujii N, Fukase K, Hirata K, Kuroki Y. 2006. Mannose-binding lectin augments the uptake of lipid A, Staphylococcus aureus, and Escherichia coli by Kupffer cells through increased cell surface expression of scavenger receptor A. J Immunol, 177(8):5517–5523.

Oo YH, Shetty S, Adams DH. 2010. The role of chemokines in the recruitment of lymphocytes to the liver. Dig Dis, 28(1):31–44.

Ospelt C, Gay S. 2010. TLRs and chronic inflammation. Int J Biochem Cell Biol, 42(4):495–505.

Ostrowska A, Gu K, Bode DC, van Buskirk RG. 2009. Hypothermic storage of isolated human hepatocytes: a comparison between University of Wisconsin solution and a hypothermosol platform. Arch Toxicol, 83(5):493–502.

Petrat F, Boengler K, Schulz R, Groot H de. 2012. Glycine, a simple physiological compound protecting by yet puzzling mechanism(s) against ischaemia-reperfusion injury: current knowledge. Br J Pharmacol, 165(7):2059–2072.

Pizanis N, Petrov A, Heckmann J, Wiswedel I, Wohlschläger J, Groot H de, Jakob H, Rauen U, Kamler M. 2012. A new preservation solution for lung transplantation: evaluation in a porcine transplantation model. J Heart Lung Transplant, 31(3):310–317.

Pless G, Sauer IM, Rauen U. 2012. Improvement of the cold storage of isolated human hepatocytes. Cell Transplant, 21(1):23–37.

Pless-Petig G, Singer BB, Rauen U. 2012. Cold storage of rat hepatocyte suspensions for one week in a customized cold storage solution--preservation of cell attachment and metabolism. PLoS One, 7(7):e40444.

Poisson J, Lemoinne S, Boulanger C, Durand F, Moreau R, Valla D, Rautou P-E. 2017. Liver sinusoidal endothelial cells: Physiology and role in liver diseases. J Hepatol, 66(1):212–227.

Prodanov L, Jindal R, Bale SS, Hegde M, McCarty WJ, Golberg I, Bhushan A, Yarmush ML, Usta OB. 2016. Long-term maintenance of a microfluidic 3D human liver sinusoid. Biotechnol Bioeng, 113(1):241–246.

Puts CF, Berendsen TA, Bruinsma BG, Ozer S, Luitje M, Usta OB, Yarmush ML, Uygun K. 2015. Polyethylene glycol protects primary hepatocytes during supercooling preservation. Cryobiology, 71(1):125–129.

Raasch M, Rennert K, Jahn T, Gartner C, Schonfelder G, Huber O, Seiler AEM, Mosig AS. 2016. An integrative microfluidically supported in vitro model of an endothelial barrier combined with cortical spheroids simulates effects of neuroinflammation in neocortex development. Biomicrofluidics, 10(4):44102.

Ramachandran P, Pellicoro A, Vernon MA, Boulter L, Aucott RL, Ali A, Hartland SN, Snowdon VK, Cappon A, Gordon-Walker TT, Williams MJ, Dunbar DR, Manning JR, van Rooijen N, Fallowfield JA, Forbes SJ, Iredale JP. 2012. Differential Ly-6C expression identifies the recruited macrophage phenotype, which orchestrates the regression of murine liver fibrosis. Proc Natl Acad Sci USA, 109(46):E3186–95.

Rashidi H, Alhaque S, Szkolnicka D, Flint O, Hay DC. 2016. Fluid shear stress modulation of hepatocyte-like cell function. Arch Toxicol, 90(7):1757–1761.

Rathinam C, Poueymirou WT, Rojas J, Murphy AJ, Valenzuela DM, Yancopoulos GD, Rongvaux A, Eynon EE, Manz MG, Flavell RA. 2011. Efficient differentiation and function of human macrophages in humanized CSF-1 mice. Blood, 118(11):3119–3128.

Rauen U, Kerkweg U, Groot H de. 2007a. Iron-dependent vs. iron-independent cold-induced injury to cultured rat hepatocytes: a comparative study in physiological media and organ preservation solutions. Cryobiology, 54(1):77–86.

Rauen U, Klempt S, Groot H de. 2007b. Histidine-induced injury to cultured liver cells, effects of histidine derivatives and of iron chelators. Cell Mol Life Sci, 64(2):192–205.

Rauen U, Petrat F, Li T, Groot H de. 2000. Hypothermia injury/cold-induced apoptosis-evidence of an increase in chelatable iron causing oxidative injury in spite of low O2-/H2O2 formation. FASEB J, 14(13):1953–1964.

Rauen U, Petrat F, Sustmann R, Groot H de. 2004. Iron-induced mitochondrial permeability transition in cultured hepatocytes. J Hepatol, 40(4):607–615.

Rauen U, Polzar B, Stephan H, Mannherz HG, Groot H de. 1999. Cold-induced apoptosis in cultured hepatocytes and liver endothelial cells: mediation by reactive oxygen species. FASEB J, 13(1):155–168.

Richardson D, Ponka P, Baker E. 1994. The effect of the iron(III) chelator, desferrioxamine, on iron and transferrin uptake by the human malignant melanoma cell. Cancer Res, 54(3):685–689.

Rodríguez-Antona C, Donato MT, Boobis A, Edwards RJ, Watts PS, Castell JV, Gómez-Lechón M-J. 2002. Cytochrome P450 expression in human hepatocytes and hepatoma cell lines: molecular mechanisms that determine lower expression in cultured cells. Xenobiotica, 32(6):505–520.

Rongvaux A, Takizawa H, Strowig T, Willinger T, Eynon EE, Flavell RA, Manz MG. 2013. Human hemato-lymphoid system mice: current use and future potential for medicine. Annu Rev Immunol, 31:635–674.

Rose KA, Holman NS, Green AM, Andersen ME, LeCluyse EL. 2016. Co-culture of Hepatocytes and Kupffer Cells as an In Vitro Model of Inflammation and Drug-Induced Hepatotoxicity. Journal of Pharmaceutical Sciences, 105(2):950–964.

Rubin K, Janefeldt A, Andersson L, Berke Z, Grime K, Andersson TB. 2015. HepaRG cells as human-relevant in vitro model to study the effects of inflammatory stimuli on cytochrome P450 isoenzymes. Drug Metab Dispos, 43(1):119–125.

Schurich A, Bottcher JP, Burgdorf S, Penzler P, Hegenbarth S, Kern M, Dolf A, Endl E, Schultze J, Wiertz E, Stabenow D, Kurts C, Knolle P. 2009. Distinct kinetics and dynamics of cross-presentation in liver sinusoidal endothelial cells compared to dendritic cells. Hepatology, 50(3):909–919.

Scott MJ, Liu S, Shapiro RA, Vodovotz Y, Billiar TR. 2009. Endotoxin uptake in mouse liver is blocked by endotoxin pretreatment through a suppressor of cytokine signaling-1-dependent mechanism. Hepatology, 49(5):1695–1708.

Seki E, Minicis S de, Osterreicher CH, Kluwe J, Osawa Y, Brenner DA, Schwabe RF. 2007. TLR4 enhances TGF-beta signaling and hepatic fibrosis. Nat Med, 13(11):1324–1332.

Seok J, Warren HS, Cuenca AG, Mindrinos MN, Baker HV, Xu W, Richards DR, McDonald-Smith GP, Gao H, Hennessy L, Finnerty CC, Lopez CM, Honari S, Moore EE, Minei JP, Cuschieri J, Bankey PE, Johnson JL, Sperry J, Nathens AB, Billiar TR, West MA, Jeschke MG, Klein MB, Gamelli RL, Gibran NS, Brownstein BH, Miller-Graziano C, Calvano SE, Mason PH, Cobb JP, Rahme LG, Lowry SF, Maier RV, Moldawer LL, Herndon DN, Davis RW, Xiao W, Tompkins RG. 2013. Genomic responses in mouse models poorly mimic human inflammatory diseases. Proc Natl Acad Sci USA, 110(9):3507–3512.

Shah C, Hari-Dass R, Raynes JG. 2006. Serum amyloid A is an innate immune opsonin for Gram-negative bacteria. Blood, 108(5):1751–1757.

Shalova IN, Lim JY, Chittezhath M, Zinkernagel AS, Beasley F, Hernández-Jiménez E, Toledano V, Cubillos-Zapata C, Rapisarda A, Chen J, Duan K, Yang H, Poidinger M, Melillo G, Nizet V, Arnalich F, López-Collazo E, Biswas SK. 2015. Human monocytes undergo functional re-programming during sepsis mediated by hypoxia-inducible factor-1α. Immunity, 42(3):484–498.

Shi C, Pamer EG. 2011. Monocyte recruitment during infection and inflammation. Nat Rev Immunol, 11(11):762–774.

Shi S, Xue F. 2016. Current Antioxidant Treatments in Organ Transplantation. Oxid Med Cell Longev, 2016:8678510.

Sica A, Invernizzi P, Mantovani A. 2014. Macrophage plasticity and polarization in liver homeostasis and pathology. Hepatology, 59(5):2034–2042.

Singer M, Deutschman CS, Seymour CW, Shankar-Hari M, Annane D, Bauer M, Bellomo R, Bernard GR, Chiche J-D, Coopersmith CM, Hotchkiss RS, Levy MM, Marshall JC, Martin GS, Opal SM, Rubenfeld GD, van der Poll T, Vincent J-L, Angus DC. 2016. The Third International Consensus Definitions for Sepsis and Septic Shock (Sepsis-3). JAMA, 315(8):801–810.

Smedsrød B. 2004. Clearance function of scavenger endothelial cells. Comp Hepatol, 3 Suppl 1:S22.

Starokozhko V, Groothuis GMM. 2017. Judging the value of 'liver-on-a-chip' devices for prediction of toxicity. Expert Opin Drug Metab Toxicol, 13(2):125–128.

Strnad P, Tacke F, Koch A, Trautwein C. 2017. Liver - guardian, modifier and target of sepsis. Nat Rev Gastroenterol Hepatol, 14(1):55–66.

Szabo G, Dolganiuc A, Mandrekar P. 2006. Pattern recognition receptors: a contemporary view on liver diseases. Hepatology, 44(2):287–298.

Tacke F, Luedde T, Trautwein C. 2009. Inflammatory pathways in liver homeostasis and liver injury. Clin Rev Allergy Immunol, 36(1):4–12.

Tacke F, Zimmermann HW. 2014. Macrophage heterogeneity in liver injury and fibrosis. J Hepatol, 60(5):1090–1096.

Takao K, Miyakawa T. 2015. Genomic responses in mouse models greatly mimic human inflammatory diseases. Proc Natl Acad Sci USA, 112(4):1167–1172.

Takeuchi O, Akira S. 2010. Pattern recognition receptors and inflammation. Cell, 140(6):805–820.

Tanaka Y, Yamato M, Okano T, Kitamori T, Sato K. 2006. Evaluation of effects of shear stress on hepatocytes by a microchip-based system. Meas. Sci. Technol., 17(12):3167–3170.

Thomas RJ, Bhandari R, Barrett DA, Bennett AJ, Fry JR, Powe D, Thomson BJ, Shakesheff KM. 2005. The effect of three-dimensional co-culture of hepatocytes and hepatic stellate cells on key hepatocyte functions in vitro. Cells Tissues Organs (Print), 181(2):67–79.

Toepke MW, Beebe DJ. 2006. PDMS absorption of small molecules and consequences in microfluidic applications. Lab Chip, 6(12):1484–1486.

Toh Y-C, Lim TC, Tai D, Xiao G, van Noort D, Yu H. 2009. A microfluidic 3D hepatocyte chip for drug toxicity testing. Lab Chip, 9(14):2026–2035.

Tomiyama K, Ikeda A, Ueki S, Nakao A, Stolz DB, Koike Y, Afrazi A, Gandhi C, Tokita D, Geller DA, Murase N. 2008. Inhibition of Kupffer cell-mediated early proinflammatory response with carbon monoxide in transplant-induced hepatic ischemia/reperfusion injury in rats. Hepatology, 48(5):1608–1620.

Toyoda Y, Tamai M, Kashikura K, Kobayashi S, Fujiyama Y, Soga T, Tagawa Y-i. 2012. Acetaminophen-induced hepatotoxicity in a liver tissue model consisting of primary hepatocytes assembling around an endothelial cell network. Drug Metab Dispos, 40(1):169–177.

Uhrig A, Banafsche R, Kremer M, Hegenbarth S, Hamann A, Neurath M, Gerken G, Limmer A, Knolle PA. 2005. Development and functional consequences of LPS tolerance in sinusoidal endothelial cells of the liver. J Leukoc Biol, 77(5):626–633.

van den Bossche J, Baardman J, Otto NA, van der Velden S, Neele AE, van den Berg SM, Luque-Martin R, Chen H-J, Boshuizen MCS, Ahmed M, Hoeksema MA, Vos AF de, Winther MPJ de. 2016. Mitochondrial Dysfunction Prevents Repolarization of Inflammatory Macrophages. Cell Rep, 17(3):684–696.

van Meer BJ, Vries H de, Firth KSA, van Weerd J, Tertoolen LGJ, Karperien HBJ, Jonkheijm P, Denning C, IJzerman AP, Mummery CL. 2017. Small molecule absorption by PDMS in the context of drug response bioassays. Biochem Biophys Res Commun, 482(2):323–328.

van Midwoud PM, Janse A, Merema MT, Groothuis GMM, Verpoorte E. 2012. Comparison of Biocompatibility and Adsorption Properties of Different Plastics for Advanced Microfluidic Cell and Tissue Culture Models. Anal Chem, 84(9):3938–3944.

Vernetti LA, Senutovitch N, Boltz R, DeBiasio R, Shun TY, Gough A, Taylor DL. 2016. A human liver microphysiology platform for investigating physiology, drug safety, and disease models. Exp Biol Med (Maywood), 241(1):101–114.

Vogel DYS, Heijnen PDAM, Breur M, Vries HE de, Tool ATJ, Amor S, Dijkstra CD. 2014. Macrophages migrate in an activation-dependent manner to chemokines involved in neuroinflammation. J Neuroinflammation, 11:23.

Wang P, Wu P, Siegel MI, Egan RW, Billah MM. 1994. IL-10 inhibits transcription of cytokine genes in human peripheral blood mononuclear cells. J Immunol, 153(2):811–816.

Wang X, Li W, Lu J, Li N, Li J. 2004. Lipopolysaccharide suppresses albumin expression by activating NF-kappaB in rat hepatocytes. J Surg Res, 122(2):274–279.

Warren HS, Tompkins RG, Moldawer LL, Seok J, Xu W, Mindrinos MN, Maier RV, Xiao W, Davis RW. 2015. Mice are not men. Proc Natl Acad Sci USA, 112(4):E345.

Weiskirchen R, Tacke F. 2014. Cellular and molecular functions of hepatic stellate cells in inflammatory responses and liver immunology. Hepatobiliary Surg Nutr, 3(6):344–363.

Wikswo JP. 2014. The relevance and potential roles of microphysiological systems in biology and medicine. Exp Biol Med (Maywood), 239(9):1061–1072.

Wille T, Groot H de, Rauen U. 2008. Improvement of the cold storage of blood vessels with a vascular preservation solution. Study in porcine aortic segments. J Vasc Surg, 47(2):422–431.

Willinger T, Rongvaux A, Takizawa H, Yancopoulos GD, Valenzuela DM, Murphy AJ, Auerbach W, Eynon EE, Stevens S, Manz MG, Flavell RA. 2011. Human IL-3/GM-CSF knock-in mice support human alveolar macrophage development and human immune responses in the lung. Proc Natl Acad Sci USA, 108(6):2390–2395.

Wu RQ, Xu YX, Song XH, Chen LJ, Meng XJ. 2001. Adhesion molecule and proinflammatory cytokine gene expression in hepatic sinusoidal endothelial cells following cecal ligation and puncture. World J Gastroenterol, 7(1):128–130.

Wu S, Wohlschlaeger J, Groot H de, Rauen U. 2009. Evaluation of a modified HTK solution containing the new iron chelator LK 614 in an isolated rat liver perfusion model. J Invest Surg, 22(5):340–347.

Wynn TA, Barron L. 2010. Macrophages: master regulators of inflammation and fibrosis. Semin Liver Dis, 30(3):245–257.

Yan J, Li S, Li S. 2014. The role of the liver in sepsis. Int Rev Immunol, 33(6):498–510.

Yu G, Jing Y, Kou X, Ye F, Gao L, Fan Q, Yang Y, Zhao Q, Li R, Wu M, Wei L. 2013. Hepatic stellate cells secreted hepatocyte growth factor contributes to the chemoresistance of hepatocellular carcinoma. PLoS One, 8(9):e73312.

Zatschler B, Dieterich P, Müller B, Kasper M, Rauen U, Deussen A. 2009. Improved vessel preservation after 4 days of cold storage: experimental study in rat arteries. J Vasc Surg, 50(2):397–406.

Zhang YS, Aleman J, Shin SR, Kilic T, Kim D, Mousavi Shaegh SA, Massa S, Riahi R, Chae S, Hu N, Avci H, Zhang W, Silvestri A, Sanati Nezhad A, Manbohi A, Ferrari F de, Polini A, Calzone G, Shaikh N, Alerasool P, Budina E, Kang J, Bhise N, Ribas J, Pourmand A, Skardal A, Shupe T, Bishop CE, Dokmeci MR, Atala A, Khademhosseini A. 2017. Multisensor-integrated organs-on-chips platform for automated and continual in situ monitoring of organoid behaviors. Proc Natl Acad Sci USA, 114(12):E2293–E2302.

Zhou Q, Patel D, Kwa T, Haque A, Matharu Z, Stybayeva G, Gao Y, Diehl AM, Revzin A. 2015. Liver injury-on-a-chip: microfluidic co-cultures with integrated biosensors for monitoring liver cell signaling during injury. Lab Chip, 15(23):4467–4478.

Zimmermann HW, Bruns T, Weston CJ, Curbishley SM, Liaskou E, Li K-K, Resheq YJ, Badenhorst PW, Adams DH. 2016. Bidirectional transendothelial migration of monocytes across hepatic sinusoidal endothelium shapes monocyte differentiation and regulates the balance between immunity and tolerance in liver. Hepatology, 63(1):233–246.

Zinchenko YS, Schrum LW, Clemens M, Coger RN. 2006. Hepatocyte and kupffer cells co-cultured on micropatterned surfaces to optimize hepatocyte function. Tissue Eng, 12(4):751–761.

B ACKNOWLEDGEMENT

Zuerst möchte ich mich bei PD Dr. Alexander Mosig als mein Mentor und Arbeitsgruppenleiter recht herzlich bedanken. Durch seine ausgezeichnete Unterstützung während meiner Arbeit hatte er entscheidenden Anteil an meiner wissenschaftlichen und persönlichen Entwicklung. Unsere Zusammenarbeit ermöglichte mir die Autorenschaft an diversen Publikationen und die Teilnahme an vielen spannenden Projekten sowie internationalen Kongressen. Vielen Dank Sandy!

Ich möchte mich außerdem bei Prof. Otmar Huber bedanken, der mir als Betreuer von Beginn an mit wissenschaftlichen Ratschlägen und anregenden Diskussionen sehr geholfen hat.

Außerdem danke ich meinem Betreuer Prof. Michael Bauer für die Hilfe zum Start meiner Karriere im CSCC und die dadurch eröffneten Möglichkeiten.

Recht herzlich möchte ich ausnahmslos der gesamten AG INSPIRE danken! Durch euch fühlte sich die Arbeit wie ein zweites Zuhause an und es war jeden Tag eine Freude mit euch im Labor zu stehen. In diesem Zuge möchte ich insbesondere Dr. Knut Rennert danken, der mir neben hilfreichen Tipps und Ratschlägen mit kurzen Gesangseinlagen im Labor von Beginn an zur Seite stand.

Weiterhin danke ich der Belegschaft vom Institut für Biochemie II, allen Kooperationspartnern und Kollegen für die Hilfe und die konstruktive Unterstützung während meiner Arbeit.

Ein ganz besonderer Dank gilt meinen Eltern Marion und Detlef, die mir jede nur erdenkliche Unterstützung gaben und mir in jeder Lebenslage zur Seite standen! An dieser Stelle danke ich auch recht herzlich meiner gesamten Familie und meinen zahlreichen guten Freunden für den Rückhalt sowie den super Ausgleich neben der Arbeit. Leider war es meinem Opa Dieter nicht vergönnt den Abschluss meiner Dissertation mit zu erleben. Ruhe in Frieden!

Last but not least, vielen Dank an die Korrekturleser PD Dr. Tony Bruns und Dr. Shishir Shetty!

C CURRICULUM VITAE

D LIST OF PUBLICATIONS

6. Gröger M, Dinger J, Kiehntopf M, Peter FT, Rauen U, Mosig AS. “Preservation of Cell Structure, Metabolism and Biotransformation Activity of Liver-on-chip Organ Models by Hypothermic Storage”, *Adv Healthc Mater.* **2018**, 7(2).

5. Gröger M, Lange M, Rennert K, Kaschowitz T, Plettenberg H, Hoffmann M, Mosig AS. “Novel approach for the prediction of cell densities and viability in standardized translucent cell culture biochips with near infrared spectroscopy”, *Eng Life Sci*. **2017**, 17(5):585–593.

4. Rennert K, Heisig K, Groeger M, Wallert M, Funke H, Lorkowski S, Huber O, Mosig AS. “Recruitment of CD16(+) monocytes to endothelial cells in response to LPS-treatment and concomitant TNF release is regulated by CX3CR1 and interfered by soluble fractalkine”, *Cytokine*. **2016**, 83:41-52.

3. Gröger M, Rennert K, Giszas B, Weiß E, Dinger J, Funke H, Kiehntopf M, Peters FT, Lupp A, Bauer M, Claus RA, Huber O, Mosig AS. “Monocyte-induced recovery of inflammation-associated hepatocellular dysfunction in a biochip-based human liver model”, *Sci Rep*. **2016**, 6:21868.

2. Press AT, Ungelenk L, Rinkenauer AC, Gröger M, Lehmann F, Mosig A, Schubert US, Clemens MG, Bauer M. “A new fluorescent dye for cell tracing and mitochondrial imaging in vitro and in vivo”, *J Biophotonics*. **2016**, 9(9):888-900.

1. Rennert K, Steinborn S, Gröger M, Ungerböck B, Jank AM, Ehgartner J, Nietzsche S, Dinger J, Kiehntopf M, Funke H, Peters FT, Lupp A, Gärtner C, Mayr T, Bauer M, Huber O, Mosig AS. “A microfluidically perfused three dimensional human liver model”, *Biomaterials*. **2015**, 71:119-131.

E AUTHOR CONTRIBUTION STATEMENT

Manuscript I

Rennert K, Steinborn S, Gröger M, Ungerböck B, Jank AM, Ehgartner J, Nietzsche S, Dinger J, Kiehntopf M, Funke H, Peters FT, Lupp A, Gärtner C, Mayr T, Bauer M, Huber O, Mosig AS. 2015. A microfluidically perfused three dimensional human liver model. **Biomaterials**, 71:119-131.

author	contribution
M. Gröger	establishment of fully assembled liver-on-a-chip models, CDF and CYP3A4 activity assays, integration and optimization of microfluidics, statistical data analysis
K. Rennert	planning and performing experiments, writing of the manuscript
S. Steinborn	performing experiments, integration optimization of microfluidics
B. Ungerböck, J. Ehgartner, T. Mayr	establishment of oxygen measurement, sensor spot integration
A.M. Jank	establishment of basic microfluidic techniques
S. Nietzsche	scanning electron microscopy analysis
J. Dinger, F.T. Peters	analysis of CYP3A4 metabolite formation
M. Kiehntopf	measurement of lactate, glucose, albumin, urea, ASAT, ALAT, GLDH and LDH
H. Funke	writing of the manuscript
A. Lupp, M. Bauer	writing of the manuscript
C. Gärtner	contributed to biochip design
O. Huber	writing of the manuscript
A.S. Mosig	design and supervision of the study, writing of the manuscript

Manuscript II

Gröger M, Rennert K, Giszas B, Weiß E, Dinger J, Funke H, Kiehntopf M, Peters FT, Lupp A, Bauer M, Claus RA, Huber O, Mosig AS. 2016. Monocyte-induced recovery of inflammation-associated hepatocellular dysfunction in a biochip-based human liver model. **Scientific Reports**, 6:21868.

author	contribution
M. Gröger	performing all monocyte perfusion experiments, flow cytometry analysis, immunofluorescence staining, cytokine measurements, statistical data analysis, writing of the manuscript
K. Rennert	performing experiments, design of the study, writing of the manuscript
B. Giszas	*in vivo* experiments (mouse model)
E. Weiß	performing experiments
H. Funke	writing of the manuscript
M. Kiehtopf	measurement of lactate, glucose, albumin, urea, ASAT, ALAT, GLDH and LDH
J. Dinger, F.T. Peters	analysis of CYP3A4 metabolite formation
A. Lupp	study design, writing of the manuscript
M. Bauer	writing of the manuscript
R. Claus	supervision of *in vivo* experiments (mouse model), writing of the manuscript
O. Huber	writing of the manuscript
A.S. Mosig	design and supervision of the study, writing of the manuscript

Manuscript III

Gröger M, Dinger J, Kiehntopf M, Peter FT, Rauen U, Mosig AS. 2018. Preservation of cell structure, metabolism and biotransformation activity of liver-on-chip organ models by hypothermic storage. **Advanced Healthcare Materials**, 7(2).

author	contribution
M. Gröger	design of the study, planning and performing all experiments, statistical data analysis, writing of the manuscript
J. Dinger, F.T. Peters	analysis of 1-OH-midazolam and 4-hydroxy-diclofenac formation
M. Kiehntopf	measurement of lactate, glucose, albumin, urea, ASAT, ALAT, GLDH and LDH
U. Rauen	provision of storage solutions, writing of the manuscript
A.S. Mosig	design and supervision of the study, writing of the manuscript

Ort, Datum

Prof. Dr. Otmar Huber

F EHRENWÖRTLICHE ERKLÄRUNG

Hiermit erkläre ich, dass mir die Promotionsordnung der Medizinischen Fakultät der Friedrich-Schiller-Universität bekannt ist,

ich die Dissertation selbst angefertigt habe und alle von mir benutzten Hilfsmittel, persönlichen Mitteilungen und Quellen in meiner Arbeit angegeben sind,

mich folgende Personen bei der Auswahl und Auswertung des Materials sowie bei der Herstellung des Manuskripts unterstützt haben: Prof. Otmar Huber (Betreuer) und PD Dr. Alexander S. Mosig,

die Hilfe eines Promotionsberaters nicht in Anspruch genommen wurde und dass Dritte weder unmittelbar noch mittelbar geldwerte Leistungen von mir für Arbeiten erhalten haben, die im Zusammenhang mit dem Inhalt der vorgelegten Dissertation stehen,

dass ich die Dissertation noch nicht als Prüfungsarbeit für eine staatliche oder andere wissenschaftliche Prüfung eingereicht habe und dass ich die gleiche, eine in wesentlichen Teilen ähnliche oder eine andere Abhandlung nicht bei einer anderen Hochschule als Dissertation eingereicht habe.

Ort, Datum Unterschrift von Marko Gröger